DESIGN OF A PYROLYSIS OIL GASIFIER

Design and implementation of a DKR350 pyrolysis oil gasifier in a waste to energy unit and the construction, commissioning and testing of a gasifier prototype

WASTE 4ME®
POWERING THE FUTURE WITH WASTE FROM THE PAST

TU Delft Delft University of Technology

Author:
Jesse-Jan Wisman
Studentnumber 4487184

Supervisors:
Prof. Dr. Ir. Wiebren de Jong
Ir. Vincent Toepoel

October 2021

Abstract

In this study a design is proposed and experimentally validated for the gasification of waste plastic pyrolysis oil at small scale for energy applications. The gasifier is designed to be implemented at an existing waste energy recycling (WER) unit at Waste4me B.V. which processes up to 250 kg/h of waste streams in a pyrolysis reactor which converts the waste into pyrolysis oil, pyrolysis gas and a solid residue. The pyrolysis oil investigated in this study was produced from a DKR350 mixed plastics waste stream and was produced at a rate of 50 kg/h with a lower heating value of 36.1 MJ/kg. Because the pyrolysis oil is currently not usable as a fuel or chemical feedstock due to the high oxygen content and the high level of contaminants the oil should be further converted into combustible gas which could eventually replace fossil based fuels or chemical feedstocks. To come up with a suitable design for the gasifier and the implementation of the gasifier, the current WER unit at the company is first reviewed to give context to the design. Then a literature study is done into the different gasification reactions and reactors. With this knowledge the gasifier type 'entrained flow' is selected to be implemented at the WER unit for the gasification of the DKR350 pyrolysis oil. Also, a plan for the implementation of the gasifier at the WER unit is made. Then conceptual preliminary design of the gasifier is proposed, which is a low temperature, atmospheric, air blown, non-slagging, recirculating, autothermal entrained flow gasifier. Then an experimental setup is designed to test the potential performance of the preliminary gasifier design. The main aspects that are studied in these experiments are the lower limit of operation of the equivalence ratio (ER), the effects of recirculation, the composition of the product gas at different ER and steam/fuel (S/F) ratios, the carbon conversion efficiency (CCE) and cold gas efficiency (CGE) and the performance of the oil injector and evaporator. The oil feed is approximately 4 kg/h and the ER ranges from 0.16 to 0.43, while the S/F ratio ranges from 0 to 1.16. The results of the experiments are compared to the results as computed with the Gibbs equilibrium by the process simulating software COCO. From the experiments it is concluded that the lower limit of operation of the (ER) is lower than 372 ^{o}C as the gasifier reaches steady state at this temperature. The effects of recirculation are not investigated as the performance of the recirculation system is not as designed. The composition of the product gas is determined with a gas chromatograph for different ER and S/F ratios. The highest CCE and CGE are found at an ER = 0.16 and S/F = 0 with values of 97% and 64% respectively, although to ensure a robust operation of the gasifier different settings are recommended. Generally the CCE and CGE increase with the ER, while the LHV of the dry product gas decrease with the ER. The CGE and the LHV increase slightly due to steam addition between an ER of 0.24 and 0.3. The addition of steam generally cause an increase in CO and a decrease in CO_2 concentration contradicting the results computed with the Gibbs equilibrium. At ER > 0.35 the composition, LHV, CCE and CGE becomes less dependent on the S/F ratio. The oil injector shows no charring nor clogging while the experiments show reasonable CCE's and CGE's. Therefore, it is concluded that the used oil injector is a suitable alternative for the commonly used atomizers. With the findings from the experimental validation the preliminary gasifier design and plan for implementation in the WER unit are evaluated and improved. Two implementation plans are proposed, increasing the thermal efficiency of the WER unit from 52% to 58% or to 70%. Concluding from the experimental results a periodical cleaning program is recommended to clean the system from carbonaceous deposition by combusting the deposit in a preheated reactor at T > 790 ^{o}C.

Index

List of symbols and abbreviations

Symbol	Meaning	Unit
A	Area	m^2
CCE	Carbon conversion efficiency	
CGE	Cold gas efficiency	
C_L	Aerodynamic loss coefficient	
D	Diameter	m
ER	Equivalence Ratio	
f	Friction factor	
g	Gravitational acceleration	m/s^2
ΔH	Standard enthalpy of reaction	kJ/mol
LHV	Low Heating Value	MJ/kg or MJ/Nm^3
M	Molar mass	g/mol
$\dot{m}$	Mass flowrate	kg/s
N	Molar flowrate	Mol/s
P	Pressure	Pa
Q or	Volumetric flowrate	m^3/s
R	Specific gas constant	$J{\cdot}kg^{-1}{\cdot}K^{-1}$
Re	Reynolds number	
R_m	Mass entrainment ratio	
SMD	Sauter mean diameter	µm
T	Temperature	K
X	Mass fraction	
Y	Volume fraction	K
u	Velocity	m/s
γ	Heat capacity ratio	
µ	viscosity	mPa·s or Pa·s
ρ	Density	kg/m^3
σ	Density ratio	
ϕ	Amount in mass, volume or number of molecules	kg, m^3 or mol

1. Introduction

The usage of fossil fuels as an energy source has caused the carbon dioxide levels in the atmosphere to increase globally. The rise in carbon dioxide concentration is seen as the cause of global warming which causes sea levels to rise, causes extreme weather and can cause huge changes on many ecosystems. Therefore to conserve the environment a reduction in carbon emissions is necessary. If a higher carbon circularity can be reached the need for fossil fuels will reduce and therewith also the carbon emissions. Also on the long-term a reduction in fossil fuel consumption is required as the depletion of fossil fuels will become imminent. Besides the need for a reduction of fossil fuel consumption another challenge the world faces today is the problem of plastic pollution. Several locations in the oceans are reported to be heavily polluted by plastic waste. The plastic pollution could be solved if all the waste streams worldwide are properly processed.

At Waste4me B.V. (*Waste4me*, 2021) it is tried to deliver a solution to the need for carbon circularity as well as the need for proper waste management. The company tries to achieve this by converting waste streams into fuels or a feedstock for the chemical industry with a stand alone unit at a relatively small scale to industry. The fuels will be used for the production of heat and power, therefore it is called waste-to-energy. Also the heat produced in the process can directly be utilized which is also a form of waste-to-energy. The conversion into a chemical feedstock is called chemical recycling. As the requirements on the quality of the product are generally lower for waste-to-energy than for chemical recycling the first goal at Waste4me and therefore also in this thesis is waste-to-energy. To convert the waste into fuels a pyrolysis system is used as the first conversion unit at Waste4me because of its robustness in terms of mass flow and waste composition. The waste is thermally decomposed in a screw pyrolysis reactor. When the output gas stream of the pyrolysis reactor is condensed a slurry of condensed hydrocarbons, tars and char will come out together with a stream of gas. The slurry output stream has a high calorific value but is not of high or any economic value. This low economical value is due to the high concentrations of pollutants which are bound to organic compounds and to the solid char particles. Therefore it is desired to transform the components in this stream into hydrocarbon gasses, which have a higher economical value after the gas is cleaned of its pollutants. The condensate slurry is targeted to be gasified after condensation as this will enable the possibility to buffer the condensates which will give the ability to control the output of the pyrolysis system.

Therefore the objective of this research is to come up with a design for the gasification of the condensates of a waste processing pyrolysis system to increase the total gas yield of the system. Also the gasification system should be implementable in the current screw pyrolysis system at Waste4me. To design the gasification system the required operating conditions for the gasification of the different hydrocarbon fractions will be studied in order to determine the demand for additional utilities as heat, steam and oxygen. Then it will be studied what additional processing equipment is required to enable the gasification of the condensates. A design will be made for the additional processing equipment and whereafter the design will be validated empirically.

In figure 1 a schematic overview of the current pyrolysis system can be seen. The solid black lines in figure 1 indicate existing material streams in the screw pyrolysis system at Waste4Me. The dotted black line indicates the flue gas heating of the pyrolysis system. The gasification system marked in red and the adjacent streams marked in red are non-existing and are the parts to be designed in this study. The gasification system marked in red will consist of all the additional processing equipment that is required to enable the gasification of the condensates. To implement this gasification system the product gas should be reinjected into the system somewhere to combine the non-condensable pyrolysis gas with the gasification product gas into one product

gas outlet stream. This to be determined mixing location is indicated by the question mark at the red product stream of the gasifier in figure 1.

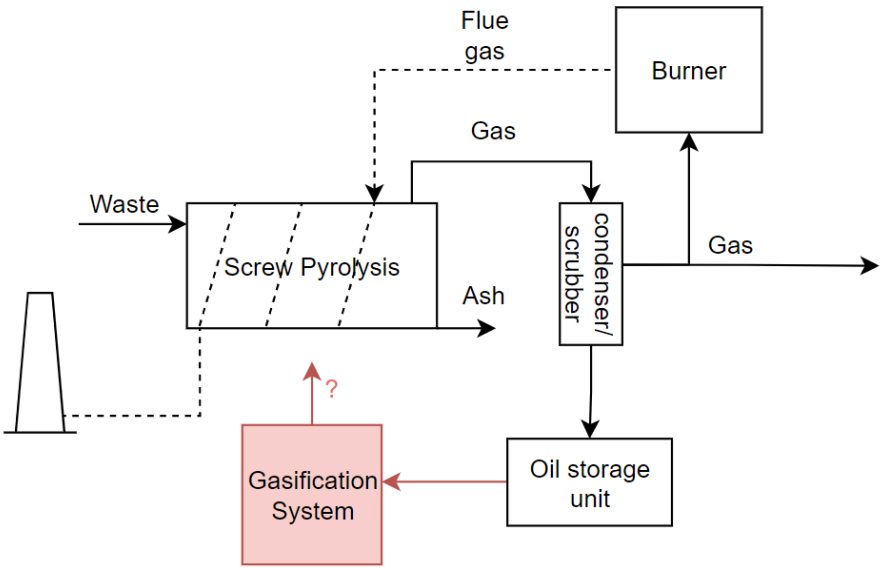

figure 1 Schematic overview of the pyrolysis system. The 'to be designed' gasification system and recirculation stream are marked in red.

The objective of this research leads to the following main research question:

How should a gasifier be designed and implemented to increase the gas yield of a DKR350 waste processing screw pyrolysis based system for heat and power applications?

1.1 Structure description

To answer the main research question several sub-questions need to be solved. This paragraph will discuss all the sub-questions which follow from the main research question. Also, it will describe how the sub-questions will be answered. In figure 2 an overview is given of the structure of this research including the main research question, sub-questions and in-between products and end products. The sub-questions are:

1. **How should the gasifier be implemented in a DKR350 waste processing screw pyrolysis based system?**
   To answer this the current waste processing screw pyrolysis system at Waste4me will be reviewed after which a plan for implementation will be made.
2. **What are the design constraints and criteria for a gasifier to be implemented in a DKR350 waste processing screw pyrolysis based system?**
   To answer this a review of the current waste processing screw pyrolysis system at Waste4me will be made and the DKR350 pyrolysis products will be studied as these will form the feed material for the gasifier. With this knowledge the design criteria and constraints will be defined.
3. **What type of gasification system should be used?**
   To answer this the different gasification reactors and reactions will be studied in a literature review. This knowledge combined with the formulated design constrains and criteria will lead to the selection of a gasification system. It will be checked if this selected gasifier can be implemented as decided in sub-question 1 and any necessary adjustments will be made in either the implementation of the gasifier or the reactor type. The product will be a gasifier selection and a final design for the implementation of it.
4. **How to design the selected gasifier concept?**
   To answer this question a gasifier design will be proposed which will be based on the selected gasifier concept that was determined in question 3, and which fulfills the constraints and criteria as determined in question 2.

5. **How to validate the preliminary gasifier design?**
   At the hand of several sub-questions the performance of the preliminary gasifier design will be validated. The performance of the gasifier will first be predicted with by several models, which are then validated with an experimental study. The exact methodology of the validation will be explained in chapter 7.
6. **How to design a test setup?**
   From methodology determined in question 5 the requirements for the test setup will follow. With these requirements a test setup will be designed. After designing the setup it is constructed and commissioned. Then the experiments from question 5 can be performed.

The actions needed to answer these sub-questions that were discussed in the previous section will define the structure of the research. The order of actions and their corresponding chapters will be:

1. Review on the Waste4me WER unit (Ch. 2)
2. Literature review on the different gasification reactors and reactions (Ch. 3,4)
3. Selection and implementation of a gasifier type (Ch. 5)
4. Design of the gasifier and literature review on gasifier components (Ch. 6)
5. Defining the methodology for the modelling of the gasifier and the validation of the gasifier performance (Ch. 7)
6. Design, modelling, building and commissioning of the test setup (Ch. 8)
7. The results and discussion of the results of both the models and experiments (Ch. 9)
8. Evaluate the preliminary gasifier design leading to a final gasifier design (Ch. 10)

The structure of the research is summarized in a flowchart which is shown in figure 2.

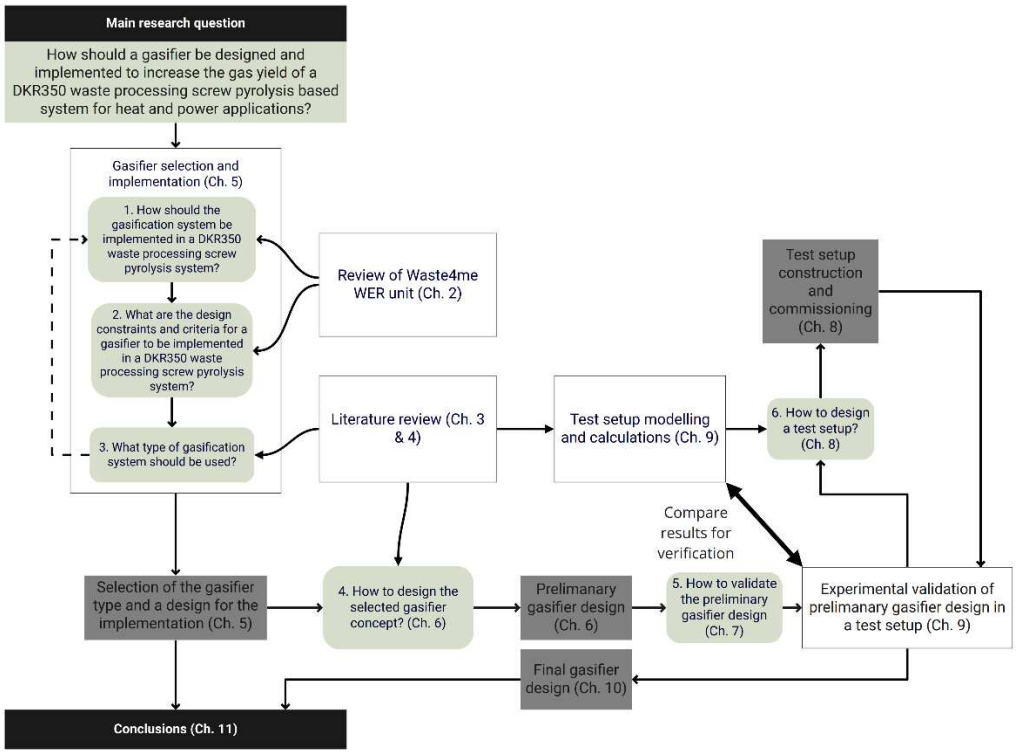

figure 2 Flowchart of the research structure including the main research question, sub-questions and in-between products and end products. Also the corresponding chapters in this report are mentioned in between brackets.

2. Waste4me WER unit

In this chapter a system description of the current screw pyrolysis system is given. This will give the context for the design and implementation of the gasification system which will be done in paragraph 5.2 & 5.3. Also the contents of the oil will be discussed which together with the context of the current system will give the motivations for the design constraints and criteria for the gasifier which will be defined in paragraph 5.1..

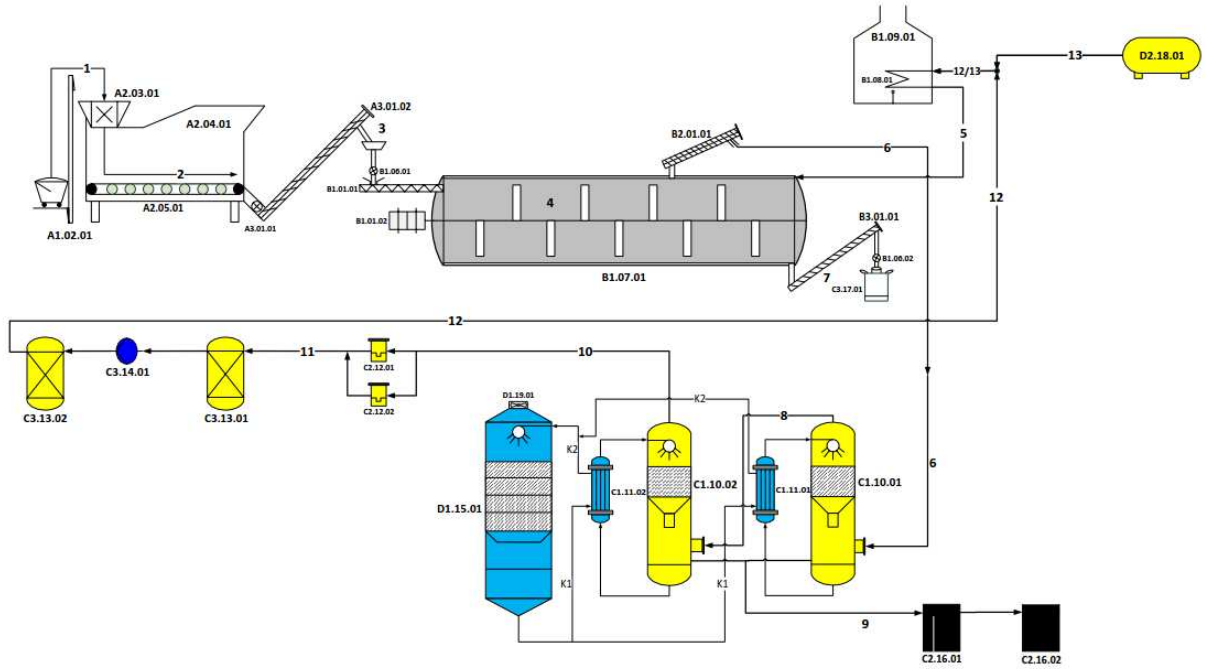

figure 3 Current Waste Energy Recycling (WER) unit at waste4me.

The current Waste Energy Recycling (WER) unit from waste4me is illustrated in figure 3. The process streams in figure 3 are numbered. The most important process steps are represented by the following points:

1. A container containing the waste is emptied into a shredder where the waste is shredded.
2. After the material goes through the shredder, it falls on a walking floor. This walking floor acts as a buffer for the system. After the walking floor the material is fed into a screw conveyor.
3. The screw conveyor raises the material and drops it into a rotary valve which feeds the material into the pyrolysis reactor at a feed rate up to 250 kg/h. The rotary valve ensures that no oxygen is fed into the reactor.
4. In the pyrolysis reactor the material is heated to 500 – 700 °C. The reactor operates slightly under atmospheric pressure. The material breaks down slowly into gasses and a solid residue. This solid residue is moved by a screw to the bottom exit of the reactor, where a screw conveyor removes the solid residue (7). The gasses exit at the top of the reactor.
5. Part of the product gas is combusted, the flue gas is used to heat the reactor externally.
6. The gasses are cooled in a screw where part of the entrained solids will settle. Then the gas is cooled in a scrubbing installation where the condensable gasses are collected.
9. The oils will float on top in the scrubbing installation, this oil layer is removed and stored in two storage vessels.

The waste stream that will be considered in this study is DKR 350. DKR 350 is a municipal waste plastic mix which typically contains packaging plastics and consists for 90 m% of PE, PP, PS and PET. Also it contains packaging parts such as caps, lids and labels which can be a source of contaminants. A specification sheet on DKR 350 waste which gives a more elaborate definition can be found in appendix F. In a previous study at Waste4me the pyrolysis of DKR 350 with the current WER unit was studied and a mass balance was

determined which is shown in figure 4. The pyrolysis oil used in this study was produced during that experiment, therefore the waste mixture used in that experiment defines the DKR 350 mixture in this study. The waste mixture was created by mixing 50 m% automotive shredder residue, 35 m% low density polyethylene and 15 m% polypropylene. The exact composition of the automotive shredder residue is unknown, however it is likely that is contains high amounts of PVC. The mixture is comparable to the DKR 350 specifications, however it contains more contaminants and the mixture does not consist of 90% of PE, PP, PS and PET. Also the feed material contains higher concentrations of PVC and lower concentrations of PET than the DKR 350 specifications require. This causes higher concentrations of chlorine in the product streams due to the PVC and a lower fraction of oxygenated hydrocarbons due to the oxygen in the PET. However, in this study the mixture is categorized as a worst case scenario DKR 350 mixture and therefore the oil produced used in this study is also labelled as DKR 350 pyrolysis oil. The mass balance resulting from the experiment can be seen in figure 4. 14 m% of the pyrolysis yield is ash, which mainly consists of carbon. The oil yield is 20 m% and the pyrolytic gas yield is 67 m%. A part of the produced gas is used to externally heat the pyrolysis reactor. In this research the main objective is to convert the 20 m% oil yield into combustible gasses. Therefore in this chapter the composition of the oil will also be discussed.

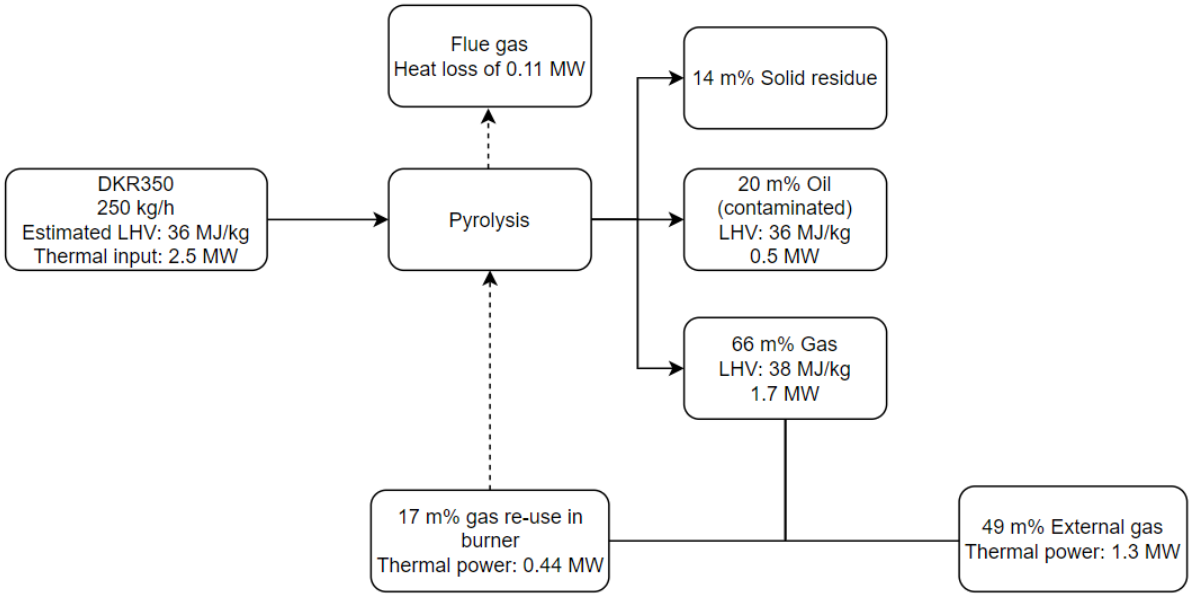

figure 4 Mass balance of the pyrolysis of a waste stream similar to DKR 350 in the Waste4me WER Unit with indications of the LHV of each stream as determined in a previous study at Waste4Me B.V. (Contin et al., 2020).

The oil contamination concentrations, molecular composition and boiling curve of DKR350 pyrolysis oil were determined by a commercial lab. The lab reports can be found in appendix A. The viscosity of the oil could not be determined due to the high fraction of solid particles in the oil. These particles are most likely char particles that were entrained in the outlet gas stream of the pyrolysis reactor. The oil however behaves comparable to water when stirred and therefore it is assumed that the viscosity of the oil is similar to the viscosity of water. The main contaminants in the oil are chlorine and iron with 0.356 m% and 0.431 m% respectively as can be found in appendix A. The main source of chlorine is the polyvinyl chloride (PVC) in the automotive shredder residue ((Perondi et al., 2019). The chloride is bound to organic molecules in the oil. The iron contamination can be caused by the corrosion of the equipment or by the iron in the feedstock. The boiling point curve from appendix A showed that 40 m% has a boiling point lower than 150 °C. 80 m% has a boiling point lower than 332 °C and the oil is fully evaporated at 566 °C.

The oil composition was determined by high temperature gas chromatography. This method cannot measure the components with a boiling point of 100 °C or lower. 53.45 m% of the oil consists of hydrocarbons, which are the molecules that contain only hydrogen and carbon atoms. The rest of the molecules were mainly organic compounds. Most of the hydrocarbons have 8 or close to 8 carbon molecules and are alkylbenzenes.

The alkylbenzenes with 8 carbon molecules are xylene and ethylbenzene, both with the formula C8H10. But the properties of these molecules are comparable and therefore the oil will be modelled as an alkylbenzene with 8 carbon molecules in the thermodynamic models in paragraph 9.1..

From the oil composition it can be concluded that the tar concentration in the oil is high. Tar is a complex mixture of mostly aromatic hydrocarbons formed during thermal decomposition of organic compounds and during secondary cracking reactions (Veksha et al., 2018). Tar is typically defined as a mixture of organic molecules with a molecular weight greater than benzene (Moersch et al., 2000). Because many of the organic molecules have a higher molecular weight than benzene this fraction of the oil could be seen as tars.

For this study also an elemental analysis was performed at a commercial lab on the DKR350 pyrolysis oil. Also the heating value of the oil and the moisture content of the oil were determined. The results of these analysis are tabulated in Table 1 and

Table 2. The lab reports on both the analysis can be found in appendix D.

Table 1 Results of the elemental analysis which was performed on the DKR350 pyrolysis oil used in this study. The lab reports can be found in Appendix D.

Element	Carbon	Oxygen	Nitrogen	Hydrogen
Mass % (as received)	82.0	6.7	0.95 (Contin et al., 2020)	8.65

Table 2 Results of the analysis on the heating value and the moisture content of the oil

Property	Value
HHV	38900 kJ/kg
LHV	36100 kJ/kg
Moisture content (by Karl Fischer titration)	10000 ppm

3. Gasification Reactions

In this chapter the different gasification reactions will be discussed. The tars and other condensable hydrocarbons can be cracked to smaller non condensable hydrocarbons. Three major reaction mechanisms are responsible for the conversion of condensable hydrocarbons into the non-condensable hydrocarbons. These are thermal cracking, dry/steam reforming and catalytic reforming. Fixed carbon and hydrocarbons can also react with oxygen, this can lead to partial or stoichiometric combustion. The thermal cracking, dry/steam reforming, catalytic reforming, char reduction and hydrocarbon combustion reactions will be shown in the paragraphs of this chapter. In the first paragraph the most important parameters for gasification and cracking will be discussed.

3.1 Gasification parameters

There are several parameters that characterize the gasification. For steam reforming the steam over carbon ratio is used (S/C) which can be defined as a molar or mass ratio. Usually the moisture content of the feedstock is also accounted for in the calculation of the S/C ratio (Leijenhorst et al., 2014). For the gasification with air or oxygen the equivalence ratio (ER) is generally used. The ER is defined as the ratio between the amount of oxidizer and the amount of oxidizer required for stochiometric combustion. The ER can be calculated with the following equation:

$$\mathrm{ER} = \frac{\phi_{\mathrm{O_2}}}{\phi_{\mathrm{StC}}} \qquad \text{(Eq. 3.1)}$$

Where $\phi_{\mathrm{O_2}}$ is the amount of oxidizer supplied and ϕ_{StC} the amount of oxidizer required for stoichiometric combustion (Leijenhorst et al, 2014). The determination of $\phi_{\mathrm{O_2}}$ and ϕ_{StC} are further explained in paragraph 7.3. To evaluate the performance of a gasifier the parameters carbon conversion efficiency and the cold gas efficiency can be used. The carbon conversion efficiency is the ratio between the amount of carbon in the product gas stream and the amount of carbon in the feed stream as described by the following equation:

$$\mathrm{CCE} = \frac{\phi_{\mathrm{c_{gas}}}}{\phi_{\mathrm{c_{feed}}}} \qquad \text{(Eq. 3.2)}$$

The cold gas efficiency presents the thermal efficiency of the gasifier. It is the ratio of the total calorific output of the product gas stream and the total calorific output of the feed oil stream. It can be calculated with the following equation:

$$\mathrm{CGE} = \frac{\dot{V}_{\mathrm{dry}}\,\mathrm{LHV}_{\mathrm{dry}}}{\dot{m}_{\mathrm{oil}}\,\mathrm{LHV}_{\mathrm{oil}}} \qquad \text{(Eq. 3.3)}$$

Where $\mathrm{LHV_{dry}}$ is the lower heating value of the dry product gas per unit volume and $\dot{V}_{\mathrm{dry}}$ is the volumetric flow of the dry product gas. $\mathrm{LHV_{oil}}$ is the lower heating value of the oil feed going into the reactor per unit mass and $\dot{m}_{\mathrm{oil}}$ is the mass flow rate of the oil feed.

3.2 Thermal cracking

Under high temperature conditions the organic compounds will break down into smaller molecules. Generally a higher temperature leads to a higher yield of non-condensable gaseous products (Scheirs & Kaminsky, 2006) For the production of condensables a lower temperature is preferred, according to Schiers & Kaminsky for the production of a diesel mixture from waste plastics the optimal temperature should be between 390 – 425 °C. However the products of thermal cracking are often low value because of their broad range which can extend from hydrogen to coke. At high temperatures the formation of coke or char is unavoidable. The coke is formed due to the carbon surplus when the organic compound is cracked into smaller molecules. The thermal cracking, and therewith also the formation of coke, can be described by the following equation (Li et al., 2020):

$$C_xH_yO_z \xrightarrow{\text{crack}} \text{Tar} + (H_2 + CO + CO_2 + CH_4 + \text{other hydrocarbon gasses}) + \text{Coke} \quad \text{(Re. 1)}$$

According to Creager (2016) the coking starts at approximately 100 °C for a biomass derived pyrolysis oil. Shin et al. (2001) found that under pyrolysis and gasification conditions higher than 700 °C the formation of thermally stable aromatics and polycyclic aromatic hydrocarbons increases significantly. Marda et al. (2009) found that the concentration of aromatics will reduce if the equivalence ratio is increased.

3.3 Dry/steam reforming

The dry and steam reforming reactions are defined as the reactions of the organic compounds with carbon dioxide and steam. The reaction that gives the equilibrium between the steam and carbon dioxide concentrations during gasification is the water-gas-shift-reaction. It is described by the following equation:

$$CO + H_2O \rightleftharpoons CO_2 + H_2 \quad \text{(Re. 2)}$$

The water-gas-shift-reaction is moderately exothermic. This causes a shift in equilibrium to the left side of the equation at high temperatures, and thus promoting the formation of carbon monoxide and steam. The organic compounds can also react with the steam and carbon dioxide. These reactions are strongly endothermic and are therefore favored at higher temperatures. The following equation describes the steam and dry reforming (Basu, 2018):

$$C_nH_x + nH_2O \rightarrow (n + x/2)H_2 + nCO \quad \text{(Re. 3)}$$

$$C_nH_x + nCO_2 \rightarrow (x/2)H_2 + 2nCO \quad \text{(Re. 4)}$$

3.4 Catalytic gasification

For the gasification of the organic compounds and the solid char catalysts can be used. Catalysts can reduce the activation energy for the reaction and it can increase the reaction rate of the reactions. This can cause a reduction in the required gasification temperature and a reduction in the required residence time. Also it can improve the quality of the product due to an improved selectivity. Besides the catalytic effects some catalysts also act as an absorber of contaminants. In literature alkali salts with lithium, sodium, potassium, calcium and metal(oxide)s alumina and nickel are often proposed as catalyst for hydrocarbon and char gasification (Furusjö et al., 2018) (Postma et al., 2016). Furusjö et al. found that also char particles can have a catalytic effect on the gasification of tars.

There are two most promising tar removal catalyst systems for commercial application: The first one is with the use of calcined dolomites or limestone at temperatures above 850 °C. The other one is hydrocracking or steam reforming with the use of nickel based catalyst (Dou et al., 2003). Some studies show that complete tar conversion can be achieved with synthetic catalyst above 900 °C. However these catalysts are relatively expensive and suffer from coke deposition on the catalyst. Dou et al. also experimentally studied the catalytic cracking of tar components in high temperature fuel gas. Dou et al. studied the tar conversion of Y – Zeolite, NiMo, Limestone, Alumina, and Silica catalysts between 250 – 650 °C. Also the durability of the catalyst was studied. From this study it was concluded that only the Y – Zeolite and NiMo catalysts showed almost 100% conversion at 550 °C and were stable in a durability test of 168 h. The process variables temperature and space velocity showed significant effects on the tar conversion.

With some catalysts it is possible to reduce the HCl emissions by physicochemical adsorption to the solid fraction and while also acting as a catalyst for the cracking reactions (Perondi et al., 2019). Perondi et al. studied the role of limestone and its influence on chlorine during the thermochemical conversion of automobile shredder residue. This shredder residue has a high chlorine concentration, mainly due to the presence of polyvinyl chloride. Perondi et al. found that the chlorine was adsorbed by the limestone where it formed $CaCl_2$. However it should be mentioned that this process could cause problems in the case of gasification, where generally temperatures above the melting point of 782 °C of $CaCl_2$ are used. Besides

catalyst deactivation due to a layer of molten salt on the surface the molten salt can also evaporate. This phenomena of evaporation of salts can occur for multiple alkali metal salts.

Catalyst deactivation can become a problem in long term operation. Therefore the catalyst has to be properly regenerated or replaced in time. Two main catalyst deactivation mechanisms are char formation on the catalyst surface and accumulation of molten ash on the catalyst surface. Both these phenomena will reduce the catalyst surface area and therefore reduce the catalyst activity.

Veksha et al. (2018) investigated the catalyst resistance to HCl poisoning of Ni/Limestone, Ni/Alumina and two commercial alumina supported catalysts at 790 °C. The Ni/Limestone catalyst showed instable behaviour in the presence of HCl, probably due to the formation of molten $CaCl_2$. The other catalysts where stable in terms of naphthalene conversion, but the water gas shift activity was reduced due to irreversible HCl poisoning. These losses were lowest for Ni/Alumina catalysts. However these test were conducted with low tar concentrations (0.14 v%) and low HCl concentrations (0.2 v%). However in a research which aimed at hydrogen production from bio-oil with high tar and chlorine concentrations it was concluded that the Ni/al catalyst almost completely loses its activity due to chlorine poisoning (Magrini-Bair et al., 2002).

Another catalyst deactivation for nickel catalysts is oxidation. The catalysts are active if the nickel is not in oxidized form. Therefore a high oxygen content will deactivate the catalyst. This can be reversed or prevented by a small amount of hydrogen in the gas stream (Magrini-Bair et al., 2002).

3.5 Gasification with oxygen

The oxidation reaction of the gaseous components with the oxygen are all highly exothermic. Therefore the oxidation reactions generally deliver the heat that is required for the endothermal gasification reactions. The main combustion reactions of the gaseous components can described by the following set of equations:

$$2\,CO + O_2 \rightarrow 2\,CO_2 \qquad \text{(Re. 5)}$$

$$2\,H_2 + O_2 \rightarrow 2\,H_2O \qquad \text{(Re. 6)}$$

$$C_nH_x + (x/2 + n)O_2 \rightarrow (x/2)H_2O + nCO_2 \qquad \text{(Re. 7)}$$

Note that during gasification often only partial combustion is reached. Then the products will also consist of carbon monoxide and hydrogen. The water-gas-shift-reaction will give the equilibrium between the hydrogen, carbon monoxide, carbon dioxide and steam.

The combustion of a carbonaceous slurry droplet is described by a book on combustion physics by Law (2010). A possible route of carbonaceous slurry droplet combustion was described where the droplet first partially evaporates due to the heat and mass transfer at the droplet surface. Then the solid particles will get concentrated at the surface until a shell is formed. Due to the heat transfer into the shell a gas bubble will form inside and eventually the shell will explode due to the pressure buildup. The leftovers of the droplet will then combust. This route of droplet combustion can be seen in figure 6.

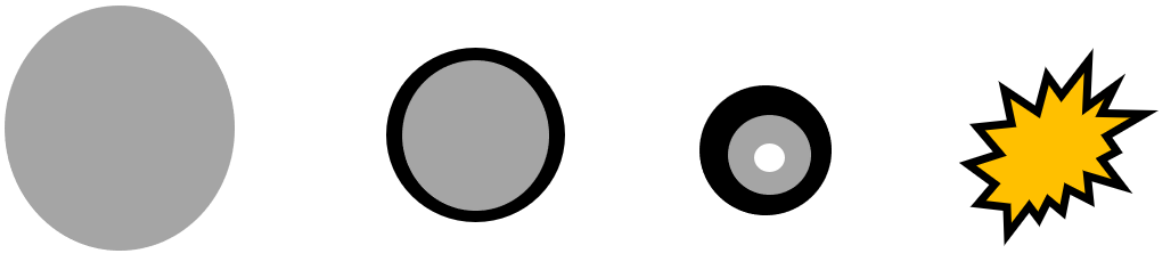

figure 5 A possible route of the combustion of a carbonaceous slurry as proposed by Law (2010) with from left to right: 1. evaporation of droplet 2. Shell formation at the surface due evaporation of the liquid fraction at the surface 3. Gas buildup inside the shell due to heat tranfer into the shell 4. Shell explodes and combusts.

3.6 Char gasification

The char particles will react in a heterogeneous reaction, in this case it is defined as a reaction of a gas with a solid. First the gas molecules are transported towards the char surface where they react whereafter the gas molecules will be transported away from the surface. The gasification reactions of char and their corresponding reaction rates at 1073 K and 0.1 atm are shown in Table 3. Reaction number 1 is often proposed as the first stage of reaction number 2, whereafter the carbon monoxide fully combusts into carbon dioxide. Note that the oxidation reactions are at least 4-5 orders of magnitudes faster than the gasification reactions with H_2, CO_2 and H_2O. However, these reaction rates are also dependent on the temperature and the reactive surface area of the char.

Table 3 Major global reactions of char combustion and gasification (Lewis, 2014)

Reaction number		$\Delta H_{reaction}$ (kJ/mol) (Higman and Burgt, 2003)	Approximate relative global rates at 1073 K and 0.1 atm and constant particle size (Walker et al., 1959)
Re. 8	$C + \frac{1}{2} O_2 \rightarrow CO$	−111	N.D.
Re. 9	$C + O_2 \rightarrow CO_2$	−394	1×10^5
Re. 10	$C + H_2O \rightarrow CO + H_2$	+131	3
Re. 11	$C + CO_2 \rightarrow 2\ CO$	+172	1
Re. 12	$C + 2\ H_2 \rightarrow CH_4$	−75	0.003

3.7 Gasification temperature and reaction rate

Gasification with an oxidizer can be seen as partial combustion. The flame temperature during combustion will be determined by the equivalence ratio. Due to the exothermal reactions during combustion the temperature will increase if the equivalence ratio increases to 1. Above the equivalence ratio of 1 there will be unreacted oxygen left in the flue gas. The oxidizer will therefore only dilute the flame while increasing its heat capacity, therefore the flame temperature will decrease. The adiabatic flame temperature for varying fuel equivalence ratio's is shown in figure 6.

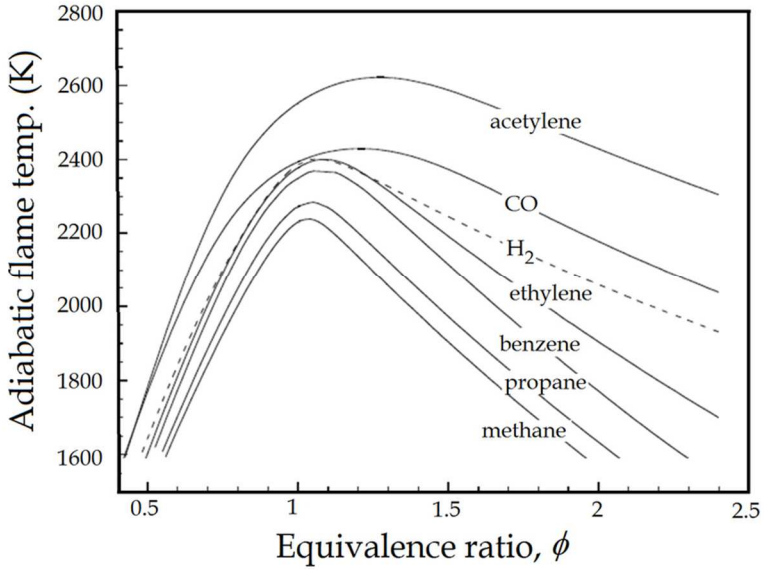

figure 6 The adiabatic flame temperature for several fuels as a function of the fuel equivalence ratio (Law, 2010, pp. 41)

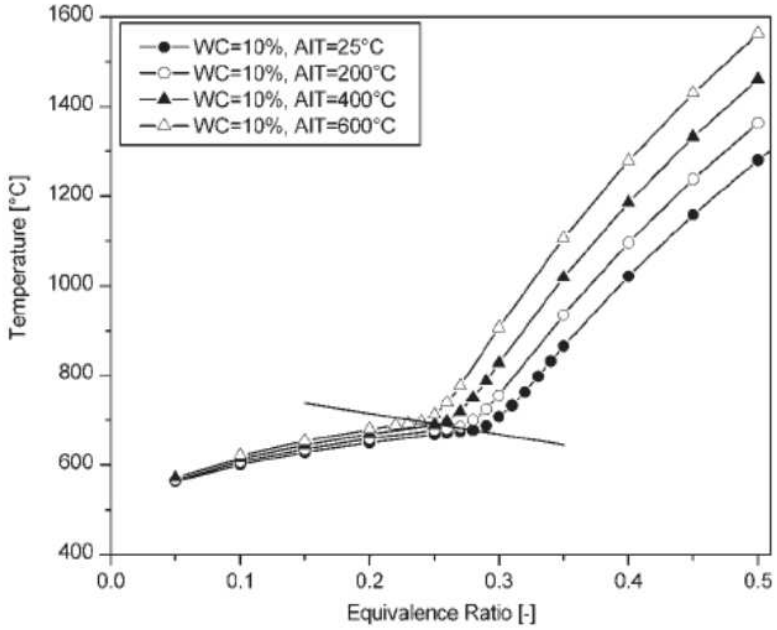

figure 7 The adiabatic flame temperature as a function of the equivalence ratio for the gasification of wood at different air inlet temperatures (AIT) and fixed water content (WC) (Mevissen et al., 2009)

During gasification however the ER is always below 1. The adiabatic temperature will reduce with the ER as shown in figure 7. Mevissen et al. (2009) found that the adiabatic flame temperature of biomass did not vary much for equivalence ratios under the solid carbon formation boundary. The found relation between the equivalence ratio and the adiabatic flame temperature can be seen in figure 7. The solid carbon formation boundary indicates the point where no fixed carbon is left in the system if the equivalence ratio is increased. Below this equivalence ratio the endothermic reactions of methanation, steam reforming and dry reforming with fixed carbon will reduce the effect of the exothermal oxygenation reactions on the adiabatic flame temperature. If hydrocarbon fuels have a relatively high carbon content in relation to the oxygen and hydrogen content, then fixed carbon will be formed if the fuel is brought into chemical equilibrium at high temperatures (Prins, 2005). To prevent the formation of fixed carbon the hydrogen and oxygen content should be increased so that the carbon will react into CH_4, CO and CO_2 molecules.

A high temperature will increase the reaction rates and will therefore increase the flame speed through the unburned gas. Therefore also an equivalence ratio close to 1 will increase the flame speed due to the higher temperatures. A high pressure will decrease the flame speed. The laminar flame speed as a function of the equivalence ratio at different pressures and temperatures for n-butane can be seen in figure 8. N-butane is not the main component of the produced gas in this study, however the effects of the ER, temperature and pressure will be comparable for the product gas in this study. The laminar flame speed is generally lower than the turbulent flame speed (Vargas et al., 2020). The laminar flame speed varies for different gas compositions as shown in a study of Magalhaes (2011) who studied the laminar flame speed of different syngas compositions.

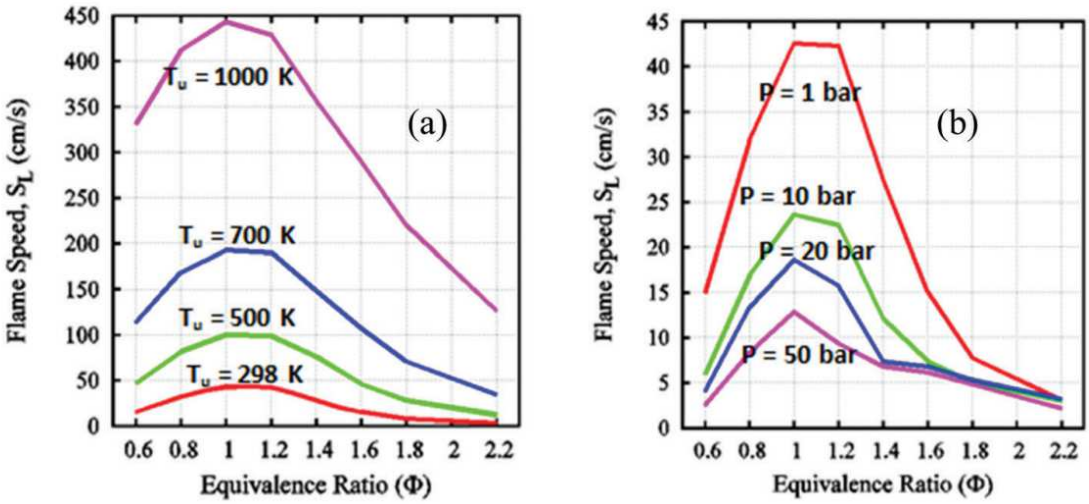

figure 8 The laminar flame speed as a function of equivalence ratio for n-butane at a) different temperatures and b) at different pressures (Ashraf et al., 2017)

Law (2010) describes the combustion of non-premixed flames in turbulent flows by the mixture fraction model. It states that when the reaction rates are rapid enough that everywhere chemical equilibrium is maintained, then the properties of the flame at a certain location can be determined by the local ER. This means that if the ER is stable in a certain area, then the temperature will be stable in that area and so a stable combustion can be ensured. A stable ER distribution can be ensured with a proper mixing system.

If the mixture reaches autoignition temperature the gas will self-ignite without the need of a propagating flame front. The autoignition temperature of different carbonaceous fuels in atmospheric conditions can vary greatly between approx. 200 °C and 750 °C (*Fuels and Chemicals Autoignition Temperatures*, 2003). Generally the autoignition temperature of a hydrocarbon will decrease if the number of carbon atoms in the hydrocarbon increases (Law, 2010). Unsaturated hydrocarbons have a higher autoignition temperature than the alkanes with the same carbon number. For the different C8H10 compounds the autoignition temperatures ranges from 432 to 528 °C at atmospheric pressure (Shen & Oehlschlaeger, 2009). Elies (2012) investigated the autoignition temperature of hydrogen. At pressures of 10 to 15 bar autoignition temperatures were found of 840-890 K. The addition of CO to the gas mixture reduced it by 8 to 23 K. At higher pressures the autoignition temperature was lower. A decrease in equivalence ratio led to an increase of the autoignition temperature.

4. Gasification Reactors

From literature four different commercially applied gasifier types can be distinguished, namely: entrained-flow, fluidized bed, fixed bed reactors and molten salt bed reactors. For large scale applications in industry the entrained flow and fluidized bed gasifiers are generally used. The four different kinds of gasifiers can be seen in figure 9. In the following chapters these different gasifiers and the relevant literature for DKR350 oil gasification will be discussed.

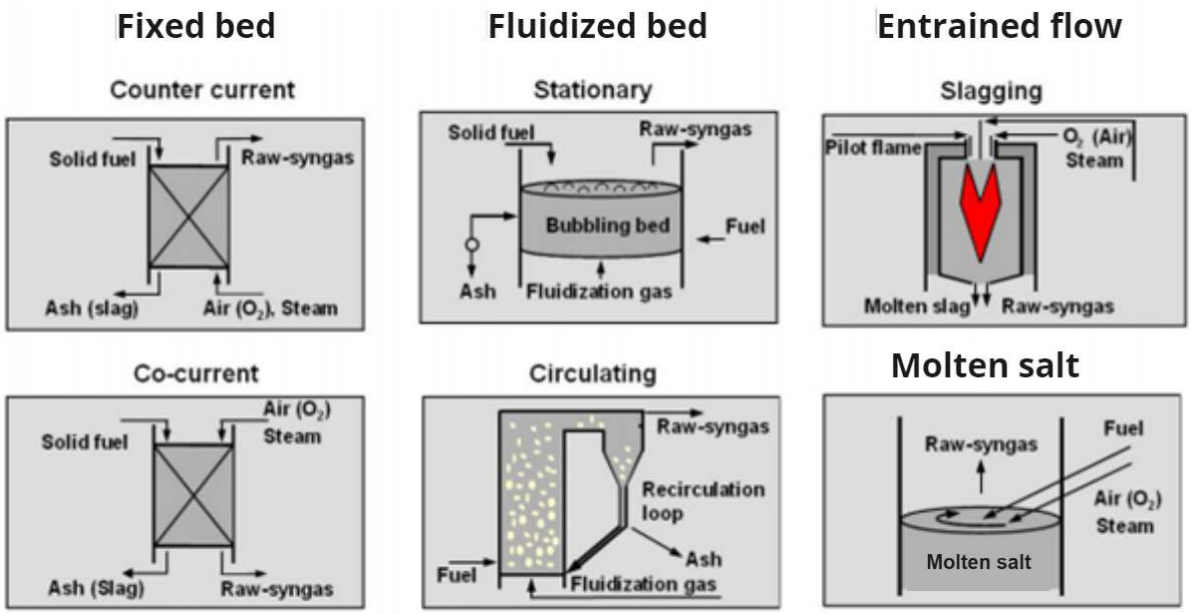

figure 9 Overview of the four different reactor concepts discussed in this thesis with different variations (Dahmen et al., 2012)

4.1 Entrained flow

Entrained flow gasifiers gasify a spray of liquid fuel, fine solid fuel particles, or fuel slurries with air or oxygen as a gasifying agent. Also steam can be added as an extra gasifying agent. The heat in the gasifier is delivered with the exothermal gasification reaction of the fuel with the oxygen. Due to the high temperatures the residence time is short, usually a few seconds. The tar conversion is high due the high temperature which causes the tars to crack to light hydrocarbons. Also the char conversion is high due to the high temperatures and due to the fast reaction kinetics of carbon with oxygen. Because the fuel mostly requires pre-treatment the application of entrained flow reactors are limited to large-scale plants (Pang, 2016). A slagging entrained flow gasifier is shown in figure 10.

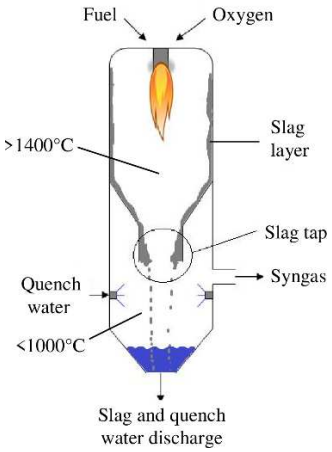

figure 10 Sketch of a slagging single stage entrained flow gasifier (Duchesne, 2012)

Different entrained flow gasifier configurations can be found in literature. A distinction can be made between slagging and non-slagging gasifiers. The main difference in operating conditions between a slagging and a non-slagging gasifier is its operating temperature. A non-slagging gasifier typically operates between 700-1000 °C, whereas a slagging gasifier operates between 1250-1500 °C (Creager et al., 2016). In table 4 the process parameters of multiple slagging and non-slagging entrained flow gasifiers found in literature are shown. The low temperature for a non-slagging gasifier will prevent the ashes from melting and therefore no slag removal system is required. Also at these low reactor temperatures the material requirements are mild, therefore the non-slagging configuration can be advantageous. The non-slagging configuration is suitable for feedstocks with a low ash content or an ash melting point higher than the operating temperature.

Another difference in reactor configurations besides the slagging or non-slagging is the number of gasification stages. In a single stage reactor there is only one location for the fuel injection, in a multiple stage reactor the fuel is injected at multiple locations. As part of the 'EAGLE project' a 2 stage gasifier was designed for the gasification of coal with oxygen (Francisco et al., 2000). The reactor is shown in figure 11. The first stage operates at high temperature which is maintained by the exothermic reactions caused by the oxygen rich conditions. The high temperature stabilizes the process and lowers the slag viscosity, which makes the slag removal possible. In the second stage the oxygen concentration is low and more of the secondary endothermic reactions with steam and carbon dioxide will dominate. Therefore the outlet gas temperature will decrease whereas the cold gas efficiency is increased.

table 4 Entrained flow reactors and their process parameters

Entrained flow gasifier project/source	Operating conditions	Gasifying agent(s)	Material infeed	Slagging or non-slagging	Heating method
Shell Gasification Process (Holthoon, 2010)	1300 – 1400 °C 30 – 60 bar	Oxygen	>550 ton/day Bottom-refinery residues (low ash content <0.4 w%)	Non-slagging	Autothermal
Karlsruhe Institute of Technology (Fleck et al., 2018)	1200 °C 1 atm	Air/oxygen	20 kg/h Glycol	Slagging	Externally heated
Technische Universität München (Tremel & Spliethoff, 2013)	1200 – 1600 °C 1 – 5 bar	Syngas, oxygen, steam	0.5 kg/h Char	Slagging	
Iowa State University (Creager et al., 2016)	1000 °C 1 – 6.9 bar	Oxygen/Air (Tests only with oxygen)	10 ml/min Pyrolysis bio-oil	Non-slagging	
CHOREN's Carbo-V beta plant (Vogels, 2010)	5 bar	Oxygen	Biomass pyrolysis gas & pyrolysis char from 65 kton/year dry wood	Slagging	
Biomass Technology Group (de Beld & Prins, 2002)	1000 – 1100 °C 1 atm	Air	Lab scale Bio-oil	Unkown	Externally heated
Colorado School of Mine (Marda et al., 2009)	625 – 850 °C 1 atm	Oxygen	10 ml/min Bio-oil mixed with methanol	Non-slagging	Externally heated
Northwest A&F University (Zheng et al., 2016)	1000 °C 1 atm	Air, Oxygen, oxygen enriched air	9 kg/h Bio-oil	Non-slagging	Heated mantel up to 1200 °C
University of canterbury (Patah, 2016)	600 – 1000 °C 1 atm	Oxygen	<67 ml/min Bio-oil	Non-slagging	Externally heated
EAGLE project pilot plant (Francisco et al., 2000)	1200 – 1700 °C 25 bar	Oxygen	150 ton/day Coal	Slagging	Autothermal

Zheng et al. (2016) tested the influence of the equivalence ratio on entrained flow gasification of bio-oil empirically. A peak in the cold gas efficiency was found at an equivalence ratio of 0.3. This optimal equivalence ratio was the same as the one that Fazly (2016) found in an empirical study into a non-slagging entrained flow bio-oil gasifier.

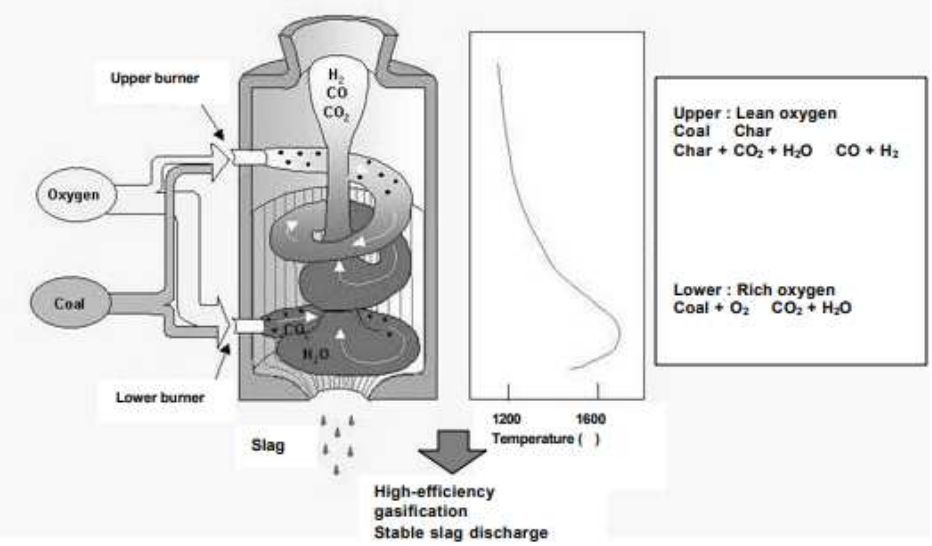

figure 11 A slagging 2-stage entrained flow gasifier designed for the EAGLE project (Francisco et al., 2000)

4.2 Fixed/packed bed

The two common configurations for a fixed bed gasifier are updraft and downdraft gasifiers. However in this research the main focus is on the gasification of the pyrolysis oils and the updraft and the downdraft configurations are both designed to gasify solid feedstocks. Therefore these fixed bed configurations will not be of any use in this study on pyrolysis oil gasification. A configuration that could work that could also be categorized as a fixed bed gasifier is the packed bed or monolith gasifier. This gasifier uses a packed bed or a monolith as the catalyst for the gasification of the pyrolysis oils. The feedstock of these gasifiers should be a gas stream. Therefore the oils should first be evaporated before they could be gasified in the catalytic gasifier. Leijenhorst et al. (2014) did an experimental study into the autothermal gasification of biomass derived pyrolysis oil on a monolith catalyst. A nearly tar and methane free product gas was produced with a space time of 1.3 s and an ER of 0.36. There was some char formation, especially when the equivalence ratio was reduced. However it was stated that the use of a monolith catalyst will reduce the risk of clogging in comparison to a packed catalyst bed.

4.3 Fluidized bed

A fluidized bed reactor has a bed of small solid particles which are fluidized by a gas. For a gasifier the solid bed material is a catalyst, non-catalytic material or a solid fuel. Besides a catalytic effect the solid material can also acts as a heat transfer medium to evenly distribute the heat to the gas. The feed-in material for the gasifier can be fed directly into the bed or it can be fed into the bed by entraining it into the fluidization gas. The feed material can be a gas, liquid or solid material. The fluidization gas for gasifiers mostly consists of steam, air or oxygen. However if the oxidizer is used as the fluidization gas it can cause problems with the temperature control of the reactor as the oxidizer also regulates the bed temperature. The typical operating temperatures for a fluidized bed vary between 800-1200 ^{o}C (Patah, 2016).

Sometimes a circulating fluidized bed configuration is used where the bed material is entrained and later separated from the product stream by a cyclone. The bed material is then reinjected into the fluidized bed. This is useful if high gas velocities are preferred or if the bed material is to be heated or regenerated in a separate reactor. Char buildup on the bed material surface can occur in fluidized bed reactors which can deactivate the catalytic effect of the bed material. The char layer can be removed by a regeneration system which combusts the char. Due to the high temperatures in a fluidized bed gasifier ash can melt or become sticky which will cause bed agglomeration.

Attrition is a destructive mechanism for catalysts in fluidized beds. Sakaguchi et al. (2010) mentions an attrition rate of 3% h^{-1} for nickel based catalysts, and 1% h^{-1} for sand. Since the catalyst usage influences the running costs, this attrition loss should be minimized.

4.4 Molten salt

Molten salts can be used in a gasifier for multiple purposes. Firstly it will stabilize the temperature in the reactor due to the significantly higher volumetric heat capacity of molten salts than the gasses in the gasification process. Secondly some salts catalyze the gasification reactions (Girods et al., 2009). Thirdly the salts can be used to purify the gas from several contaminations by chemical absorption. Contaminants that react with sodium carbonate are HCl, HBr, HF, H_2S and HCN (Kawase & Otaka, 2013).

In a molten salt gasifier (MSG) a salt melt is used to dissolve the feed stream. The feed stream of an MSG can be a coal-water slurry or other carbon containing fuels. In the salt bath the feed will react with an oxygen containing stream which is injected into the salt bath. Here the feed will be converted into a combustible gas, which contains H_2O, CO, H_2, CO_2 and CH_4. The ash is retained in the salt melt. A conceptual drawing of a test setup molten salt gasifier can be seen in figure 12. This test setup gasified a coal-water slurry with a Na_2CO_3-based salt melt and an air feed stream (Yosim, 1981). The operating pressures varied between 1-10.5 atm at a temperature of 1000 °C. The ratio between the mass flow of the coal slurry feed stream and the weight of the salt melt varied between 0.06 and 0.23 h^{-1}. The gasifier was designed to handle a ratio of 0.33 h^{-1}. The limiting factor in feed flow for this design was the entrainment of salt melt in the product gas steam. To prevent salt entrainment in the flow the gas velocity was limited to 0.6 m/s for the gas that came out of the salt melt. To maximize the feed flow at this velocity limitation a high operating pressure was preferred.

Molten salt supported on a ceramic foam can also be utilized for the reduction of soot in exhaust gasses (van Setten et al., 1999). Such a system could also be adequate to absorb the HCl and H_2S from flue gas (Lyke et al., 1983). However this configuration is for very low soot concentrations and this process uses combustion for the soot reduction. Because in this research it is the aim to gasify a high concentration carbonaceous feed stream the previously described configuration would not be suitable.

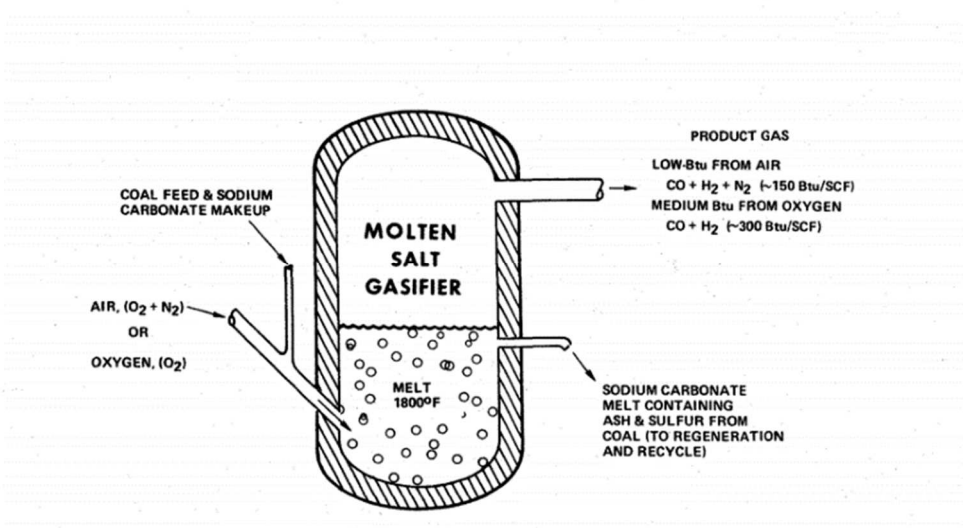

figure 12 Conceptual drawing of a molten salt gasifier (Yosim, 1981)

In literature much is known about MSG's with mainly solids in the feed stream (Barclay et al., 1977; Datta & Dittami, 2016; Li et al., 2020; Sugiura et al., 2007; Xu et al., 2018). However due to the solid phase present there will be different mass transfer phenomena and therefore the results from these reports are not representative for a reactor with mainly liquids in the feed stream. A study from (Cover & Schreiner, 1974) focused on the gasification of heavy hydrocarbons in an alkali metal carbonate molten salt. Here the MSG

setup described in patent 3,252,774 was used in the experiments (Mcmahon & Ernest, 1962). Air and steam were used to gasify a heavy oil fraction. The temperature of the melt determined the outputs of the reactor, whereas the temperature was controlled with the air flow. At a melt temperature of 926 °C no liquids were left in the product gas stream after condensation. In the related patent of Mcmahon & Ernest it was advised to inject the feed stream with a jet-like/spraying stream to ensure good mixing of the liquid into the salt bath. In patent 4,682,985 another system is described where black liquor is gasified (Arthur L Kohl & Hills, 1985). Black liquor is a byproduct of the paper industry and contains lignin, hemicelluloses and inorganic components which are used in the paper production process. The black liquor MSG from patent 4,682,985 can be seen in figure 13. In this MSG part of the liquid was gasified above the salt melt to reduce the gas velocity leaving the salt melt and therewith reduce the salt entrainment. This was done by spraying the black liquor above the salt melt, so that it partly evaporates and gasifies, whereas the heavier components fall into the salt melt where the remainder gasifies. By evaporating the spray with the heat of the product gas the gas is simultaneously cooled. This reactor configuration is also used in another patent which aims to gasify a slurry with a carbonaceous liquid and petroleum coke particles (Arthur Lionel Kohl, 2008).

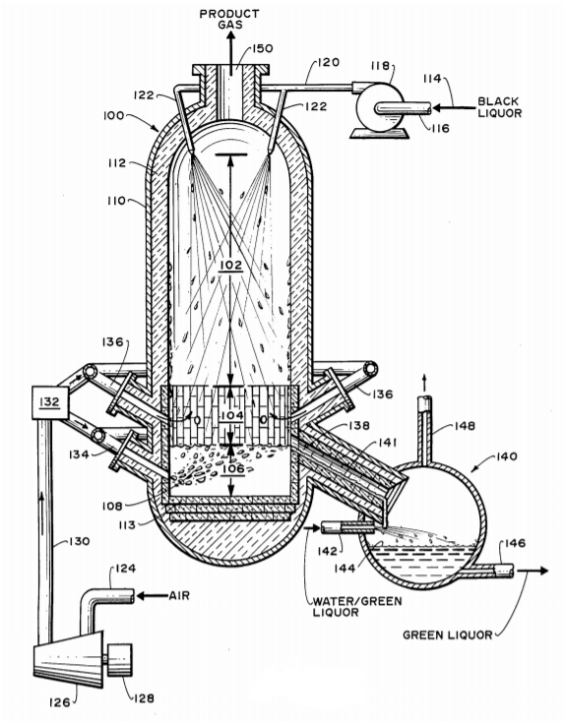

figure 13 Black liquor gasifier (Arthur L Kohl & Hills, 1985)

To minimize the heat required to melt the bath a salt with a low melting point should be chosen. However salts with a melting point that is much lower that the operating temperature mostly become unstable at high temperatures (Maund & Earp, 1988),or get close to their boiling point so that the vapor pressure of the salt will increase (Ewing & Stern, 1974). Both these effects will result in a high salt loss rate. An alternative solution to get a salt melt with a low melting point is to use an eutectic salt mixture of salts that have a high melting point. For eutectic mixtures the melting point of the mixture is lower than the melting points of the single components. An example of an eutectic mixture of two cheap salts that could be used in a molten salt gasifier is a mixture of NaCl-$CaCl_2$. These salts have a melting point of 1074 K and 1045 K respectively, however the eutectic mixture has a melting point of 779 K (Tian et al., 2016).

Ville Nikkanen (2014) mentioned several selection criteria for the salt mixture. For the selection of a suitable salt mixture one should minimize the viscosity, this will enlarge the contact area between the gas and the liquid and this would minimize the pressure drop over the reactor. Also one should minimize the surface tension of the molten salt, this will also enlarge the surface area between gas and liquid. A high solubility of the gasses into the salts is also preferred, however most suitable salts for gasification do not have this

property. Lastly it would be preferred to choose a cheap salt, so that the salt can be disposed instead of recovered which would require additional equipment.

Because of the high temperatures used in the process and the corrosivity of the salt, the material choice is important in the design of a MSG. A corrosion resistant material that can be used is Monofrax A, which is high purity, fused, cast alumina. If this is cooled at the outer side the diffused salts will freeze in the material. This material design concept was proven to be effective as a protection against molten salts (Cover & Schreiner, 1974).

5. System Design

In this chapter sub-questions 1, 2 and 3 will be answered with the knowledge that was acquired in the literature study of chapters 2, 3 and 4.

1. **How should the gasifier be implemented in a DKR350 waste processing screw pyrolysis based system?**
2. **What are the design constraints and criteria for a gasifier to be implemented in a DKR350 waste processing screw pyrolysis based system?**
3. **What type of gasification system should be used?**

5.1 Design constraints and criteria

In this paragraph the constraints and criteria are given for the gasifier to be implemented in a DKR350 waste processing screw pyrolysis based system. First al the constraints and criteria are discussed elaborately, then they are summarized in a list at the end of this paragraph.

The gasifier should eventually be implemented into the WER unit at Waste4me B.V.. As the company tries to develop a small scale stand alone waste processing unit it is important that the capital investments costs and operational costs are kept low. An easy way to reach this is by designing a gasifier with a low complexity which generally means low investment and operational costs. As explained in the introduction the WER unit could be used for waste to energy purposes or for chemical recycling purposes. However, the chemical recycling will be the next step after waste to energy as the products have much higher purity requirements. Therefore, this design will focus on designing a gasifier for waste to energy recycling purposes and therefore a high purity of the final product is not a high priority. For the implementation of the gasifier with the WER unit it is important that the energetic output of the gasifier is also controllable. This would increase the value of the whole WER unit as an energy source because it would become possible to match the local demand for power with the power of the WER unit. Because the local demand of power can have high fluctuations, it should also be important that the gasifier has a short start up time to again ensure a good match between demand and supply of power. To ensure a good security of supply it is also important that the gasifier is robust. The robustness of the gasifier holds the following aspects: Firstly it should operate stable to decrease fluctuations in the output of the gasifier. Secondly the gasifier should be as robust as possible in regard to the input of the gasifier. This means that if the oil entering the gasifier contains particles or varies in viscosity, boiling point, moisture content or heating value it should still be operational. Furthermore, a reasonable thermal efficiency and conversion should be pursued in the design. However, efficiency is more important than conversion as the non-converted hydrocarbons will recirculate trough the gas treatment system back into the gasifier. The main constraints of the design are derived from the implementation with the current WER unit. To prevent damage to the gas treatment system the product gas should approximately be at the pyrolysis gas temperature which is <600 ^{o}C. A gasifier generally uses air or oxygen for the gasification and is therefore designed for the explosion risks, however the pyrolysis reactor from the WER unit is not designed for these risks. Therefore, it should under all circumstances be prevented that the gasifier gas enters the pyrolysis unit as it could contain oxygen. From this section the design constraints and criteria are formulated. The criteria will be listed in order of priority of the criteria. The formulated constrains and criteria are listed as following:

Constraints

1. The temperature of the gasifier product gas should not exceed the maximum temperature of the gas treatment system at the point where the gas is reinjected. This means that the product gas at reinjection should not exceed 600 ^{o}C
2. The gasifier product gas may not be reinjected into the pyrolysis reactor if the gasifier product gas can contain oxygen.

Criteria

1. The gasifier should be controllable

2. The gasifier should be robust as defined in previous section
3. The gasifier should have a low complexity to ensure a low CAPEX and OPEX
4. The gasifier should have a short start up time
5. The gasifier should have a reasonable cold gas efficiency and carbon conversion
6. The product gas should at least be usable for energy purposes, higher purities would be preferable for chemical recycling

5.2 Gasifier type selection

To select the best suitable reactor type the advantages and disadvantages of each gasifier type discussed in the literature study were formulated and are shown in Table 5. Both the molten salt reactor and the fluidized bed reactor have a high complexity of gasifier design which will increase the CAPEX and OPEX costs. Also due to the weight of the beds the reactors require a significant amount of time for start up. Besides both reactors need a treatment system for the bed material which also increases the operational costs. Due to these reasons these gasifier designs will not be selected.

The choice should then be made between the entrained flow and the packed bed reactor. The packed bed reactor is comparable to the entrained flow reactor, as the oil should first be atomized and gasified as in an entrained flow gasifier whereafter it enters the catalyst bed. The catalyst bed is meant to enhance the conversion of the feed material or decrease the production of unwanted by products. In this study the entrained flow reactor will be chosen over the packed bed because the entrained flow reactor is the system with the simplest setup. This will reduce the CAPEX and OPEX. If the experimental study into the conversion, cold gas efficiency or product gas purity of the produced gas shows a poor performance of the entrained flow gasifier, a catalyst bed could still be added to upgrade the system to a packed bed reactor.

To match the constraints and criteria for the gasifier with the design of the selected entrained flow gasifier, the design of the gasifier will be futher specified. The entrained flow gasifier will be a ‘non-slagging autothermal entrained flow low temperature gasifier’. That is because it offers the following advantages:

- Lower heat losses due to lower system temperature
- Low material requirements for the gasifier at low temperature reducing CAPEX
- No slag production so no slag removal system required which reduces CAPEX
- Less quenching required or heat exchanging required to bring the gas back to 600 ^{o}C as described by one of the design constraints
- Less dilution of the product gas by nitrogen due to the low ER, which increases gas purity
- Low startup time as the operational temperature is low

In Ch. 6.1 the non-slagging entrained flow gasifier design will be further specified into a conceptual preliminary gasifier design.

Table 5 The advantages and disadvantages of the different gasifiers for the gasification of DKR350 pyrolysis oil

	Entrained Flow	Molten Salt	Packed/Fixed bed	Fluidized bed
Advantages	• High char and tar conversion • Possible Cl capture by lime addition to slurry • Low complexity • Low startup time	• High char and tar conversion • Possible Cl capture by lime addition to salt bath • High stability • High controllability	• Low complexity • Low temperature (>1000 °C)	• Low temperature (>1000 °C)
Disadvantages /Challenges	• High operating temperature (1000-1500 °C) • High operating pressure (5-50 bar) • Slag removal system required • Low stability at low gasification temperature	• High temperature (1000 °C) • High operating pressure (1-30 bar) • Complicated startup • Entrained and evaporated salt in product gas • Complicated setup • Salts are highly corrosive	• Low char and tar conversion • Char buildup on catalyst surface • Molten ash buildup on catalyst surface • Cl poisoning of catalyst	• Low char and tar conversion • Char buildup on catalyst surface • Molten ash buildup on catalyst surface • Cl poisoning of catalyst • Attrition of catalyst bed • Complexity due to need of fluidized bed

5.3 Implementation of the gasifier

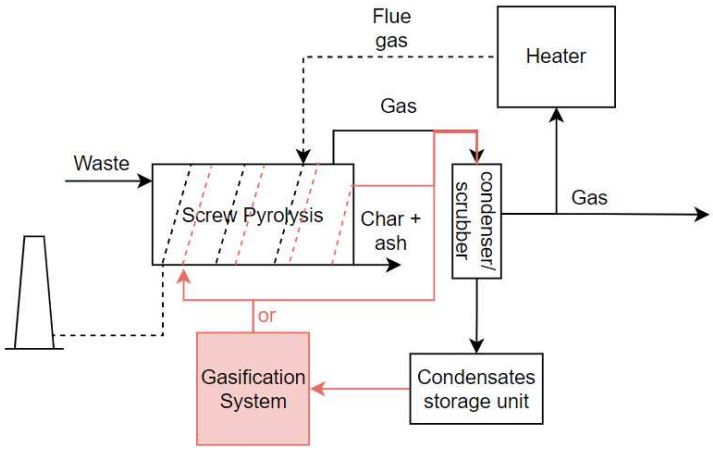

figure 14 Implementation of the gasification system with both the options of: 1. Cooling of the product gas and simultaneous heating of the pyrolysis reactor and 2. The direct mixing of the product gas with the pyrolysis gas.

The gasifier will be implemented after the condensate storage unit. The location of the reinjection of the product gas depends on the quality of the product gas of the gasifier. For this implementation plan it is assumed that the product gas still contains a significant amount of tars, char particles and other contaminations and should therefore be condensed and cleaned. The product gas will be circulated around the pyrolysis reactor to heat the reactor externally and simultaneously cool the product gas whereafter it will be injected into the pyrolysis reactor outlet stream. If the product stream is already at the same temperature as the pyrolysis gas it will directly be reinjected into the pyrolysis outlet gas stream. In both cases the same gas

treatment system can be used as for the pyrolysis gas. In this manner only one gas treatment system is required which will be dimensioned for the desired maximum volumetric product gas flowrate. If two separate gas treatment systems would be used then both gas treatment systems should be dimensioned for the desired maximum volumetric product gas flowrate which increases the CAPEX. It should however be noted that the actual composition and volumetric flowrate of gasifier product gas will determine if the same gas treatment system can be used as for the pyrolysis gas.

6. Preliminary design of the gasifier and its components

In this chapter research question 4 will be discussed, namely: How to design the selected gasifier concept? The gasifier that was selected in chapter 5 was a non-slagging low temperature entrained flow gasifier. In this chapter a preliminary conceptual design of the gasifier will be made in paragraph 1. Also the theoretical knowledge required to design, select, or dimension the different gasifier components will be discussed in paragraph 2 to 4. In paragraph 5 the relevant knowledge found in literature about gasifier modelling which could be used for designing and dimensioning the gasifier will be discussed.

6.1 Gasifier design

The preliminary gasifier design is shown in figure 15. At the top the slurry or oil enters where it is atomized by a small amount of atomizing fluid, which could be steam or air. This high velocity atomizer stream will act as an ejector. It will draw in some of the high temperature product gas into the evaporation section where it will be used to evaporate the oil droplets. At the bottom of the reactor where the oil is fully evaporated air is added as the gasifying agent. At the bottom of the reactor the gasifying agents, being air and optionally steam, are blown into the system. This will cause the gasification reactions to start. After gasification part of the flow is recirculated and part of the flow will leave the system as product gas.

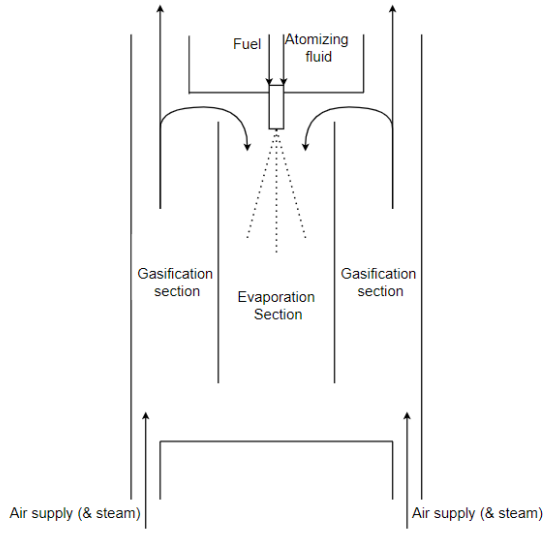

figure 15 Conceptual drawing of the preliminary gasifier design

Table 6 The design constraints as formulated in chapter 5.1 with the solutions to realize these constraints that were employed in the preliminary gasifier design

Design specification	Description	Solutions
High stability/robustness	The process should be stable for variations in the reactor inflow as viscosity, moisture content, boiling curve and varying LHV	• The evaporation and the gasification will occur in separate stages, this will prevent the dependency of combustion stability on the spray quality and rate of evaporation • There will be a high recirculation of hot gas in the reactor to ensure a good temperature distribution and therewith a stable gasification also at lower temperatures
High controllability	The process conditions and outputs should be controllable so that the process can be adjusted for different inflows and so that the product output can be controlled	• Air, steam and oil flow are controlled to control the ER and S/F of the reactor. This will give control to the reactor temperature and heating value of the output.
High carbon conversion	The oil containing aromatics, tars and chars should be converted in gas	• By the addition of air in a later stage the aromatics, tars and chars will be gasified with the reactive oxygen • The use of an atomizer will lead to high heating rates and therefore lower carbon formation • Steam can be added as the atomizing fluid control the S/F ratio which could lead to a reduction in char formation
High cold gas efficiency	The cold gas efficiency of the gasifier should be reasonably high to	• Operation at low ER together with a high carbon conversion will lead to a high caloric output
Low Capex/Opex	Low investment and running costs	• Low compression costs due to minimal usage op pressurized gasses • Low operation temperature leading to low material requirements and a non-slagging system which both reduces the Capex.

In Table 6 the design constrains from chapter 5.1 are shown that were not fulfilled with the gasifier selection and implementation. The solutions to meet the design constraints in this preliminary design are also summarized in the table.

A thorough search of the relevant literature and patents delivered no comparable designs to recirculation design as the one described above and as shown in figure 15, therefore it is assumed that this is a unique design. Research has already been done into non-slagging entrained flow gasification of pyrolysis oils by Patah (2016) and Creager et al. (2016). However the gasifiers in these studies do not operate autothermal. Also Creager encountered problems with the atomization of the oil. Therefore in this design it is aimed to create an autothermal gasifier which can operate stable at low temperature regardless of the atomization quality.

The design of the gasifier will include the design of the ejector, the selection of a suitable atomizer, the modelling of the droplet evaporation, thermodynamic modelling of the gasifier and the dimensioning of the reactor main components of the gasifier. The theoretical basis for the design of the circulating non-slagging entrained flow gasifier is partially based on the knowledge that was obtained in chapter 2 to 4, and the theoretical knowledge for the design of the ejector, selection of an atomizer and the thermodynamic modeling can be found on the following paragraphs 2, 3, 4 and 5 in this chapter.

6.2 Ejectors

An ejector utilizes the kinetic energy of the primary fluid to entrain a low pressure secondary fluid. After this entrainment the mixed stream will divert in a diffuser to raise its static pressure. A schematic representation of an ejector is shown in figure 16. The performance of an ejector system can be quantified by the entrainment ratio and the pressure ratio. The entrainment ratio is the volumetric or mass ratio between the primary fluid and the secondary fluid, the pressure ratio is the ratio between the pressure of the outgoing mixed flow and the pressure of the ingoing secondary fluid (Singh et al., 2003). The pressure difference of the outgoing mixed flow and the ingoing secondary flow is also called the back pressure.

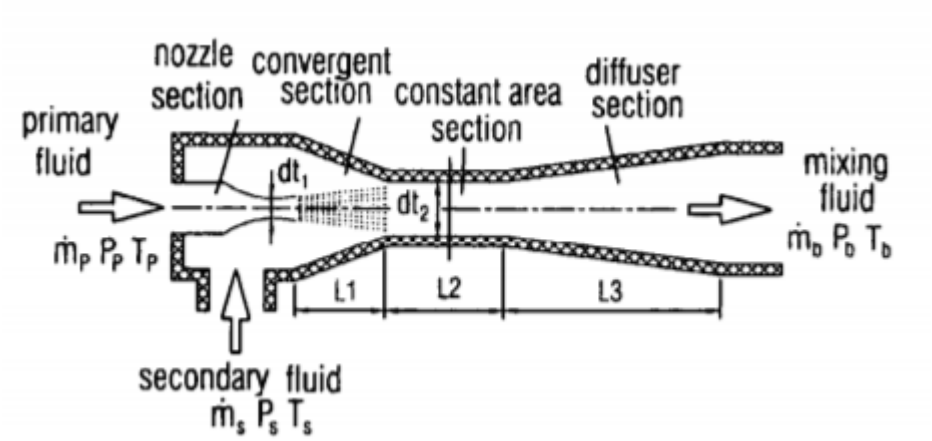

figure 16 Schematic representation of an ejector (Chang, 2000)

A liquid-gas ejector uses liquid as the primary fluid and a gas as the secondary fluid. The advantage of using a liquid is that the kinetic energy of the primary liquid can be generated with a pump which is more efficient than a compressor which would be required for a gas. However, the main disadvantage for liquid-gas ejectors is that the entrainment ratio is low. That is because the gas with a low density is mixed with a liquid with a much higher density, although the volumetric entrainment ratio can be high, the mass entrainment ratio will be low. In a recent study on the influence of nozzle design for ejectors in jet loop reactors a maximum entrainment of 0.45% was measured in an experimental setup (Deepanker, 2017). In another experimental research from Ben Brahim (1983) a maximum entrainment of 0.15% was measured.

A gas-gas ejector uses a gas as the primary and secondary fluid. The mass flow rate of the primary flow at chocked conditions for an isentropic flow can be calculated with the following equation (Huang, 1998):

$$\dot{m} = \frac{PA_t}{\sqrt{T}} \times \sqrt{\frac{\gamma}{R}\left(\frac{2}{\gamma+1}\right)^{(\gamma+1)/(\gamma-1)}} \qquad \text{(Eq. 6.1)}$$

Where $\dot{m}$ is the mass flow rate at chocked flow condition. T is the stagnation temperature, P the stagnation pressure, A_t the nozzle throat area, y the heat capacity ratio and R the specific gas constant.

Ejectors are generally used for high back pressure applications. Therefore they are not designed for high entrainment ratios. However for the design of burners high entrainment ratios are required. Pritchard (1977)

derived an equation for the entrainment of gasses in confined jets based on the conservation of momentum. The equation for the volumetric entrainment ratio R derived by Pritchard is given by:

$$R = \frac{-(1+\sigma)}{2} + \sqrt{\frac{\sigma A_T}{A_0(1+C_L)}} \qquad \text{(Eq. 6.2)}$$

The equation for the mass entrainment ratio R_m in a confined jet is then given by:

$$R_m = \frac{\rho_\infty Q_\infty}{\rho_0 Q_0} = \frac{-(1+\sigma)}{2\sigma} + \sqrt{\frac{A_T}{A_0(1+C_L)\sigma}} \qquad \text{(Eq. 6.3)}$$

Where ρ is the density, Q is the volumetric flowrate, A is the area, $\sigma(=\rho_0/\rho_\infty)$ is the density ratio and C_L is the friction loss factor. The ∞ and 0 annotations denote the location in the system, where ∞ corresponds to the entrained flow, and 0 corresponds to the jet. The configuration with the variables used in this equation can be seen in figure 17.

Singh (1999) compared and confirmed the equation derived by Pritchard with a numerical study. His results were later confirmed empirically by the results of Namkhat & Jugjai (2010) who studied the entrainment of air in an ejector of a self-aspirating burner. The results of this study and a comparison with the study of Singh (1999) can be seen in figure 18.

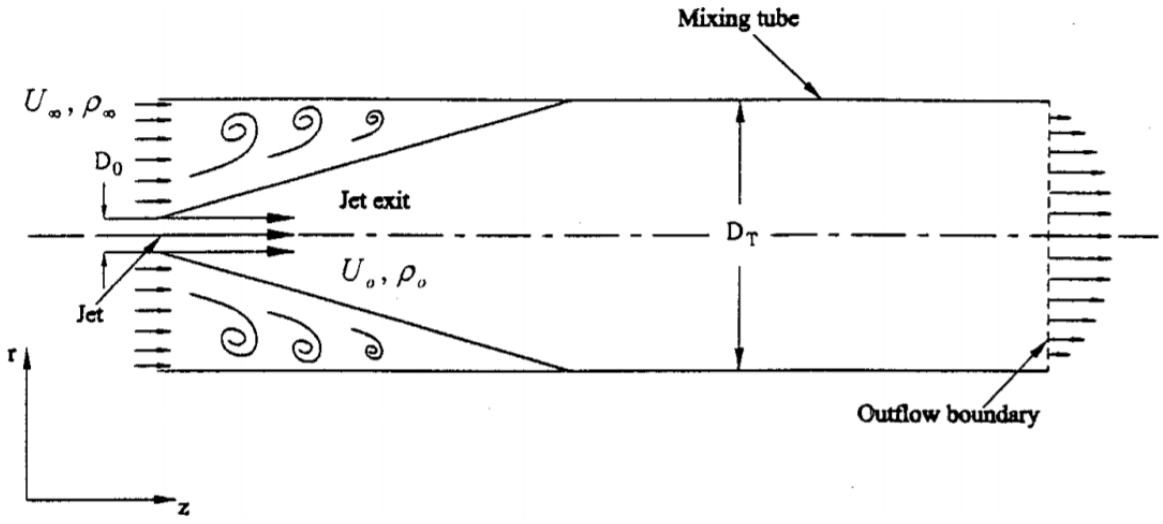

figure 17 The configuration of the jet entrainment that was studied in the study of Singh (2010)

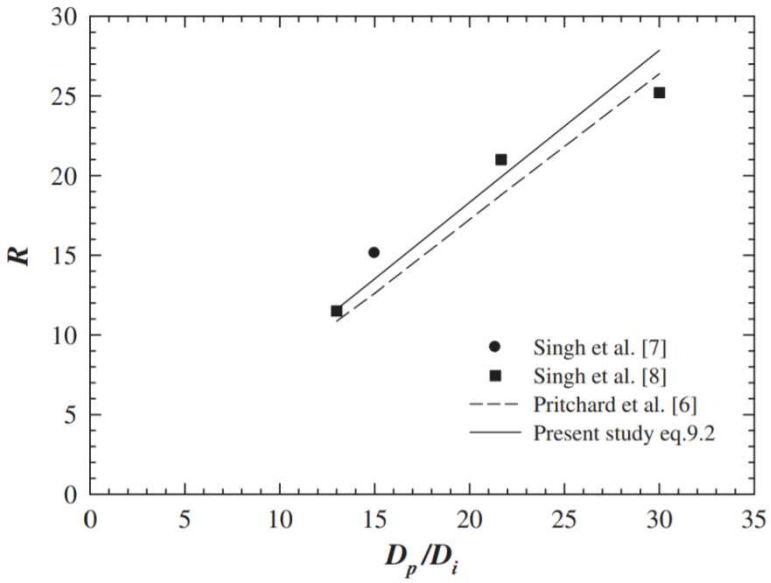

figure 18 Volumetric entrainment ratio for a self-aspirating burner as a function of the ratio of the ejector outlet diameter over the jet diameter. Equation 6.2 is indicated by the curve labelled as Pritchard et al. (Namkhat and Jugjai, 2010)

Sovani et al. (2001) investigated the entrainment of air in confined liquid sprays created by a fluid atomizer. Entrainment ratios up to 29 were found. However this entrainment ratio is dependent on the spray charactiristics, which vary for different operating conditions.

6.3 Atomizers

For the atomization of a slurry different atomizing systems are available. The different techniques will result in different spray characteristics as: spray pattern, spray dimensions, droplet size, jet breakup distance, and droplet velocities (Patah, 2016). The different atomizer nozzles are:

1. Single fluid
   In a single fluid atomizer the fluid atomizes when its is forced through a orifice at a high pressure difference. In the high velocity jet instabilities will occur which causes the jet breakup into smaller droplets. The spray characteristics are mainly dictated by the liquid flow rate and the discharge orifice (Williams, 1990).
2. Twin fluid
   In a twin fluid atomizer a gas stream and a liquid stream are involved. The spray characteristics are strongly determined by the velocities of both streams. The twin fluid atomizer produces fine droplets which will give a large contact area between the gas and the liquid. There are two different configurations: Internal mixing and external mixing. In internal mixing the fluids are already mixed before exiting the nozzle, for external mixing the fluids come in contact at the exit of the nozzle.
3. Ultrasonic
   In an ultrasonic atomizer the atomization is caused by high frequency vibrations in the liquid. Which will cause small droplet formation at the gas-liquid interface. The main advantage is that the atomization performance is not dependent on the liquid flow rate.

For a gasifier the contact area between the gas phase and the liquid is an important parameter because it characterizes the liquid evaporation and the reactions of the gas phase with the liquid phase. The Sauter Mean Diameter (SMD) characterizes the contact area of a spray and is defined as the diameter of a sphere with the same volume-to-surface area ratio as the spray of interest (Wang, 2013). A high viscosity of the liquid will increase the SMD of the spray because it stabilizes the liquid, whereas a higher surface tension reduces the SMD (Sovani et al., 2001). A higher injection pressure will generally decrease the SMD. An increasing mass gas-to-liquid ratio (GLR) will generally decrease the SMD.

6.5 Thermodynamic Modeling

In this chapter the modelling of gasification found in literature will be discussed. This will give a theoretical basis for the modelling of the gasification reactor that will be used as a comparison for the empirical results from the test setup.

Eikeland et al. (2015) modelled a steam gasification system of biomass with Aspen Plus with a CSTR and a RGIBBS reactor as the reactor models. The results were compared with experimental data from biomass gasification plant in Güssing (Güssing Renewable Energy). This comparison can be seen in table 7. The difference between the results from the RGIBBS reactor and the experimental data was large. That is because this equilibrium would be reached only in infinite time, and in a real reactor there is only finite time. Especially a large difference in methane concentration between the RGIBBS reactor and the experimental data can be noted. The CSTR reactor gave a more realistic description of the process. The volume fraction of the main gas components as a function of the CSTR temperature at a residence time of 1.7 s can be seen in figure 19. The inflection point of all reaction sets in gasification are typically around 800 °C. This causes the steep increase/decrease in concentrations in figure 19.

table 7 Comparison of the main components after steam gasification of wood chips at a steam to fuel mass ratio of 1 and at atmospheric pressure of a CSTR and Gibbs equilibrium reactor model and experimental data (Eikeland et al., 2015).

	CSTR	*Gibb*	*Experimental data (Güssing Renewable Energy)*
Residence time [s]	1.7		
CH_4 *(vol % dry basis)*	16.4	0.012	~10
CO *(vol % dry basis)*	44.1	25.8	~24
CO_2 *(vol % dry basis)*	15.6	16.8	~23
H_2 *(vol % dry basis)*	24.0	57.5	~44
LHV [MJ/m^3]	14.0	9.5	~13-15
Volume reactor[m^3]	0.48		
Gasification temperature [°C]	850	850	850

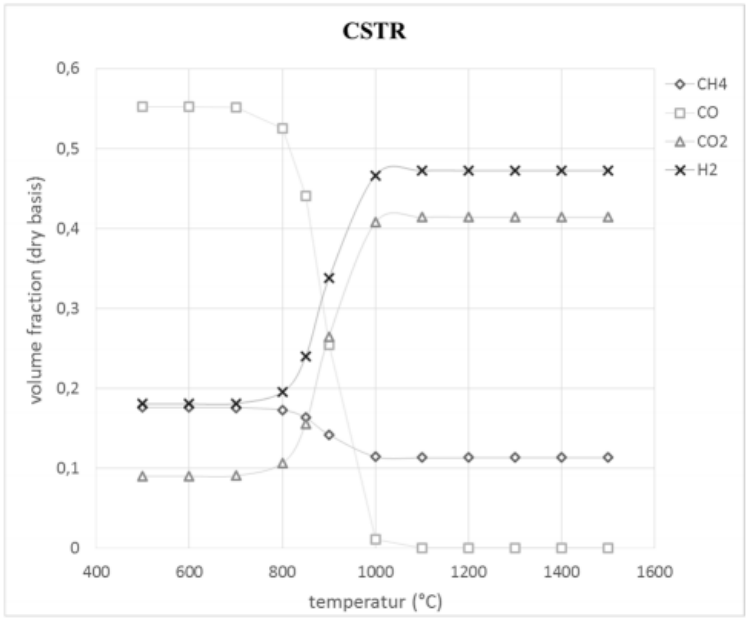

figure 19 The results of a CSTR at atmospheric pressure and 1.7 s residence time computated with available reaction kinetics (Eikeland et al., 2015)

Eikeland et al. used the RKS-BM cubic equation of state. The RKS-BM property method is used for nonpolar or mildly polar mixtures. Examples are hydrocarbons and light gases, such as carbon dioxide, hydrogen sulphide, and hydrogen. The RKS-BM property method is consistent in the critical region. The results have the lowest accuracy in the region near the critical point. Saleh et al. (2020) modelled the gasification of biomass and used the Peng Robinson cubic equation of state. This model can be used for the same mixtures as for the RKS-BM model.

7. Methodology

In this chapter the methodology behind the modelling and the experimental validation of the gasifier will be discussed. In the first paragraph the methodology of the experimental validation of the gasifier will be discussed. The next paragraph shows the methodology of the fluid dynamics modelling needed to design the recirculation, and it shows the methodology used for the thermodynamic modelling of the reactor. The third paragraph shows the equations that are used to derive the gasifier performance from the measured data.

7.1 Methodology of experimental validation of the gasifier

In this paragraph the methodology of answering sub-question 5: 'How to validate the preliminary gasifier design?' will be discussed. For the validation of the gasifier design an experimental study will be performed on a test setup. The results of this experimental study will be compared to the results of the models used in chapter 6 for the gasifier design or the results will be compared to data found in the literature review. The different sub-questions to validate the performance of the preliminary gasifier design and their corresponding methodology are:

5.1 What is the added stability/robustness by variation in injection location?

Stability/robustness of the gasifier is one of the design criteria. With this sub-question it becomes clear if the oil should be injected with the inlet air or in the recirculating product gas when one wants to maximize the robustness of the gasifier. The robustness of the gasifier in this case is defined as the ability of the gasifier to operate with a wide range of reactor feed properties, which are differences in LHV and water content of the gasifier feed. Variation in the LHV and water content of the reactor feed could lead to a reduction in temperature and eventually flameout of the gasifier. A reducing ER will also result in a lower reactor temperature which will result in lower reaction rate which causes a reduction in flame front propagation as can be seen in figure 8 of paragraph 3.7. Eventually the gas velocity will become higher than the flame front propagation, at this point a flame-out of the reactor will occur. The effects of a reducing ER can be comparable to the effects of a variation of the reactor feed composition and therefore the range of operation of the ER will represent the robustness of the gasifier. Because the upper range of operation of the ER will be >1 and will therefore be outside the gasification region, the upper range of operation will not be tested. Therefore, the lower limit of operation of the ER will characterize the robustness.

To perform the tests firsts an injection location will be set. The ER will be lowered by reducing the air supply until the gasification stops. The temperature at different locations will be monitored in the reactor to see if and at what reactor inlet and outlet temperatures are right before the reactions stop and the reactor temperature drops rapidly. To perform this test the air inflow should be measured, the oil flow should be measured and the reactor inlet and outlet temperatures should be measured.

5.2 What is the added stability/robustness by product gas recirculation?

This question is also aimed at the stability/robustness of the gasifier just as the previous question. The definition of stability/robustness for this question can also be found in question 5.1. In this test also the lower limit of operation for the ER will characterize the robustness of the gasifier just as explained in previous question. The lower limit of operation of the ER will be determined for different levels of recirculation inside the gasifier. The results can be used to determine the level of recirculation that is required for a certain lower limit of operation for the ER, and thus for a certain level of robustness.

To perform this test again the ER must be lowered by reducing the air supply until the reactions stop. This temperature at which this happens is the lower limit of operation. The temperature of the reactor will also be measured. To control the ER the air flow and oil flow also must be measured. Also the amount of recirculating flow should be measurable.

5.3 What is the performance of the gasifier for different ER, injection locations and S/F ratios?

The gas yield, product stream composition, LHV of the product gas, carbon conversion efficiency and cold gas efficiency will characterize the performance of a gasifier. To find the optimal configuration for the injection location, steam to fuel ratio and equivalence ratio the gas yield, LHV of the producer gas, CCE and CGE of the gasifier will be determined. This will give the optimal gasifier configuration for this setup and from the results at this optimal configuration it can be derived if the gasifier performance is reasonable in comparison to gasifiers found in literature. Also the results will be compared to the results that could be expected from the theoretical gibbs equilibrium.

The test will be performed when the gasifier is in steady state after the to-be-tested gasifier configuration is set. The product gas stream of the gasifier will be extracted and cooled. The condensables and solid particles will be separated from the stream and measured. The composition of the remaining gas will also be determined.

5.4 How does the recirculation compare to the design specifications?

An analytical will be made to simulate the gas dynamics inside the gasifier. However the real performance of the recirculation system should be measured to verify the model and to ensure a proper functioning of the experimental setup. If the model is experimentally verified it could also be used if the reactor with the recirculation system were to be built on larger scale.

The model will be based on chapter 6.2 for the dimensioning of the ejector and some simple pressure drop calculations for the dimensioning of the tubes in the gasifier. The model will be experimentally verified by setting a certain level of recirculation and measure the realized level of recirculation with a pitot tube inside the reactor. Also the gasifier temperature will be measured to estimate the density of the gas.

5.5 What is the performance of the evaporative system?

To simplify the design of the gasifier the atomizer is replaced by an injector which sprays the oil on the hot reactor walls. Such a system is less sensitive to clogging, which happens faster in small scale gasification due to the small channels in atomizers designed for such low flow rates. However, due to the lower heating rate of the oil on the hot reactor wall in comparison to the heating rate of small atomized droplets, the conversion of oil into char is probably higher. To quantify the level of solid char formation inside the reactor the carbon conversion into the gas and condensables will be studied. Also, after the experiments the reactor will be opened to inspect the reactor wall on char formation.

7.2 Methodology of gasifier modelling

Fluid dynamics Pressure drop and flow calculations for the recirculation system

The recirculation system should be dimensioned in such a way that it enables a proper recirculation. In this chapter the methodology of the flow calculations will be discussed. These flow calculations will be used to dimension the ejector and the diameters of the pipes used in the system.

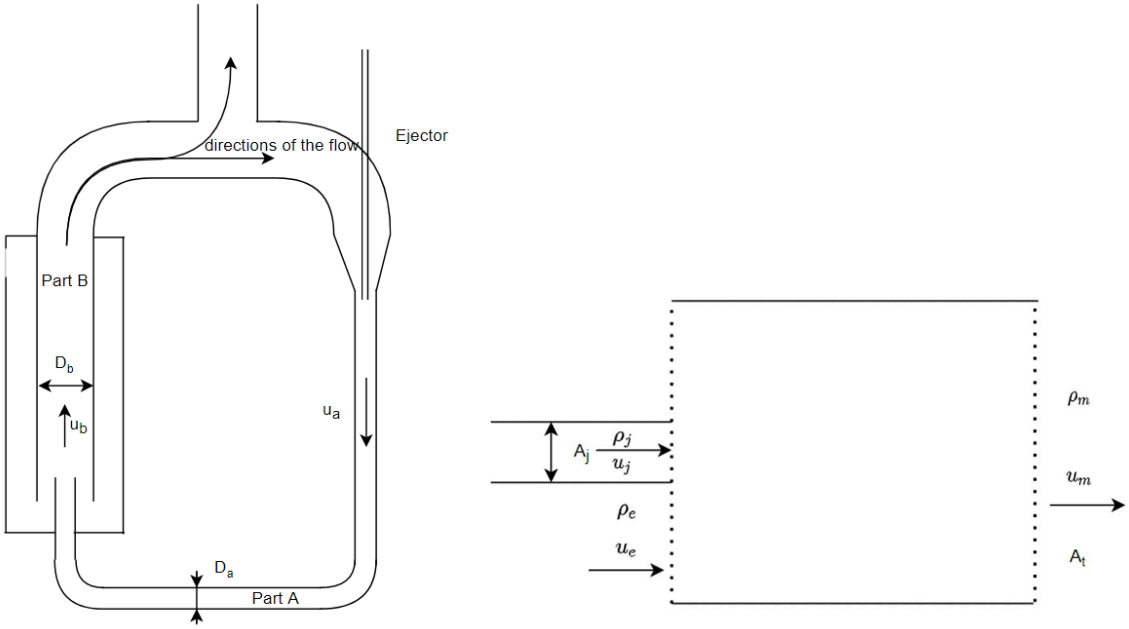

figure 20 (left) Schematic overview showing the variables used in this paragraph of the experimental gasifier setup showing the recirculation system consisting of a tube (part A) and an ejector. (right) Schematic representation of the ejector with the variables shown used in this paragraph.

First a simplified model will be discussed where no combustion takes place. The jet is in chocked flow. It is assumed that A_t>>A_j. Then equation 6.3 applies for the mass entrainment of the confined jet:

$$R_m = \frac{\rho_e Q_e}{\rho_0 Q_0} = \frac{-(1+\sigma)}{2\sigma} + \sqrt{\frac{A_T}{A_0(1+C_L)\sigma}} \qquad \text{(Eq. 6.3)}$$

Where σ is the density ratio ρ_j/ρ_∞, A_t is the throat area, A_j is the area of the jet nozzle, C_L is the friction loss coefficient which is calculated with the following equation:

$$C_L = \mathrm{f}\frac{L}{D} \qquad \text{(Eq. 7.1)}$$

Where f is the friction factor from the moody friction chart.

The C_L friction loss coefficient will however represent the head loss in both part A and part B. Therefore equation 7.1 is not valid and a C_L should be derived which represents the loss in part A and B. Let u_b=k u_a where k is a constant. The total head loss can then be calculated with the following equation:

$$h_{total} = h_a + h_b = \mathrm{f_a}\frac{\mathrm{L_a}}{\mathrm{D_a}}\frac{u_a^2}{2g} + \mathrm{f_b}\frac{\mathrm{L_b}}{\mathrm{D_b}}\frac{u_b^2}{2g} = \mathrm{f_a}\frac{\mathrm{L_a}}{\mathrm{D_a}}\frac{u_a^2}{2g} + \mathrm{f_b}\frac{\mathrm{L_b}}{\mathrm{D_b}}\frac{k^2u_a^2}{2g} \qquad \text{(Eq. 7.2)}$$
$$= \left(\mathrm{f_a}\frac{\mathrm{L_a}}{\mathrm{D_a}} + k^2\mathrm{f_b}\frac{\mathrm{L_b}}{\mathrm{D_b}}\right)\frac{u_a^2}{2g} = C_L\frac{u_a^2}{2g}$$

And thus C_L is then calculated with the following equation:

$$C_L = \mathrm{f_a}\frac{\mathrm{L_a}}{\mathrm{D_a}} + k^2\mathrm{f_b}\frac{\mathrm{L_b}}{\mathrm{D_b}} \qquad \text{(Eq. 7.3)}$$

If no flow is added in part B, then the constant k is a function of D_a and D_b. It can be described by the following equation: $k = \frac{D_a^2}{D_b^2}$

Thermodynamic modelling

The process simulation software COCO is used with the gibbs equilibrium reactor to determine the equilibrium composition of the gasifier product gas. For determining the physical properties COCO will use the Peng-Robinson equation of state. More details on the model can be found in paragraph 9.1.

7.3 Methodology of the gasifier performance calculations

Schematic overview with definition of variables

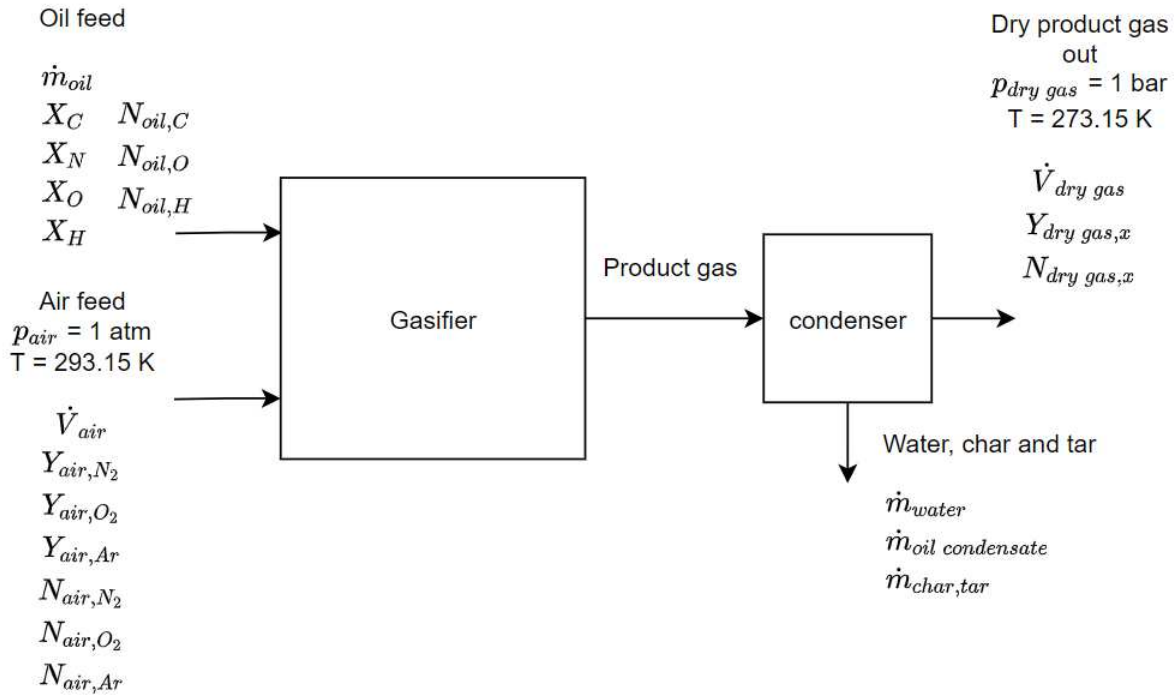

figure 21 Schematic overview of the gasifier with the with the definition of the variables used in the calculations of this paragraph. X represents a mass fraction, Y a volumetric fraction and N a molar flowrate.

In the following calculations it is assumed that the gasses behave as an ideal gas. For an ideal gas the moles per unit volume can be calculated as following:

$$\frac{n}{V} = \frac{P}{RT} \qquad \text{(Eq. 7.4)}$$

Determination of the equivalence ratio

The equivalence ratio can be determined with equation 3.1 which is the following:

$$ER = \frac{\phi_{O_2}}{\phi_{StC}} \qquad \text{(Eq. 3.1)}$$

ϕ_{StC} is determined from the stoichiometric ratios required for combustion of the carbon and hydrogen molecules in the oil. This is corrected for the oxygen in the oil. With the variables defined in this paragraph equation 3.1 then becomes:

$$\mathrm{ER} = \frac{\phi_{O_2}}{\phi_{StC}} = \frac{1/2\ N_{air,O_2}}{2N_{oil,C} + 1/2\ N_{oil,H} - N_{oil,O}} \quad \text{(Eq. 7.5)}$$

Determination of the gasifier gas composition

The gas is sampled in gasbags at the outlet of the pump after the condensation column. The gasbags are transported to a laboratory and are measured within 24 hours to minimize the gas dilution by diffusion through the gasbag. The gas composition is determined on a Trace 1300 Gas Chromatograph of Interscience Thermo Scientific at the laboratory of KIWA. The composition is given in dry basis volumetric concentrations. The molecules that all samples were tested on are the following: H_2, O_2, N_2, CO_2, CO, CH_4, C_2H_2, C_2H_4, C_2H_6, and C_3H_8.

Determination of the dry gas flow rates and yields

First the measured volumetric gas concentrations are corrected for the amount of oxygen that is present in the gas sample. That is because during sampling, storage and analysis ambient air can mix with the gas samples. It is assumed that in the product gas there is no unreacted oxygen left. The oxygen that is present in the samples is assumed to have leaked in by dilution with ambient air. The gas composition will be corrected for the amount of oxygen that is measured.

To determine the dry gas yield the nitrogen concentration in the product gas will act as a tracer gas. In the calculations the nitrogen in the air feed was assumed to be inert and all the nitrogen present in the oil was assumed to be converted into nitrogen gas. For nitrogen the molar flow then becomes:

$$N_{n_{2in}} = Y_{n_{2air}} \dot{V}_{air} \frac{P}{RT} + \frac{\dot{m}_{oil} X_{n_{oil}}}{M_{N_2}} \quad \text{(Eq. 7.8)}$$

Where P is the ambient pressure, T the ambient temperature and R the gas constant. Then the dry gas flow rate can be determined as following:

$$\dot{V}_{dry} = \frac{N_{n_{2in}} RT}{Y_{n_{2dryproduct}} P} \quad \text{(Eq. 7.9)}$$

Where if P and T are set to the normal conditions, $\dot{V}_{dry}$ will give the normalized flow rate.

Determination of the Carbon Conversion Efficiency

To calculate the carbon conversion efficiency equation 3.2 is modified for to the mass flow rate format:

$$\mathrm{CCE} = \frac{\phi_{c_{gas}}}{\phi_{c_{feed}}} = \frac{\dot{m}_{C_{dryproduct}}}{\dot{m}_{C_{oil}}} \quad \text{(Eq. 7.10)}$$

Where:

$$\dot{m}_{C_{oil}} = X_{C_{oil}} \dot{m}_{oil} \quad \text{(Eq. 7.11)}$$

And:

$$\dot{m}_{C_{dryproduct}} = \sum M_C\ N_{x_{dryproduct}}\ x\ \#\ of\ C\ atoms\ in\ molecule\ N_x \quad \text{(Eq. 7.12)}$$

Where x represents all the different molecules that were measured in the gas.

Determination of the LHV

The low heating value can be determined by the following equation:

$$\mathrm{LHV_{dry}} = \frac{\sum N_{x_{dryproduct}}\, LHV_x}{\dot{V}_{dry}} \quad \text{(Eq. 7.13)}$$

Where x represents the gasses H_2, CO, CH_4, C_2H_2, C_2H_4, C_2H_6, C_3H_6, C_3H_8 and LHV_x is in kJ/mol and LHV_{dry} in kJ/Nm^3. The used LHV_x values used in the calculations are summarized in the following table:

Table 8 LHV and enthalpy of formation of the components used for calculating the LHV_{dry}.

	LHV in kJ/mol	ΔH_f° in kJ/mol (*NIST WebBook*, 2021)
Hydrogen	241.8	0.0
Carbon monoxide	297.9	-110.5
Methane	802.5	-74.6
Acytelene	1256.2	227.4
Ethylene	1323.1	52.47
Ethane	1428.6	-83.8
Propene	1926.3	20.41
Propane	2043.0	-104.7
Carbon dioxide	0.0	-393.5
Water	0.0	-241.8 (g), -285.8 (l)
Oxygen	0	0.0

These are calculated as following:

$$LHV_x = \Delta H^\circ_{rxn} = \Delta H^\circ_{f,\,prod} - \Delta H^\circ_{f,\,reac} \quad \text{(Eq. 7.14)}$$

Where the enthalpy of formation ΔH_f° of each component can be found in the NIST Webbook (2021) and are also listed in Table 8. Note that for the calculation of the lower heating value the enthalpy of formation of water in vapour phase should be used.

Determination of the cold gas efficiency

The cold gas efficiency (CGE) is determined with equation 6.3:

$$CGE = \frac{\dot{V}_{dry}\, LHV_{dry}}{\dot{m}_{oil}\, LHV_{oil}} \quad \text{(Eq. 6.3)}$$

Where LHV_{dry} is in kJ/m^3 and LHV_{oil} is in kJ/kg.

Determination of oil condensate and water yield

The condensation system used to determine the condensate yield is discussed in paragraph 8.4. The pump after the condensation column will run for a set amount of time. Then the condensate is collected at the opening at the bottom of the condensate column. The oil fraction will be separated from the water fraction whereafter both yields will be determined on a scale wherefrom $\dot{m}_{\mathrm{oil\ condensate}}$ and $\dot{m}_{\mathrm{water}}$ can be determined. The condensate and water yield will be presented in $g/Nm^3{}_{dry\ gas}$.

Determination of the tar and char yield

The tar and char in the product gas stream is adsorbed by steel wool that is in the condensation column which will operate for a set amount of time. The steel wool will be measured before and after each experiment. From that the $\dot{m}_{\mathrm{char,tar}}$ can be determined.

Determination of the recirculating flow

The recirculating flow can be derived from the measured dynamic pressure in the pitot tube. The gas in the reactor is assumed to behave as an ideal gas. Also because the composition of the gas will mostly exist of nitrogen like air and the density of the rest of the products gasses do not drastically differ from the other components in air the product gas in the reactor is assumed to have the same density as air. The recirculating flow can then be calculated with the following equations:

$$\Delta p_{pitot} = p_{dynamic} = \frac{1}{2}\rho_{air} u_{rec}^2 \quad \text{(Eq. 7.15)}$$

Where Δp_{pitot} is the pressure difference measured over the pitot tube. The mass flow rate can be calculated with $\dot{m}_{\mathrm{rec}} = \mathrm{u}_{rec}\rho_{air}A_{rec}$, if u_{rec} is derived from equation 7.15, then the mass flow rate can be calculated with:

$$\dot{m}_{\mathrm{rec}} = \mathrm{u}_{rec}\rho_{air}A_{rec} = \sqrt{\frac{2p_{dynamic}}{\rho_{air}}}\rho_{air} \quad \text{(Eq. 7.16)}$$

Where the density of the gas ρ_{air} at the reference conditions can be calculated with:

$$\rho_{air} = \frac{P_{ambient}M_{air}}{\mathrm{RT}} \quad \text{(Eq. 7.17)}$$

8. Test Setup Development

In this chapter sub-question 6 will be answered, namely: How to design a test setup? This test setup should be able to perform the tests defined in chapter 11. The knowledge and models that were found in chapter 6 to 8 was used to design and dimension the test setup.

8.1 Construction & Design of the test setup

In this section the process in the experimental setup and its components will be described. The characterizing parameters of the design of the gasifier are shown in Table 9. The dimensioning of the gasifier was done by aiming at an oil feed flow of 4 kg/h with a residence time which is always larger than 2 s. The components described in this section can be found with their corresponding component numbers in figure 22. In figure 23 also two photo's of the experimental setup are shown with numbered components. The numbers used in this section correspond to figure 22. The main air supply for the gasifier is injected into the mantle of the gasifier with air ejector 1 (#1) where it recirculates around the gasifier chamber in a 324 mm OD tube before it enters the 219 mm OD reactor chamber. If a high air supply is required the valve of the ejector can be opened to entrain ambient air into the gasifier air feed. Ejector 2 (#2) is meant to recirculate the product gas in the system and is designed to have a minimal air consumption. The oil can either be injected directly into the gasifier chamber (#5) with oil injector 1 (#3), or in the recirculation tube (#6) with oil injector 2 (#4). The oil will evaporate on the reactor wall or the wall of the recirculation tube. To prevent charring of the oil the oil injection lances have a water cooled mantle as can be seen in figure 24. Also the diameter of the oil injector tube is relatively large for the flow (10 mm) to prevent charring. Steam can also be injected into the outer mantle of the reactor (#7). A propane burner (#8) is used to preheat the gasifier chamber before operation with oil. After the oil and air have reacted in the gasifier chamber it travels to a 160 mm OD stack (#9). There a part of the gas is sucked into the condenser (#10) with a pump for gas analysis and sampling. The other part of the product gas is mixed with ambient air by natural convection in the flare (#11) where it is fully combusted with the help of a pilot flame.

Table 9 Characterizing parameters of the designed experimental gasifier

Parameters	Values
Internal volume of reactor chamber + stack	69 l + 40 l =109 l
Design temperature	600-1000 °C
Pressure	1 atm
Design oil feed flow	1.11 g/s or 4 kg/h
Design steam feed flow (at 100 °C)	0 - 9.6 kg/h
Air feed	5 tot 25 Nm^3/h
Residence time	>3.6 s
Maximal thermal power based on LHV oil feed	40 kW

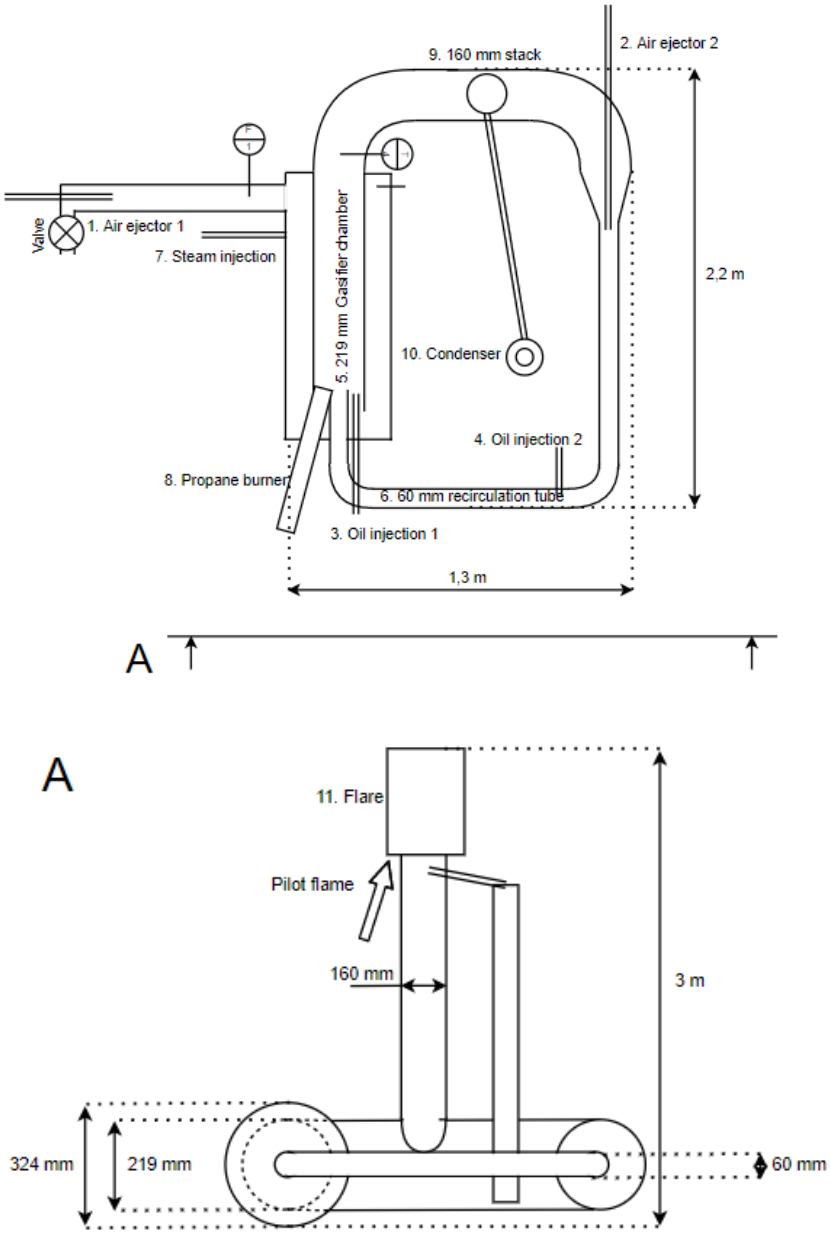

figure 22 Overview of the gasifier installation with its numbered components and main dimensions.

The test setup was built with 2 mm aisi 304 stainless steel as it is widely commercially available and it has a relatively high tensile strength at elevated temperatures. It has a higher corrosion resistance than regular steel, but it can still be subject to corrosion when contacted with chlorides. The flanges used have a PN16 pressure class rating. The gaskets used are made of Thermiculite 815® which are rated for temperatures up to 1000 °C. The isolation used on the setup consisted of two layers. The first layer contacting the reactor wall was made of ceramic wool of 25 mm which rated for temperatures up to 1260 °C. The second layer consists of a 120 mm stone wool.

To identify the problems and risks of operating the gasifier a Hazard and Operability (HAZOP) was performed. The complete HAZOP study can be found in appendix C. The recommendations for the control of the reactor formulated in this study are strictly followed to ensure safe operation.

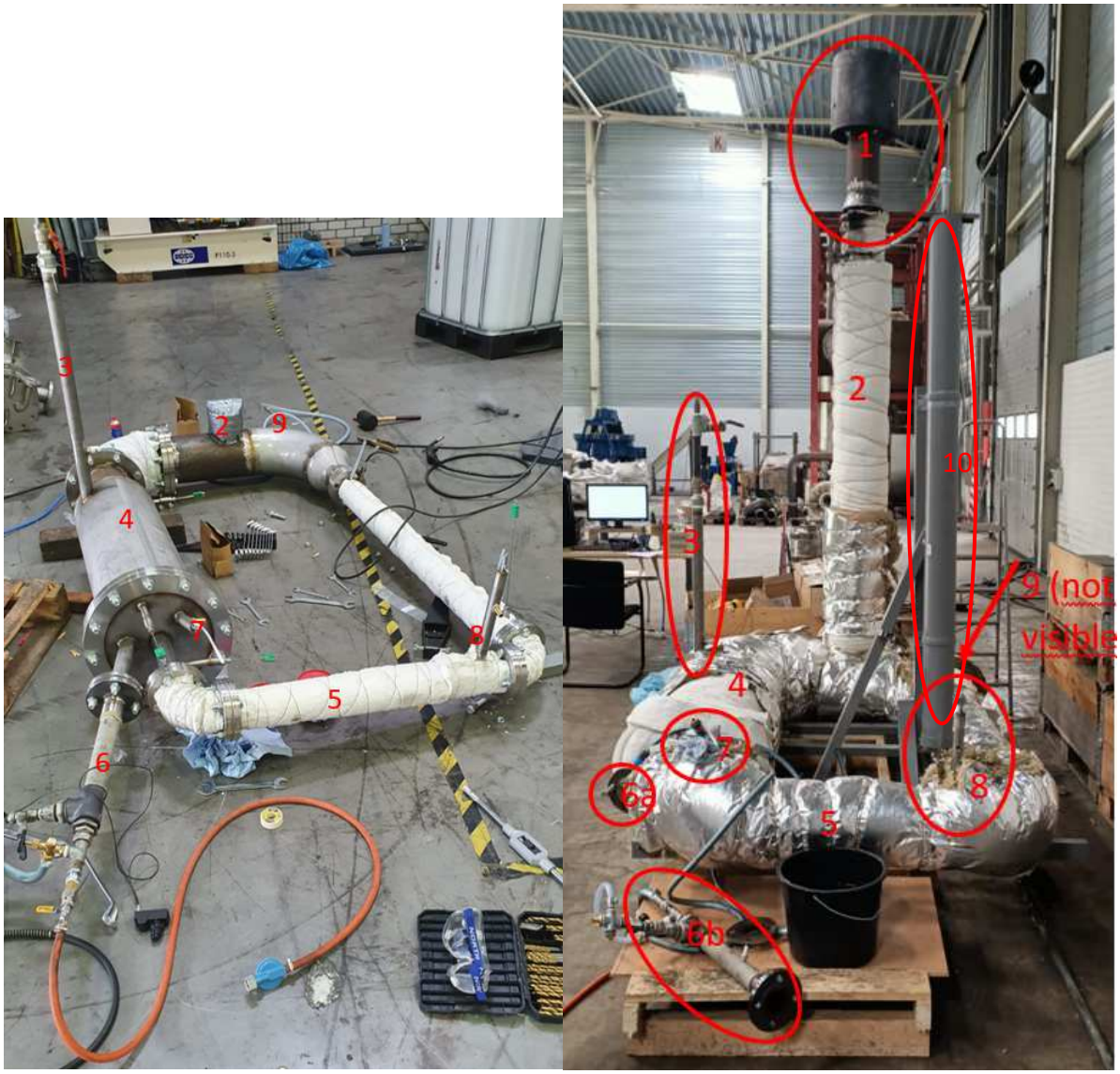

figure 23 Picture of the gasifier with insulation mounted where the numbers assign to the following components: 1. Flare, 2. 160 mm stack, 3. Air ejector 1, 4. 219 mm reactor chamber, 5. 60 mm recirculation tube. 6a. propane burner mounting flange, 6b. propane burner, 7. Oil injector 1, 8. Oil injector 2, 9. Air ejector 2. 10. Condenser.

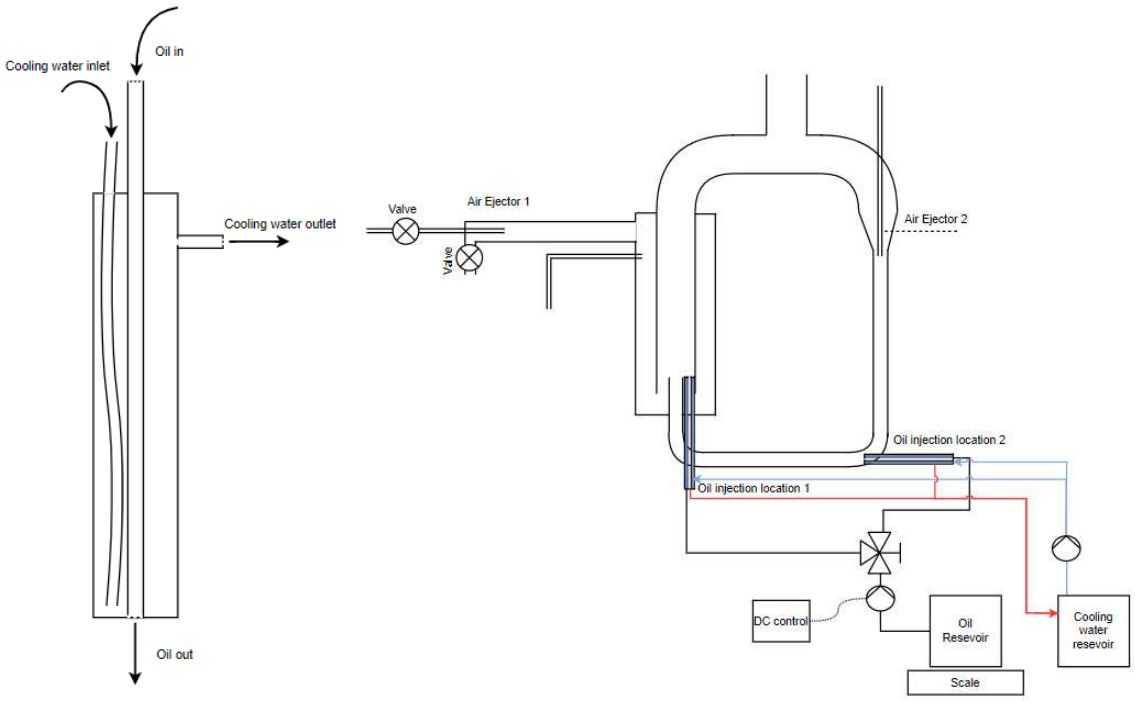

figure 24 (left) Schematic representation of one of the oil injector lances with a tube wherethrough the cooling water enters . (right) Schematic representation of the experimental setup with the cooling cycle

8.2 Dimensioning of the recirculation tube and ejector

For the calculations in this section the formulas from Ch. 7.2 are used. The gas in the reactor is assumed to have the physical properties of air. The gas in the reactor will be 1000 ^{o}C at maximum, the density will then be 0.28 kg/m^3. The diameter of the reactor tube is fixed on 0.22 m with a length of 2 m. The length of the recirculation tube is fixed on 3 m and the diameter should be determined. The mass entrainment ratio should be maximized and at least be 10 to ensure a low dilution and cooling of the recirculated gas. Choked flow will be assumed in the nozzle of the ejector and the discharge losses will be neglected. It should be kept in mind that the dynamic pressure of the resulting flow should be measurable with the accuracy of the pitot tube and the differential pressure meter used. Because the accuracy of this pitot tube is +-0.2 Pa the dynamic pressure of the gas should always at least be a 1 Pa. The recirculation flow should at least have a flow of 15 kg/h so that approximately half of all the product gas can be recirculated. The flow is assumed to be turbulent. The friction factors are determined to be 0.053 for the reactor tube and 0.065 for the recirculation tube according to the moody diagram in fig. 6.13 in White (2011) at Re = 4000. The wall roughness was assumed to be 2 mm as a lot of particle deposition on the walls is expected.

figure 25 shows the influence of the ejector nozzle diameter on the performance of the ejector when the reactor is at its maximum temperature and thus the performance of the ejector is lowest. A nozzle diameter of 1 mm is selected as this will deliver sufficient recirculation of 15 kg/h while the mass entrainment ratio is maximized for this minimal amount of recirculation.

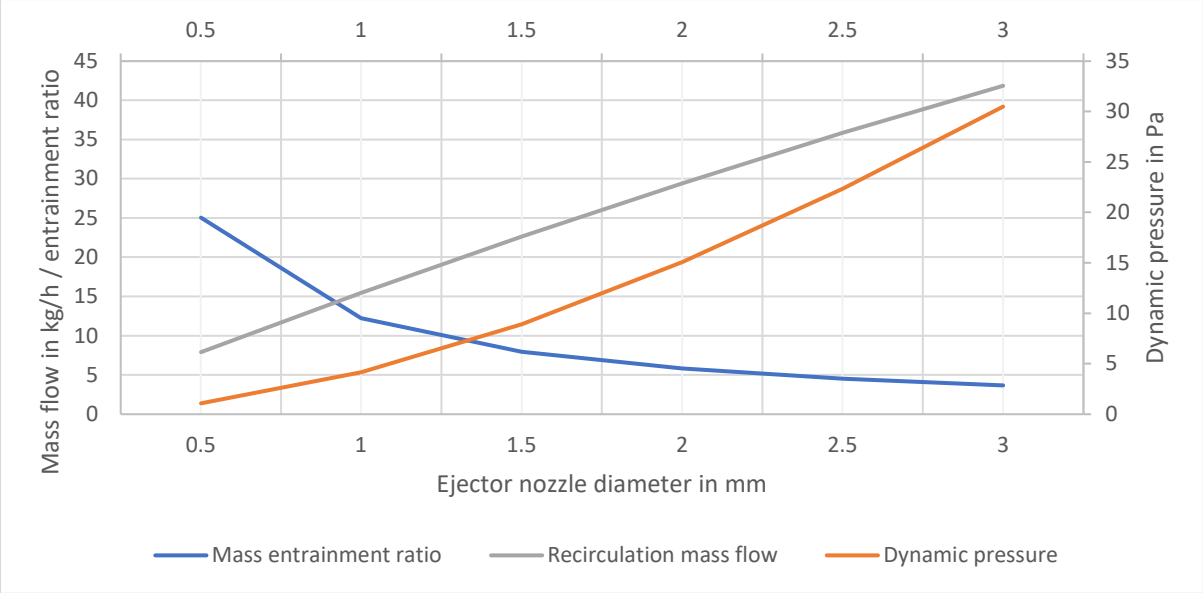

figure 25 The influence of the ejector nozzle exit diameter on the performance of the ejector in the system at T = 1000 °C and p_{ej}=1.8 bar and tube diameter of 60 mm

In figure 26 the influence of the diameter of the recirculation tube on the performance of the ejector is shown. To be able to measure the flow the dynamic pressure should at least be 1 Pa. The dynamic pressure for the 60 mm tube will be approximately 4 Pa, if the recirculation flow is set to half of the maximum amount of recirculation this will still be a dynamic pressure of 1 Pa. Therefore 60 mm is the maximum diameter for the recirculation tube to still be able to measure the dynamic pressure of the recirculation flow. Because the recirculation massflow and the entrainment ratio both increase with the tube diameter, 60 mm is selected as the size of the recirculation tube.

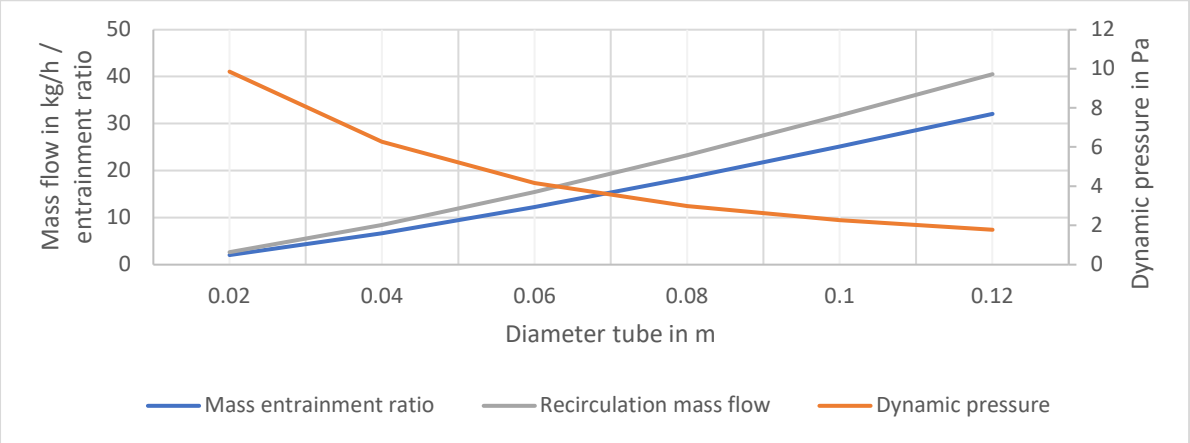

figure 26 The influence of the recirculation tube diameter on the ejector performance at T = 1000 °C and p_{ej}=1.8 bar and a nozzle diameter of 1 mm.

The effect of the temperature of the entrained gas on the gasifier performance can be seen in figure 27. The performance of the ejector reduces with temperature because the density ratio of the jet and the entrained gas increases. The formula for the mass entrainment ratio of an ejector showed in ejector 7.2 shows that the mass entrainment will reduce when the density ratio increases.

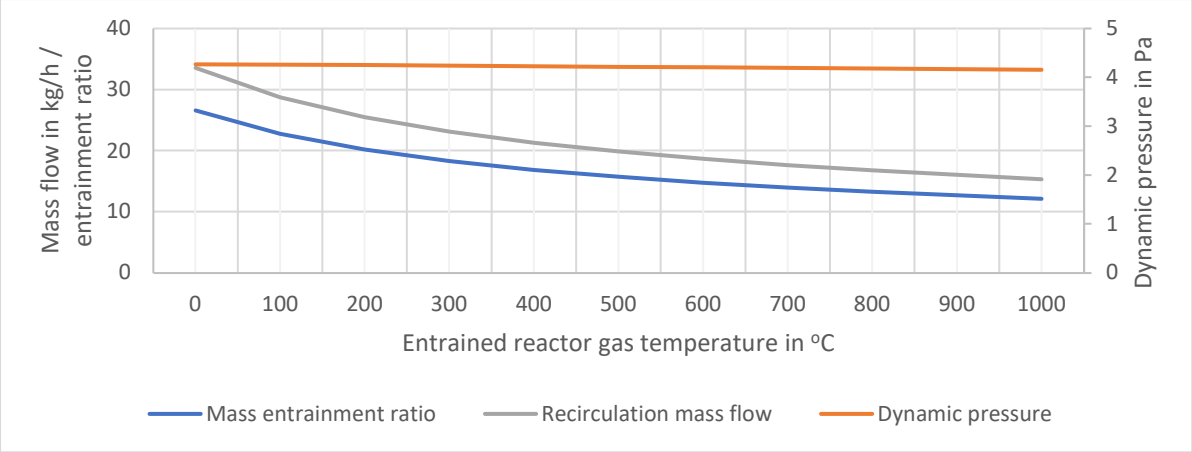

figure 27 The influence of the gasifier temperature on the ejector performance with a tube diameter of 60 mm, p_{ej}=1.8 bar and a nozzle diameter of 1 mm.

In figure 28 the influence of the static pressure of the ejector on the ejector performance is shown. The mass entrainment ratio reduces slightly with the ejector pressure, while the entrained mass flow rate increases strongly with the ejector pressure. Therefore the ejector pressure is a proper parameter to control the recirculation mass flow rate, and a graph as in figure 28 can be used to find the appropriate ejector pressure. It should be kept in mind that the calculations are not valid above the choking point of 0.89 bar gauge pressure, therefore the performance of the ejector will deviate from the curve in figure 28 above this choking pressure. The actual entrainment will be lower than the predicted entrainment ratio above the chocking point because the calculations assume the flow to become supersonic after the nozzle. When a laval nozzle is added the stream can become supersonic and the formula could be valid again, which improves the entrainment ratio in this region.

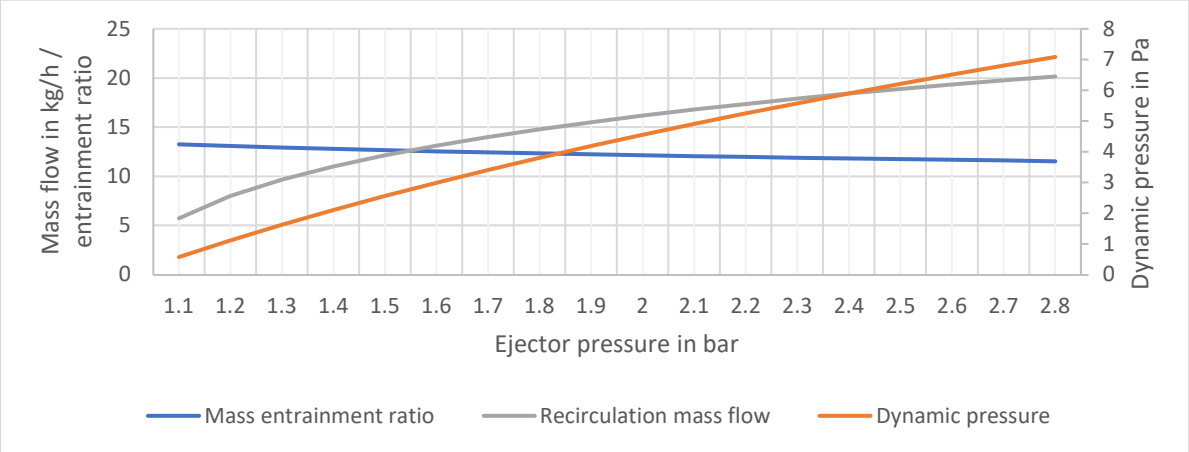

figure 28 The influence of the static pressure of the compressed air in the ejector on the ejector performance with a tube diameter of 60 mm, T=1000 °C and a nozzle diameter of 1 mm.

8.3 Control of the test setup

To perform the tests described in chapter 7.1 two parameters need to be controlled. Firstly the equivalence ratio. This means that both the oil inflow and the air inflow need to be regulated. Secondly the recirculation needs to be controlled. This will be done by varying the compressed air inflow into air ejector 2.

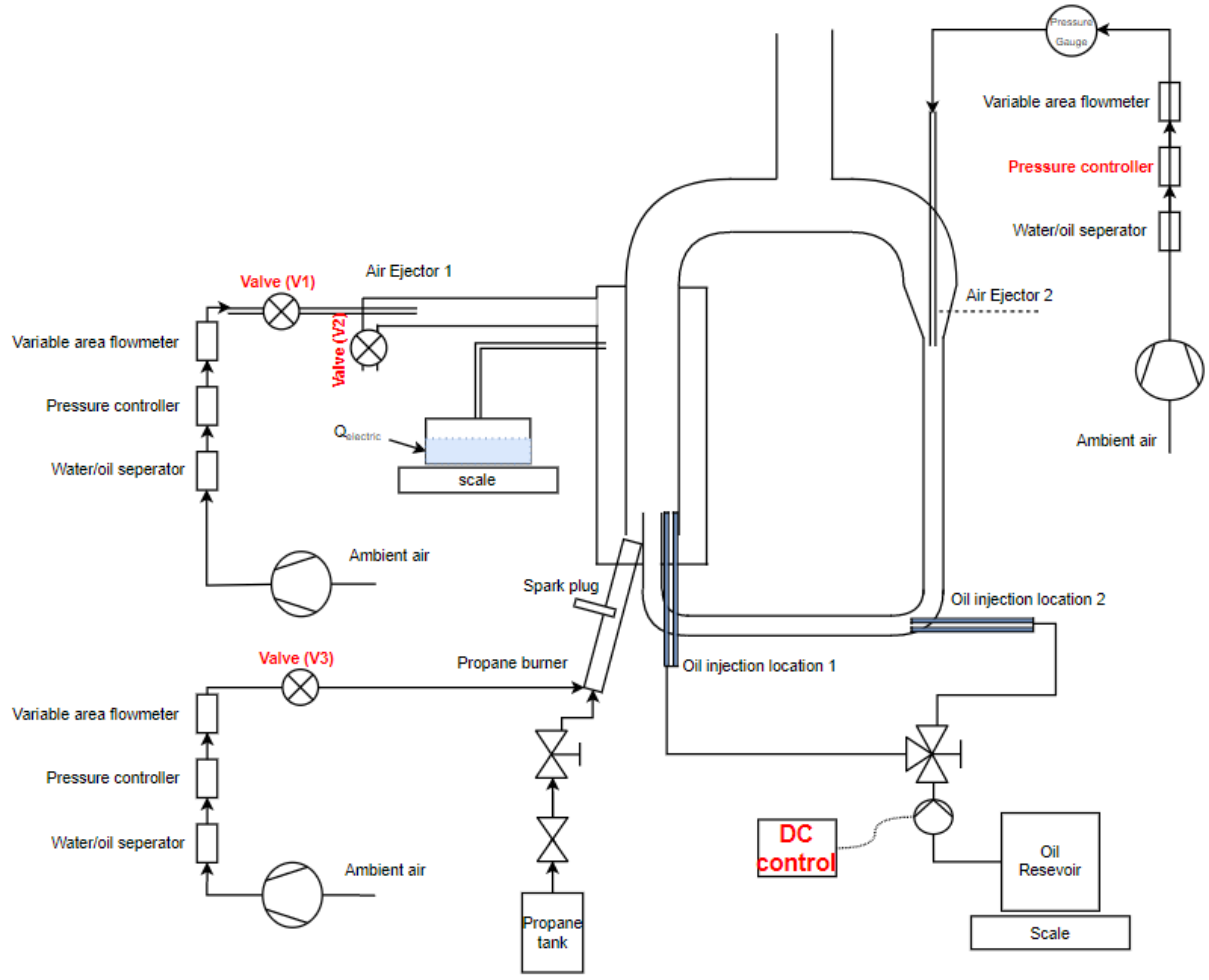

figure 29 Schematic overview of the test setup including the control valves, pressure controller, steam generator and DC controller used to control the equivalence ratio, the amount of recirculation in the system and the amount of steam added to the system.

A schematic overview of the test setup with its control valves that will be used can be seen in figure 29. To control the equivalence ratio the air inflow will be controlled with the following valves and controllers. The main air flow will be delivered with air ejector 1. Valve V1 controls the compressed air flow, whereas valve V2 controls the amount of ambient air that is entrained in the air jet created by the compressed air. The flow of compressed air in air ejector 2 is controlled with a pressure controller.

The oil is pumped with a DC peristaltic pump into the injector lances at injection location 1 or 2. The rotational speed of the pump, and therewith the volumetric flowrate of the oil, is controlled with a DC controller.

The amount of steam added to the system is controlled by switching on the power of the 2 kW steam generator. If a higher amount of steam is desired than the single steam generator can deliver then additional steam generators can be added.

The propane burner which is used for the preheating of the reactor during startup needs to be controllable firstly to create a proper mixture for ignition during startup, and secondly to control the heating rate of the reactor during preheating. The air flow of the propane burner is controlled with a variable area flowmeter. The propane flow is controlled with a ball valve. During startup the initial ignition of the propane burner is caused by a spark plug.

8.4 Measurement Devices

In this paragraph the measurement devices will be discussed. In figure 30 a schematic overview can be seen of the test setup with all the sensors that will be used. The letters T indicate a temperature sensor and the letter F a flow sensor. The numbers in the figure will be used in this paragraph to refer to the sensors.

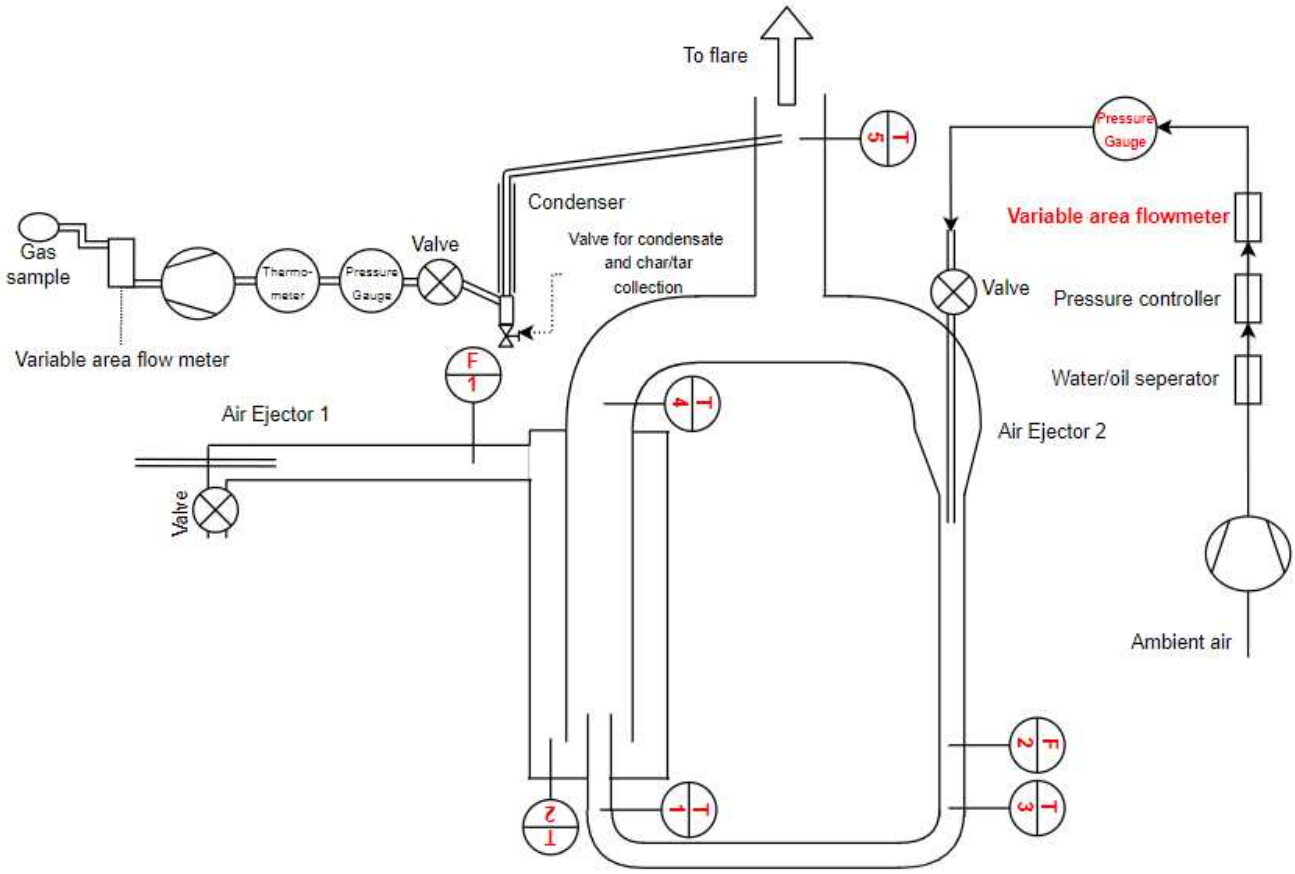

figure 30 Schematic overview of the test setup with all the flow (F) and temperature (T) sensors.

Temperature in the reactor

For the temperature measurements 5 thermocouples type-K will be used. The sensors are protected by a stainless steel cover and are heat resistant up to 1100 °C. The output of these sensors is 4-20 mA. With these thermocouples the reactor inlet temperature of the preheated air (T2) and of the recirculating inlet gas will be measured (T1). Also the temperature of the reactor outlet (T4), the stack temperature (T5) and the temperature of the recirculating stream (T3) before the evaporating section are measured and logged in a PLC.

Flow into and in the reactor

The volumetric flow or flow velocity will be measured and logged at 3 different locations in the system. The 3 different locations are labeled and can be found in figure 30. To determine the flow of the main air supply the flow velocity after air ejector 1 will be determined with a Delta OHM thermal anemometer (F1) with an accuracy of ± 3% of the measured value (F1). The thermal anemometer determines the flowrate by quantifying the heat capacity of the flow with a hot wire while assuming the specific heat capacity of air. The dynamic pressure of the flow after air ejector 2 (F2) will be measured with a pitot tube. Together with the temperature (T3) and the assumption of an ideal gas with the physical properties of air an estimation of the recirculating flow velocity can be made. Due to the high temperatures at the location of the pitot tube a 10 mm OD stainless steel Prandtl pitot tube from manufacturer Paul Gothe GmbH will be used which can resist

temperatures up to 1100 °C. The pressure differential over the pitot tube will be measured with the differential manometer Setra 267 with a range of 0-50 Pa and a minimal accuracy of ± 0.2 Pa. Thirdly to measure the flow of air which is added to the system by air ejector 2 the flow (F3) will be measured with a Key Instruments MR3000 variable area flow meter with a range of 2 – 30 L/min and an accuracy of ± 1.2 L/min. To determine the normalized air flow rate also the pressure directly after the variable area flow meter is measured.

Product gas condenser and sampling system

To analyze the dry gas product gas composition and to quantify the amount of condensables and char/tar in the gas a gas extraction and condensation system was designed. The condenser tube consists of a 20 mm ID 2 m long tube which is cooled with water at ambient temperature. A schematic representation of the condenser system can be found in figure 30, also the condenser is labelled as #10 in figure 22 and figure 23. The gas is pumped through the condenser with a constant volume pump with a constant RPM. The volumetric flow can be measured at the outlet of the pump with a variable area flow meter. The flow through the pump can be regulated by reducing the pressure with the valve in between the condenser and the pump. The temperature and the pressure of the flow going into the pump are measured with an analog thermometer and pressure gauge. An estimation of the flow can then be made if the flow is assumed to be ideal and the physical properties of the gas are derived from the composition of the gas. The composition of the gas was determined in a commercial lab with a gas chromatograph. The gas samples were sampled at the outlet of the variable area flow meter and were transported to the lab in 1 liter multifoil gas bags.

Oil flow and steam flow

The total oil and steam usage are measured per experiment. The weight of the water basin and of the oil reservoir are measured at the start and at the stop of each experiment. The weight scale has an accuracy of ± 1 g. The average oil and steam flow are then given if the oil and steam consumption are divided by the time of the experiment.

8.5 Complete overview of the experimental setup

In figure 31 a complete schematic overview of the experimental setup as build is shown. All the components that were discussed in previous paragraphs are shown in the figure.

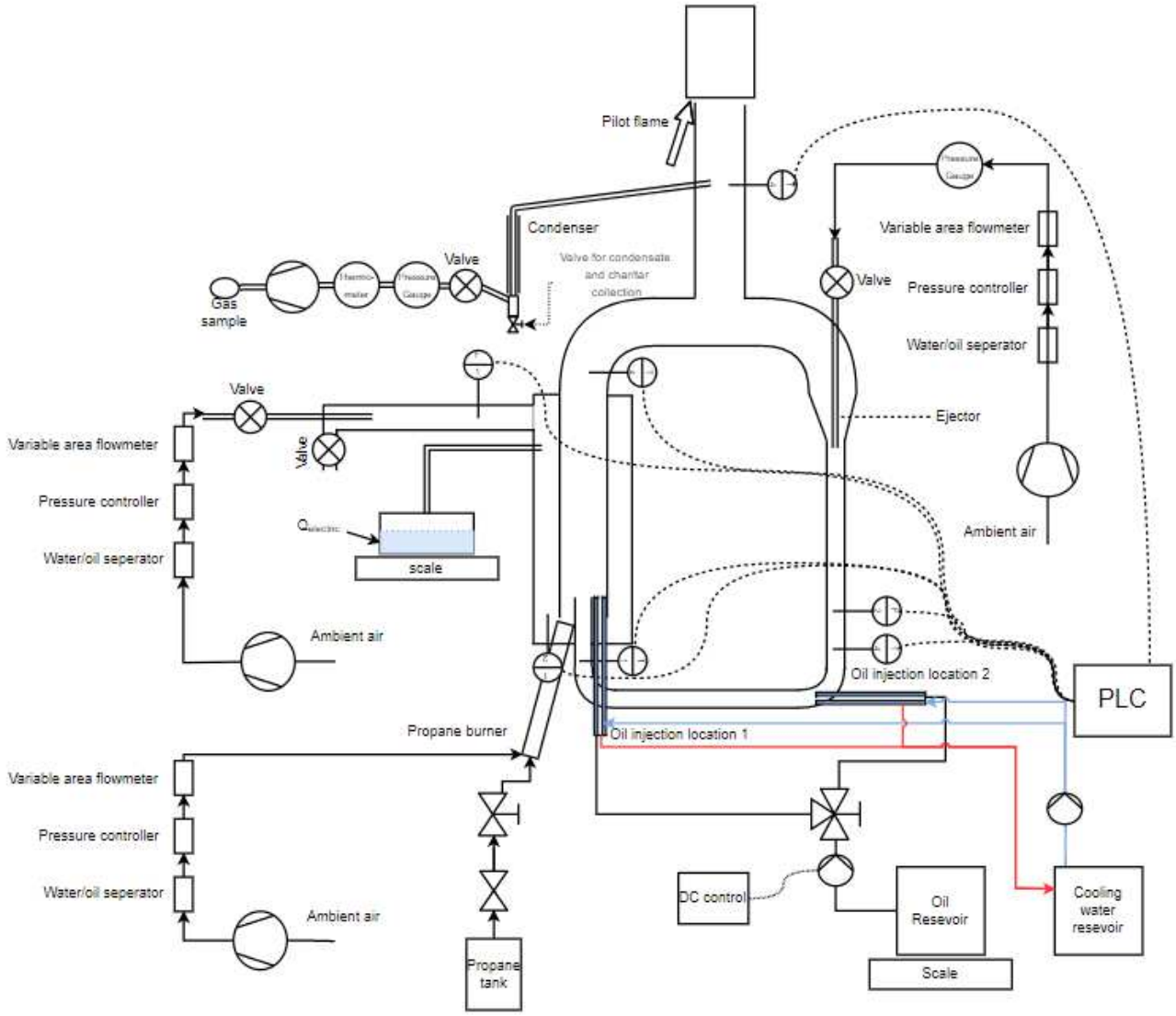

figure 31 A complete schematic overview of the experimental setup with all instruments, measurement devices and control devices that were used

8.6 Commissioning

Startup of the reactor

The startup of procedure requires approximately 2 hours to ensure proper warm up of the reactor components. For the experiments this is important to enable the steady state experiments without wasting the pyrolysis oil on the heating of the reactor. The startup of the reactor after 15 min can be seen in figure 32. The startup is relatively slow, this is because gasifier is constructed with thick PN10/16 stainless steel flanges. These absorb a lot of heat and therefore the reactor has to be heated for a long time to be able to operate in steady state. However, in normal operation the oil can be injected much earlier (e.g. at T reactor = 500 ^{o}C). This would only require 15 min of preheating with the current propane burner. If a larger propane burner is installed, this startup time could even be shorter.

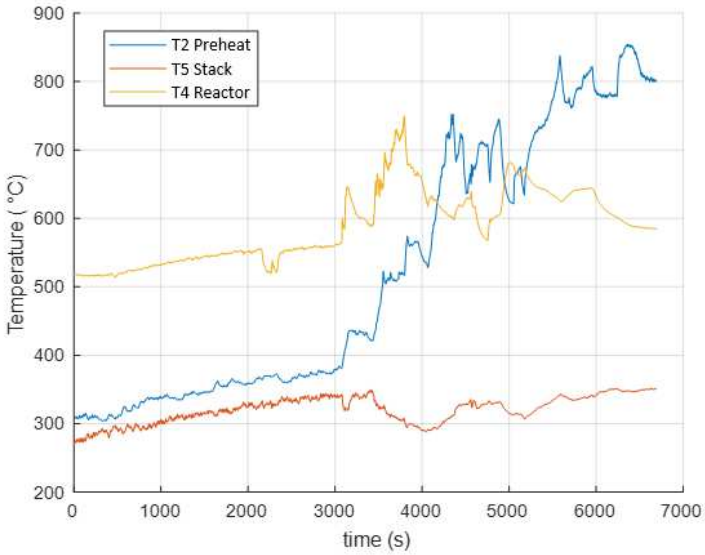

figure 32 The preheating of the reactor with propane gas until t = 3070 s. Then the propane flow is stopped and diesel is added to the system whereafter the reactor settings are readjusted several times causing fluctuations in the reactor temperature. The locations of T2, T4 and T5 are indicated in figure 30.

Testing and evaluation of recirculation system

The performance of the recirculation system was first tested with a reactor at ambient temperature. The results of this test can found in Table 10. The predicted performance of the ejector is calculated the model from chapter 8.2. The measured recirculation at the pressure setting of 0.8 bar gauge pressure on the ejector is 2.15-2.63 times higher than the predicted recirculation as can be seen in Table 10 row 7. This could be caused by an overestimation of the pressure drop in the system, as this was based on a turbulent system with rough walls. However when the reactor was cold all the walls were still clean from tars and the flow in the reactor was probably laminar instead of turbulent as the Reynolds number in these conditions is approximately 400, and thus this would reduce the pressure drop. Also due to the higher recirculation in the reactor the assumption that the velocity in the larger diameter tube before the ejector is negligible becomes invalid, causing a large deviation from the calculated recirculation. However at higher temperatures the flow is expected to be turbulent, the walls are expected to have a high roughness due to deposition of particles and the recirculation will be much lower due to the lower density of the gas.

Table 10 The measured and predicted recirculation flow at a reactor temperature of 20 °C. The location of the instruments used are indicated in figure 33.

Parameter	According to model in paragraph 8.2	Actual Value
Indicated flow at variable area flow meter (F3)		12 ± 1.2 l/min
Pressure of compressed air (P1)		1.8 bar abs
Flow rate at 1 atm		16 ± 1.6 l/min
Mass flow of compressed air		1.16 ± 1.16 kg/h
Measured recirculation flow velocity (F2)		6.00 ± 0.04 m/s
Entrained massflow	31.1 kg/h	72.1 ± 0.60 kg/h
Mass entrainment ratio	26.0	62.4 ± 6.2

During the high temperature recirculation test problems were encountered with the flow measurements due to clogging of the pitot tube. Also heavy particle deposition was observed in the recirculation tube during inspection of the insides of the reactor after operation as showed in chapter 9.2. Due to the clogging of the recirculation tube the recirculation flow dynamic pressure could not be measured. The temperatures in the recirculation tube were measured when the ejector pressure was 0.8 bar gauge and the averaged reactor temperature was 614 °C, the results of the experiment are shown in Table 11 and the numbered instruments used for the experiment are shown in figure 33. According to the model the mass entrainment ratio should have been 15. With this mass entrainment ratio the cooling effect of the cold air jet could not have caused the temperature reduction of 311 °C between the averaged reactor temperature and the temperature T3 in the recirculation tube. Heavy heat losses in the recirculation tube could be the cause of the low recirculation temperature. The heat losses can also observed between the thermocouples T3 and T1 where 75 °C of process temperature is lost. In this section no process stream is added, and thus the loss of heat is the only explanation for the reduction in temperature in this section.

Due to the heat losses in the recirculation tube it has become useless to recirculate the gasses to improve the lower operational limit of the ER. That is because the hot recirculation gasses should preheat and react with the relative cold gasses and oil in the first part of the reactor, however due to the heat losses the recirculation gasses have a lower temperature then the air preheat gasses and thus it would cool the gasses instead preheating the gasses. Also, because the recirculation temperature is far below the boiling point of the heavy fraction of the pyrolysis oil it is not a good idea to evaporate the oil in this section because the oil will not fully evaporate. It is therefore concluded from this test that the recirculation experiments cannot be performed.

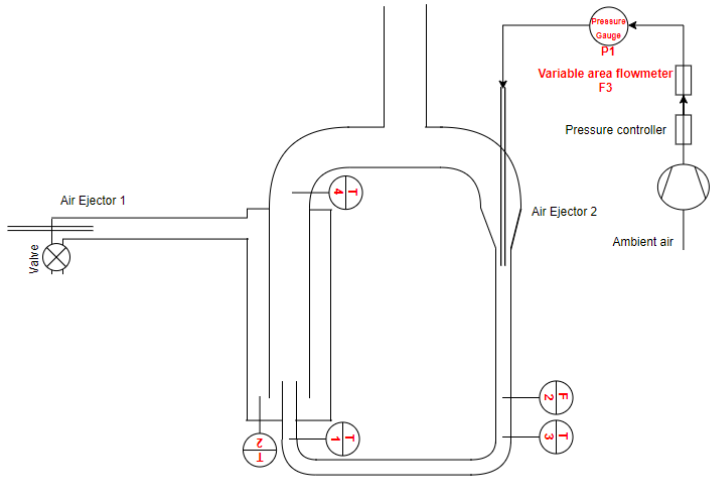

figure 33 The reactor with the thermocouples (T1-4) and pitot tube (F2) which were used in the high temperature recirculation test. Also the variable area flow meter F3 and pressure gauge P1 used are shown.

Table 11 The averaged measured parameters and values during the high temperature recirculation test during a 10 s measurement interval.

Measured system parameters	Averaged value
T1 recirculation flow	227 °C
T3 recirculation flow	303 °C
T2 preheat	395 °C
T4 reactor	614 °C
Pressure of ejector	1.8 bar abs
Normal flow rate ejector air	16 ± 1.6 l/min
Recirculation flow velocity	N.D. due to clogging of pitot tube

9. Results & Discussion

In this chapter the results of the thermodynamic modelling and the experimental validation of the gasifier are presented and discussed.

9.1 Modelling

With the methodology and matlab script that can be found in appendix E the equilibrium constants of the water-gas shift reaction and the steam reforming reaction at varying temperatures were determined. The calculated equilibrium constants can be seen in figure 34. The water-gas shift equilibrium constant decreases with temperature, meaning that at elevated temperatures the CO_2 and H_2 decrease due to this reaction. However as can be seen the steam reforming equilibrium constant increases with temperature, and becomes significantly larger than the WGS equilibrium constant at T>890 K. The steam reforming reaction will therefore cause a rise in CO_2 and H_2 concentrations at elevated temperate, counteracting the effect of the water-shift equilibrium. To solve the equilibrium composition with multiple components at different ER and S/F ratio the software COCO will be used.

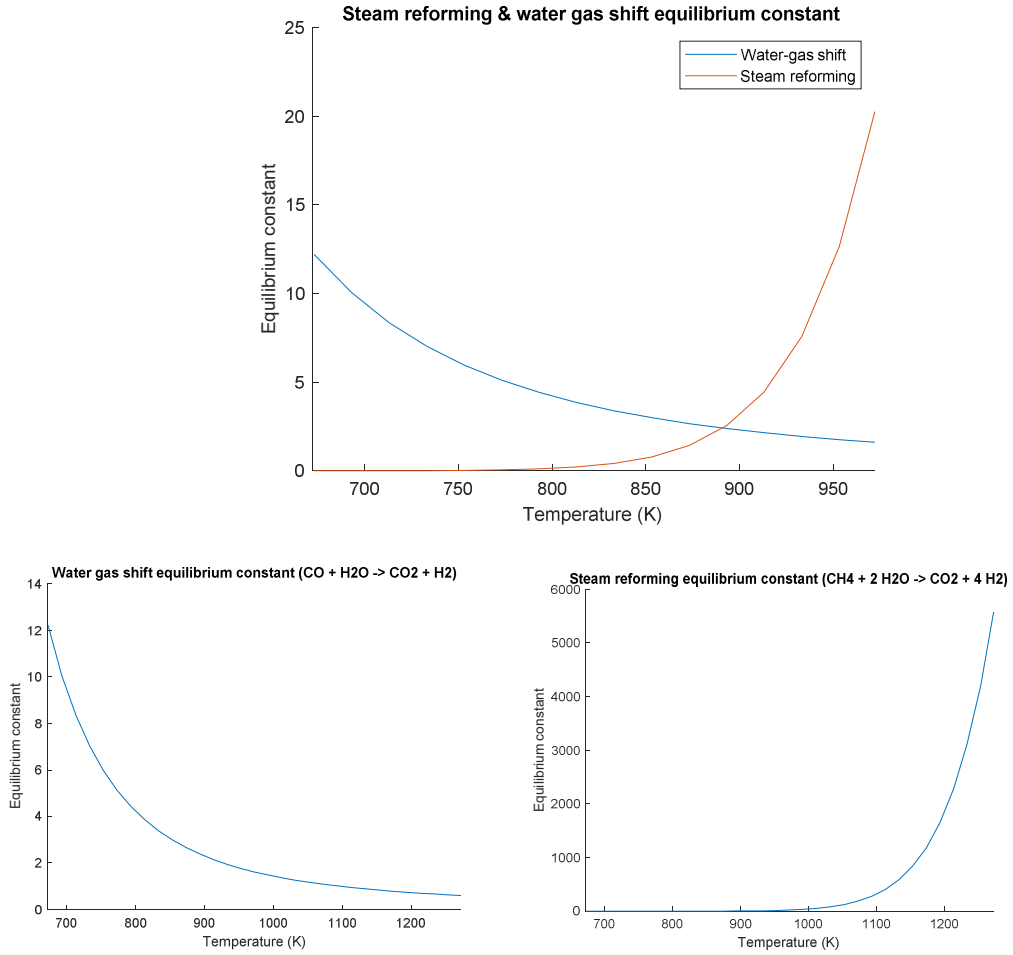

figure 34 The calculated equilibrium constants of the water-gas shift reaction and the steam reforming reaction

In the model the component ethylbenzene will be used to model the oil. That is because the molecule ethylbenzene has been quantified as the most common molecule in the oil as explained in Chapter 2. And the composition and heat of combustion are slightly comparable with the composition and heat of combustion of the oil that is used. The properties of ethylbenzene are listed in Table 12.

Table 12 Properties of ethylbenzene which will be the component used to represent the DKR350 oil in the model

Element	Mass %
C	90.6
H	9.4
O	0
N	0
LHV	41.3 MJ/kg (calc. as described in Ch. 7.4)

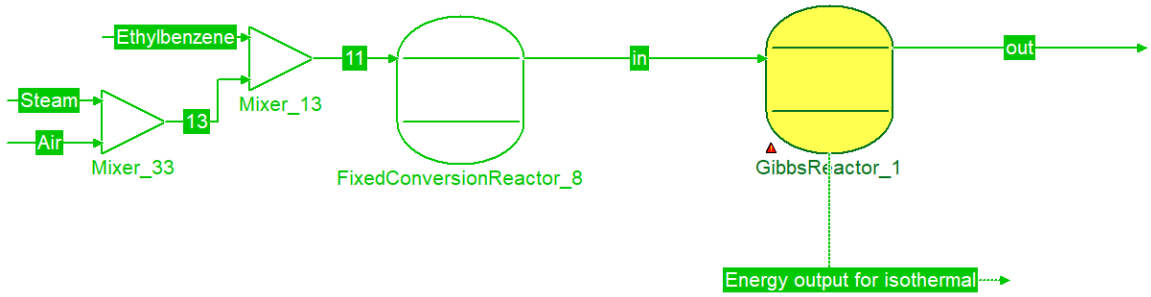

figure 35 The gibbs equilibrium reactor model in COCO that was used to simulate an isothermal reactor with the Peng-Robinson equation of state

The reactor that was used in the COCO model was an gibbs equilibrium reactor with the Peng-Robinson equation of state. Also a fixed conversion reactor was used to give an initial solution which was needed for the solver to find a valid solution for the gibbs equilibrium reactor. The model that was used can be seen in figure 35. The model was solved as isothermal and autothermal. The components that were taken into account in the model were CO, CO_2, H_2, H_2O, O_2, N_2, CH_4 and C_8H_{10}.

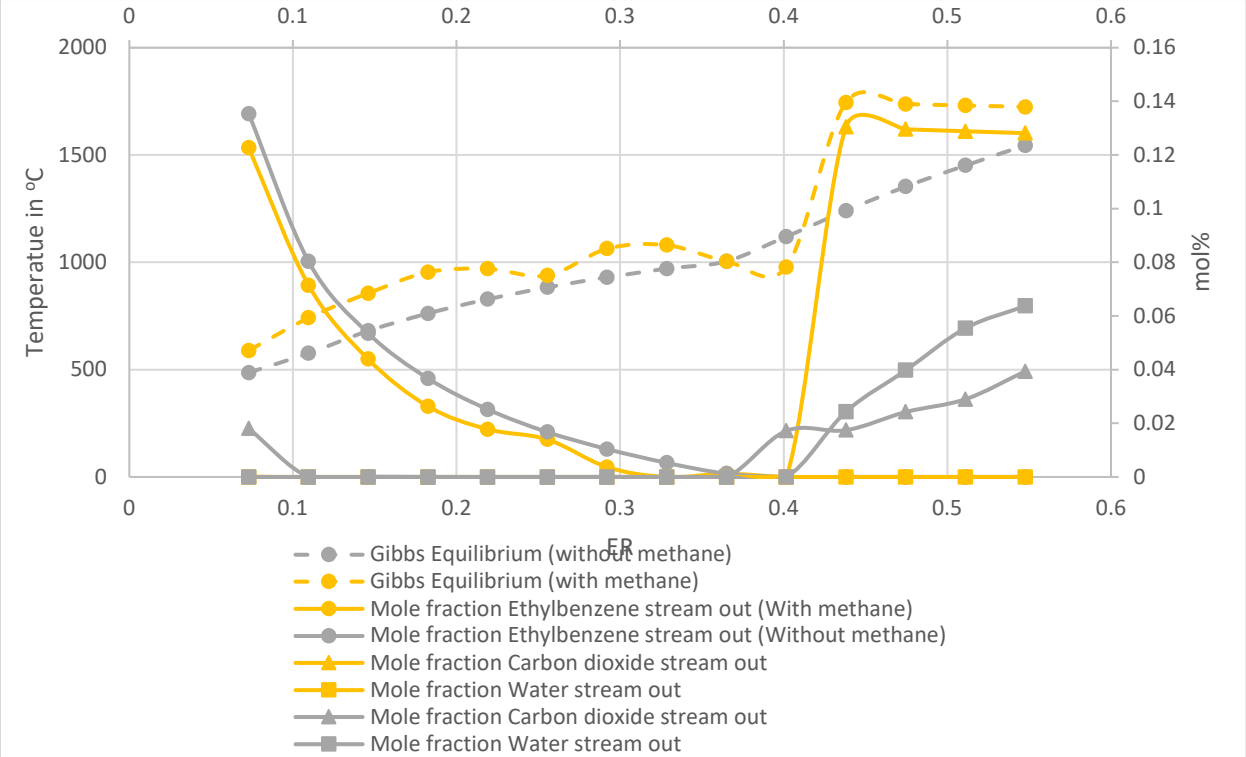

figure 36 Temperatures and concentrations of several components at the gibbs equilibrium of the gasification of ethylbenzene as calculated with COCO and the Peng Robinson equations of state. The temperature of the gibbs equilibrium where methane was taken into account shows unphysical behavior. The results are all at a pressure of 1 bar.

In figure 36 Temperatures and concentrations of several components at the gibbs equilibrium of the gasification of ethylbenzene as calculated with COCO and the Peng Robinson equations of state.figure 36 the resulting temperatures for an adiabatic reactor are shown. The adiabatic reactor simulates the case where the process operates autothermal. The gibbs equilibrium was solved for the components H_2O, H_2, O_2, CO_2, CO, N_2, CH_4 and C_8H_{10}. The gibbs equilibrium was not calculated correctly when the component CH_4 was taken into account at higher temperatures. This can be concluded from the unphysical behavior of the temperature at ER > 0.4. The temperature below ER < 0.4 is lower for the case where CH_4 was taken into account, this is because of the endothermic steam reforming reaction of CH_4. An interesting observation is that the temperature shows a slope discontinuity at approximately ER = 0.4. Concluding from the declining C_8H_{10} slope and the sudden increase of H_2O and CO_2 molecules it can be concluded that this discontinuity is caused by the depletion of unconverted oil and therewith the starting point of the full combustion into H_2O and CO_2 molecules. This is a comparable effect as discussed in Ch. 3.7 and know in literature as the solid carbon formation boundary where the depletion of solid carbon causes a discontinuity in the temperature curve. It was also tried to calculate the output of the adiabatic/autothermal gibbs reactor in the case where steam was added to the reactor. However the solver of COCO gave invalid results.

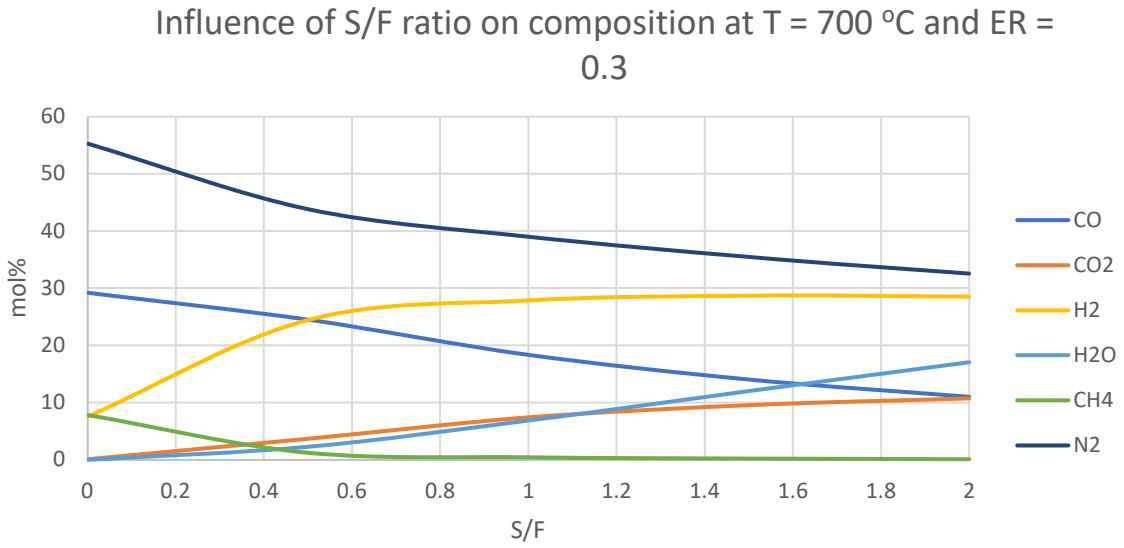

figure 37 Influence of S/F ratio on composition at T = 700 °C and ER = 0.3 , this was computed with COCO and the Peng Robinson equations of state in with an isothermal gibbs equilibrium reactor at a pressure of 1 bar.

Isothermal models were also computed with the COCO process simulation software. The results of the model where the S/F ratio was varied and the ER and the temperature were held constant can be seen in figure 37. The concentrations of C_8H_{10} and O_2 are not shown because these are zero. The influence of the S/F ratio at T= 700 °C and ER = 0.3 is highest at an S/F ratio up to 0.6. An increase in the S/F ratio leads to a decrease in the CH_4 concentration and an increase in the H_2 concentration. That is because the H_2O concentration shifts the equilibrium of the steam reforming reaction to the right, producing CO_2 and H_2. After all the CH_4 has reacted there are no rapid changes, only the water-gas shift reaction shifts to the right due to the increase in H_2O pressure.

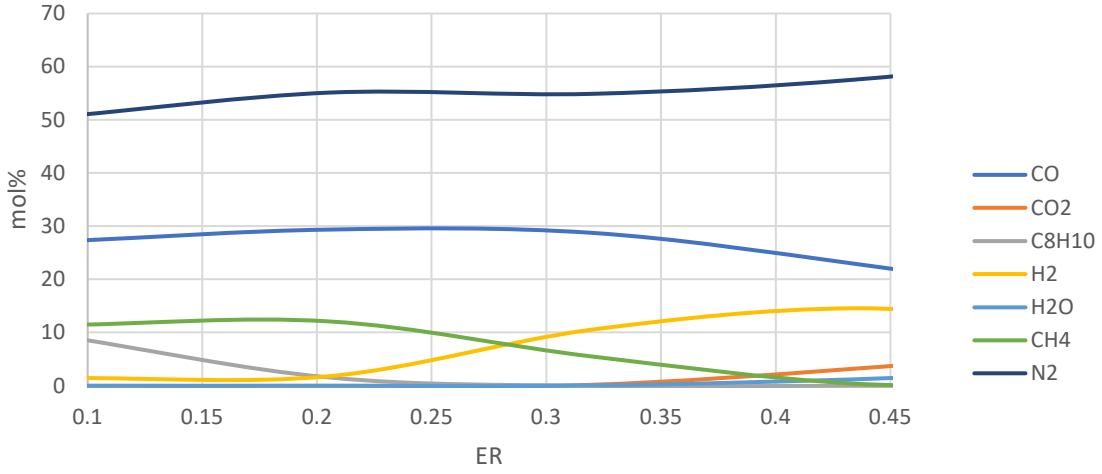

figure 38 Influence of ER on composition at T=700 °C and S/F = 0, this was computed with COCO and the Peng Robinson equations of state in with an isothermal gibbs equilibrium reactor at a pressure of 1 bar.

In figure 38 the results of the model are shown were the temperature was held constant at T = 700 °C and the S/F ratio was held constant at S/F = 0. The equivalence ratio is varied from 0.1 to 0.45. The O_2 concentration is not shown as it was zero. The C_8H_{10} has not fully converted yet at ER < 0.25. With an increasing ER the H_2, H_2O and CO_2 concentrations increase, whereas the CO and CH_4 concentrations decrease.

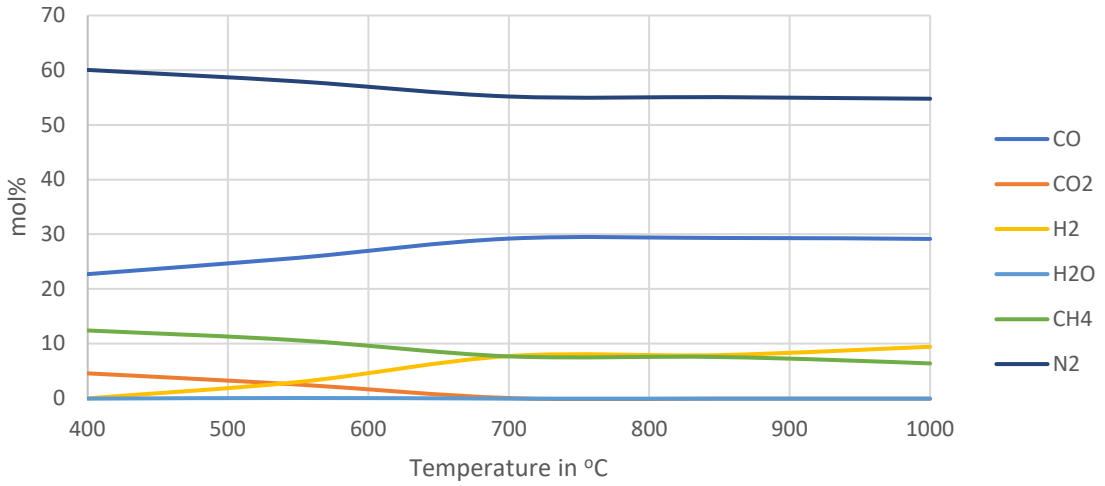

figure 39 Influence of temperature on compostition with S/F = 0 and ER = 0.3, this was computed with COCO and the Peng Robinson equations of state in with an isothermal gibbs equilibrium reactor at a pressure of 1 bar.

In figure 39 the results of the model are shown were the ER was held constant at 0.3 and the S/F ratio was held constant at 0. The temperature is varied from 0.1 to 0.45. The concentrations of C_8H_{10} and O_2 are not shown because these are zero. Until approximately 700 °C significant changes in composition can be observed. The high temperatures cause the steam reforming reaction to shift to the right causing an increase in CO_2 and H_2. However this is counteracted by the water-gas shift reaction which creates H_2O and CO from the CO_2 and H_2 produced by the steam reforming. The H_2O then stimulates the steam reforming. In figure 39 this mechanism repeats until the CO_2 concentration reaches near zero which causes a stop in the reversed water-gas shift reaction and thus consequently stopping the steam reforming of the CH_4.

9.2 Experimental

Effect of the S/F ratio and ER on the reactor temperatures

In this sub-paragraph the reactor temperatures and the influence of the S/F and ER on these temperatures will be discussed. The locations of the thermocouples discussed in this sub-paragraph can be seen in figure 40. The thermocouple in the stack (T3) seemed to be influenced by the heat coming from the flare on top of the stack. T3 generally measured higher temperatures when the flare was burning properly. To confirm this suggestion the stack temperatures were studied at the moment that the sampling pump was started which can be seen on the left side of figure 40. The stack temperature increased due to the start of the sampling pump, which probably causes a different performance of the flare which then influences the measured stack temperature. Because the stack temperature in influenced by these phenomena this temperature is not usable as a result for this study.

In figure 41 the averaged steady state temperatures of the reactor are shown. In the case that no steam is added to the system the preheat temperatures are lower than the reactor temperature at low ER (<0.2), approximately the same at an ER around 0.25 and become higher than the reactor temperature at ER > 0.25. When steam is added the reactor temperature is the same or higher than the preheat temperature. An increase in the amount of steam at low ER has a slightly decreasing effect on the system temperatures. At low ER the difference between the reactor temperatures of the experiments with steam and without steam are large, whereas this difference decreases with an increase in the ER. The temperature of the preheat is always much lower when steam is added in comparison to when no steam is added.

Note that the reactor temperatures are much lower than the temperatures calculated with the gibbs equilibrium model. Firstly this could simply be because the composition of the product gas deviates from the gibbs equilibrium composition calculated with the model. Secondly the heat losses are relatively high due to the small scale gasifier and which has a high surface/volume ratio and therefore induces heavy heat losses.

Thirdly much of the heat escapes from the gasifier due to the cooling of the oil injection lance. The lance is connected to the stainless steel lid of the 324 OD air preheating tube. This lid has a large surface area and will therefore cool the reactor gasses quite drastically.

Also note that in one experiment a steady state was reached at a temperature of 372 °C at an ER of 0.15 and an S/F ratio of 1.16. The recirculation system was partially designed to improve the lower limit of operation in terms of ER to be able to operate on low temperatures. However it can be concluded from this experiments that the lower operational limit of the ER is already far beneath the temperature at which at the pyrolysis oil is evaporated (556 °C). It is not advised to operate at these temperatures as a residue consisting of heavy oils will collect inside the reactor. Because the recommended operation temperature is much higher than the lower limit of operation, the lower operational limit is not an issue for this gasifier design.

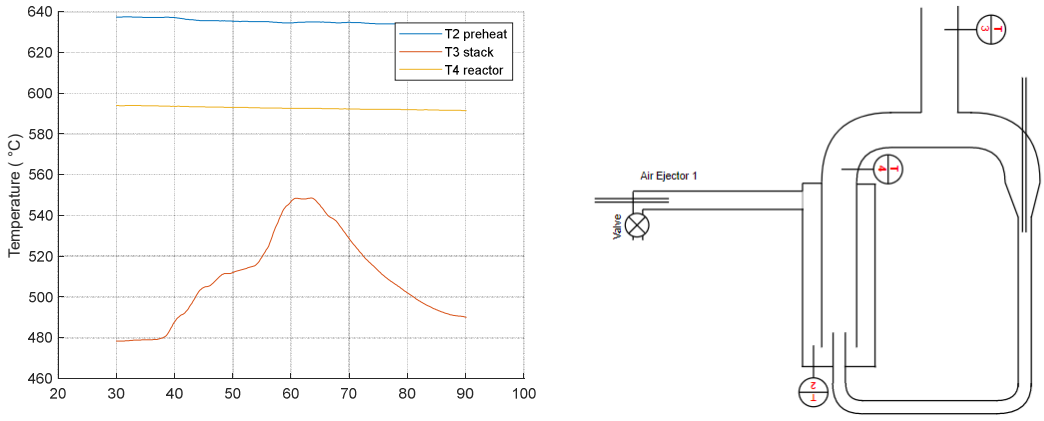

figure 40 (left) The system temperatures at the moment that gas sampling pump was started and stopped. Note that the stack temperature shows unsteady behaviour in this event. (right) The locations of the thermocouples dicussed in this sub-paragraph: T2 is the air preheat, T4 is the reactor temperature and T3 is the stack temperature.

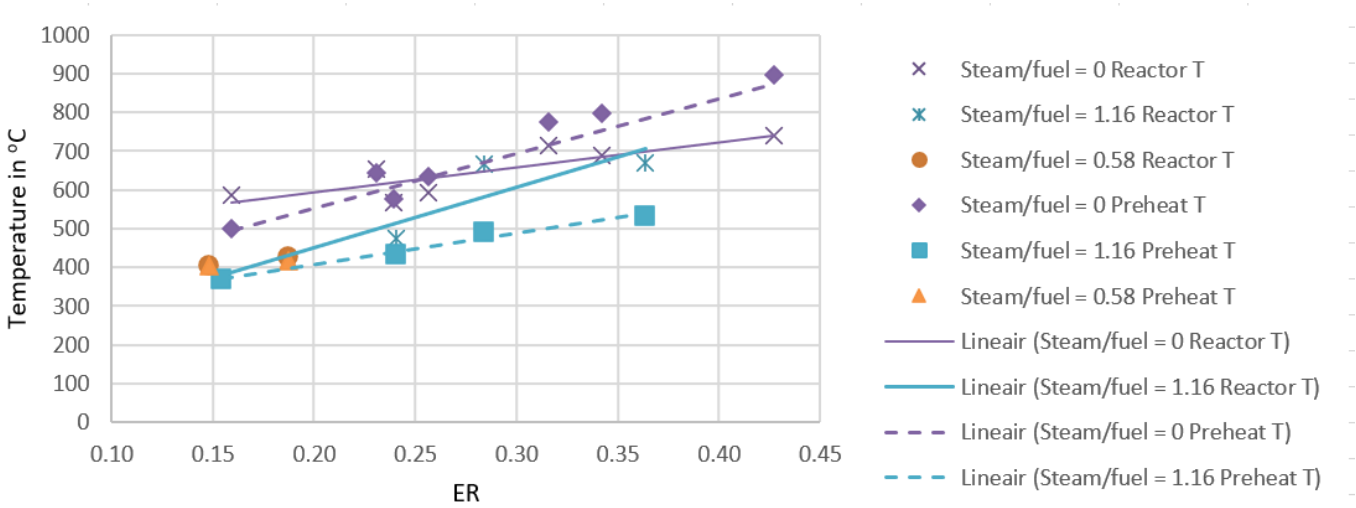

figure 41 The averaged measured steady state reactor and preheat temperatures measured during the experiments

Reactor oil usage and dry gas yield

The oil consumption measured during all the different experiments can be seen in figure 42. The oil flow during the experiments was aimed to be 4 kg/h. To have comparable experiments the oil flow should be kept constant as much as possible for the different experiments. As can be seen in figure 42 in the first experiments without steam the oil flow still fluctuated quite much because of some problems with clogging of the oil

feeding system. However in the experiments with steam these problems were solved resulted in a much more constant oil flow.

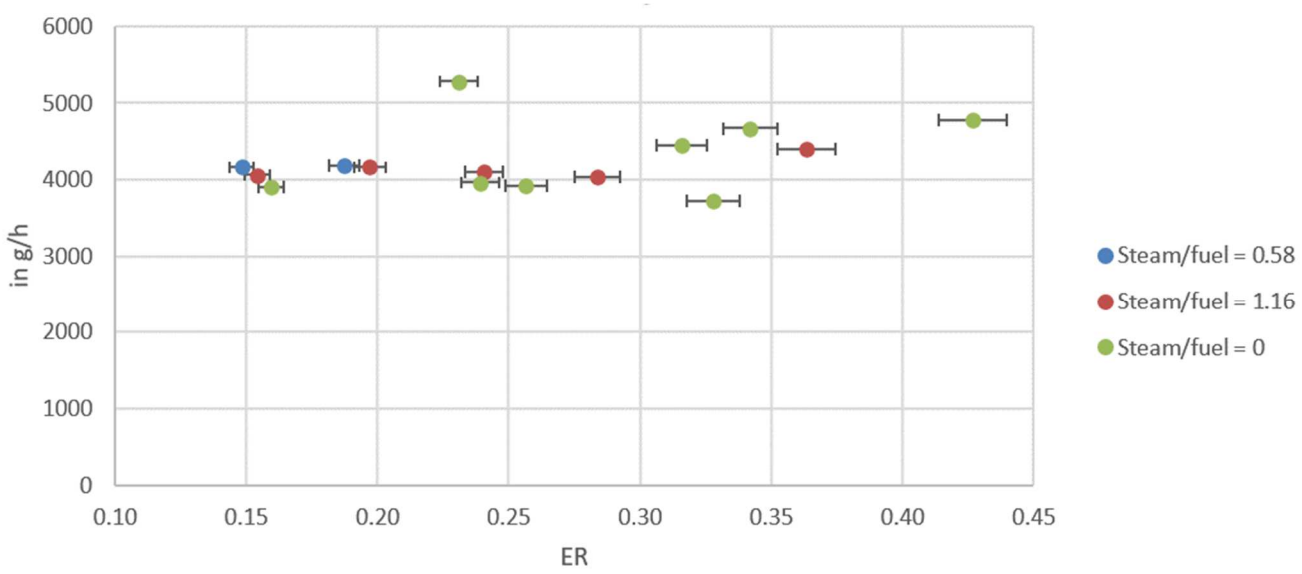

figure 42 Oil consumption during all the different experiments

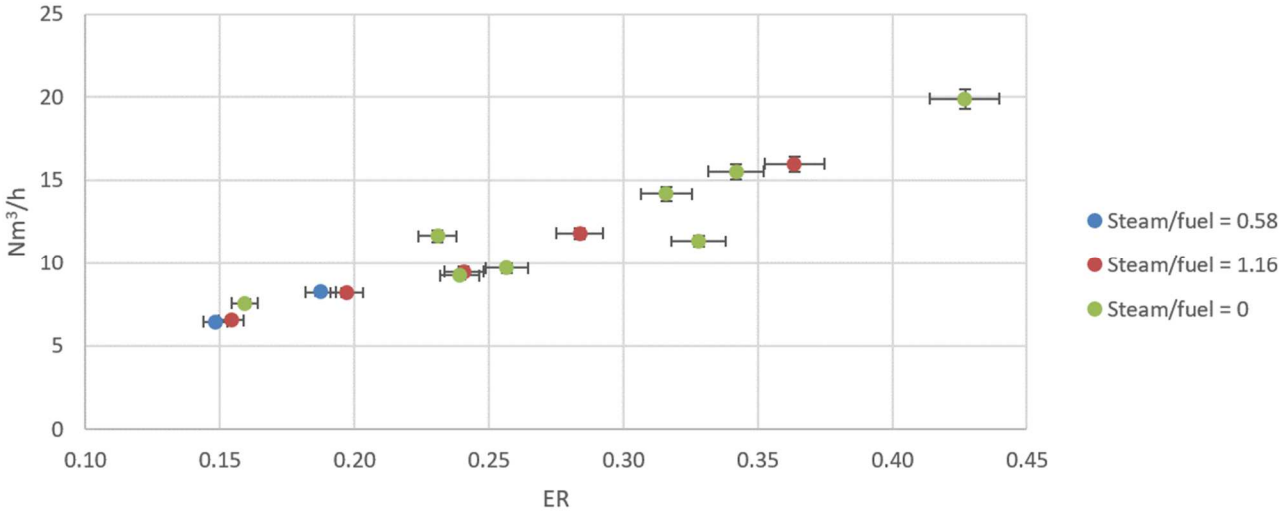

figure 43 The dry gas production during the different experiments at several ER and S/F ratio's

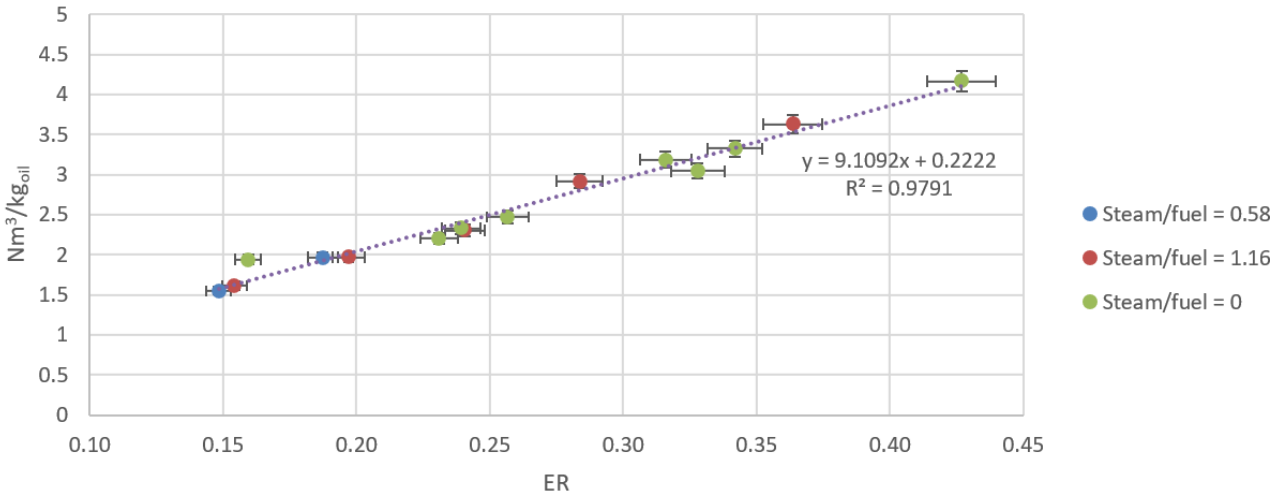

figure 44 The dry gas production per unit of oil consumption during the different experiments at several ER and S/F ratio's

In figure 43 the dry gas production is plotted for different ER and S/F ratios. If the dry gas production is expressed as a ratio between the dry gas production and the oil flow, it can be concluded that the dry gas yield per unit of oil correlates approximately linearly with the ER in the range of 0.15 to 0.43. The dry gas yield per unit of oil seems to be independent of the S/F ratio.

Effect of S/F ratio and ER on the dry gas composition and yield

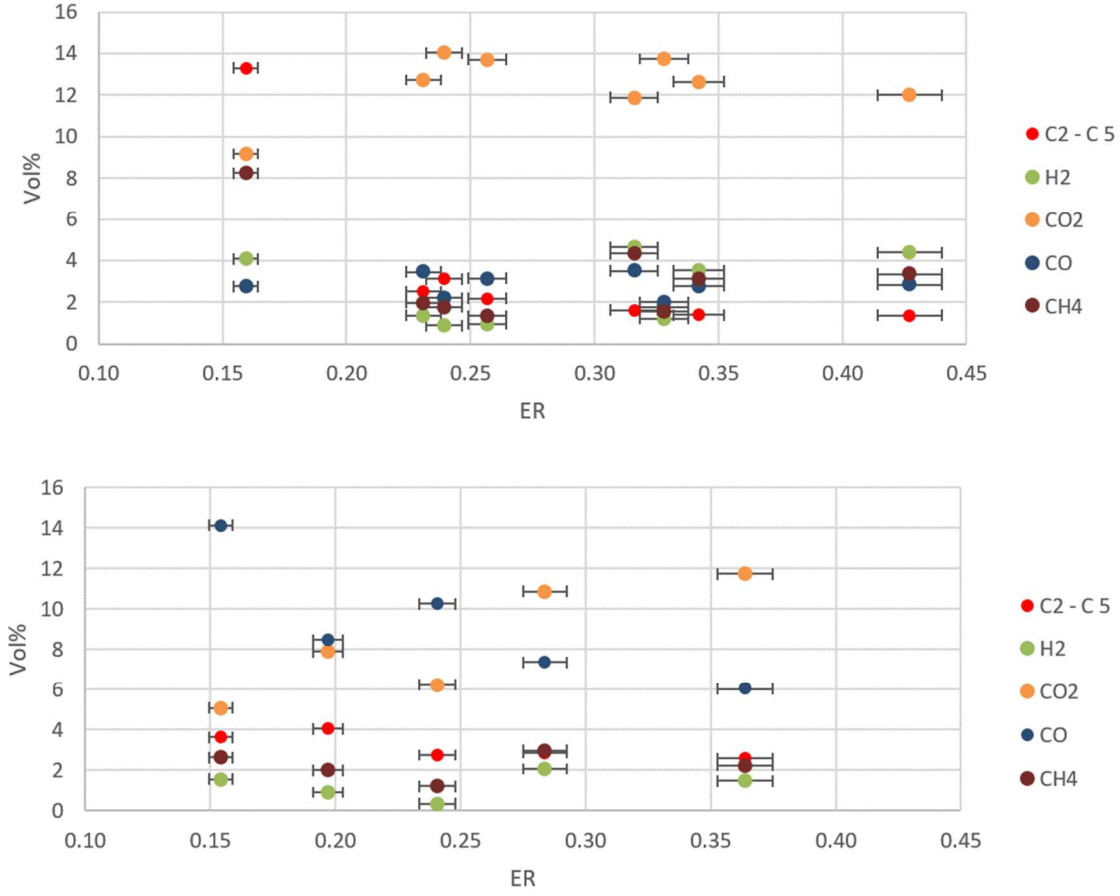

figure 45 The dry gas compositions measured where C2-C5 are all the hydrocarbons with this number of carbon molecules (upper) Measured gas composition when no steam was added (lower) measured gas composition when steam was added with an S/F ratio of 1.16

In figure 45 the gas compositions for the experiments with an S/F ratio of 1.16 and 0 are shown. Note that the CO_2 concentration is always higher than the CO_2 concentrations in the equilibrium compositions in figure 37, figure 38 and figure 39. The N_2 concentrations are not shown, but the remainder of the gas consists of N_2. In both cases an increase in ER seems to reduce C2 – C5 concentration. When no steam is added an increase in ER does not change the composition of the gas, except when ER ≈ 0.15. At this low ER the gas has a different composition, having a high C2 – C5 and CH_4 composition while having a relatively low CO and CO_2 composition. The main effect of steam addition that can be observed is a rise in CO concentration, while the CO_2 concentration decreases due to steam addition. This is contradicts the effect of steam and temperature on the equilibrium composition as shown in figure 37 and figure 39. At higher ER the effect of steam on the composition becomes less significant. When steam is added the ER has a reducing effect on the CO and an increasing effect on the CO_2 concentration, this is in accordance to the effect of the ER on the equilibrium composition as shown in figure 38. The H_2 levels are generally lower than when no steam is added. At higher ER the composition becomes more alike the composition when no steam is added.

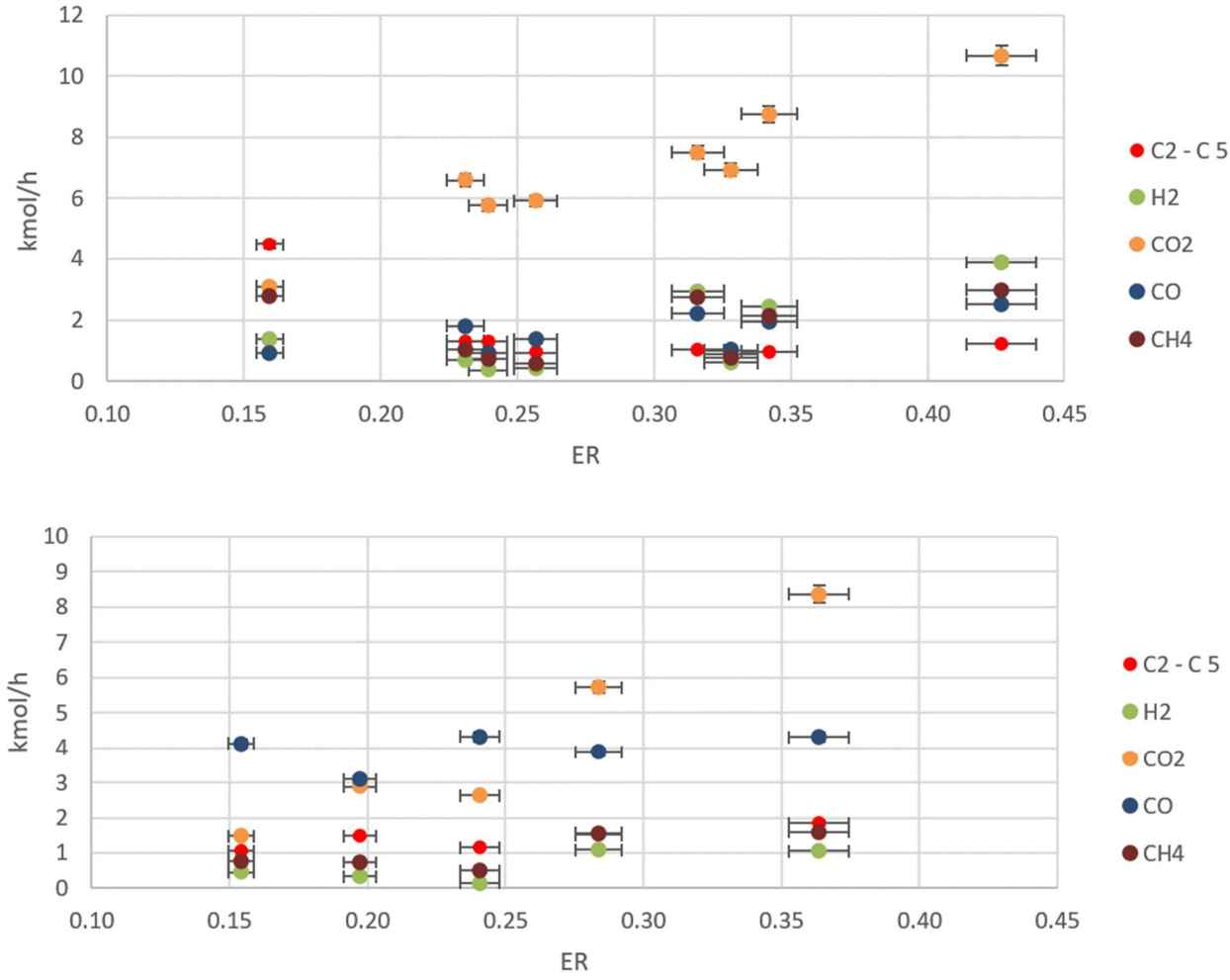

figure 46 Yield of product gas components when no steam is added (upper) and when steam is added with a S/F ratio of 1.16 (lower)

In figure 46 the total yield of the product gas components are shown for different ER and S/F ratios. This is the product of the dry gas yield with the dry gas composition. As concluded before the dry gas yield was independent of the S/F ratio and depended linearly on the ER, therefore the differences in yields of the products between de different S/F levels are mainly caused by a difference in gas composition. For both series of experiments the CO_2 concentration increases with the ER. When ER ≈ 0.15 and S/F = 0 is not taken into account all the yields of the components seem to increase for S/F = 0 with an increasing ER except for the C2 –

C5 concentration. In the case that S/F = 1.15 all the yields of the single components seem to increase with the ER except for the CO concentration.

Char, tar and condensate in the product gas

The char, tar and condensate measurements did not result in any accurate indication of the char, tar and condensate yield. The char and tar measurements were done by measuring the weight difference of the steel wool that was placed inside the condenser tube. The char and tars did deposit on the steel wool, however due to this deposition the chars and tars clogged the condenser causing a large reduction in pressure of the flow going into the constant volume displacement extraction pump. Because of the drop in pressure and thus a drop in density of the gas, the flow through the condenser was not comparable between the experiments. The depositions that were measured during the experiments are summarized in figure 47.

The condensate measurements encountered another additional problem. The condensate did not settle in the condenser so that it could be collected at the valve at the bottom of the condenser. However, it was entrained in the flow and settled in the oil of the extraction pump or was pumped out with through the gas sampling tube. It could be observed that condensed water and oil came out of the gas sampling tube, and that the oil of the extraction pump was heavily contaminated after the experiment. The temperature of the gas going into the pump was also checked and this was approximately at 25 °C, indicating proper cooling of the hot product gas. The problem with the condenser is probably that the gas velocity is to high for the condensate to settle on the walls.

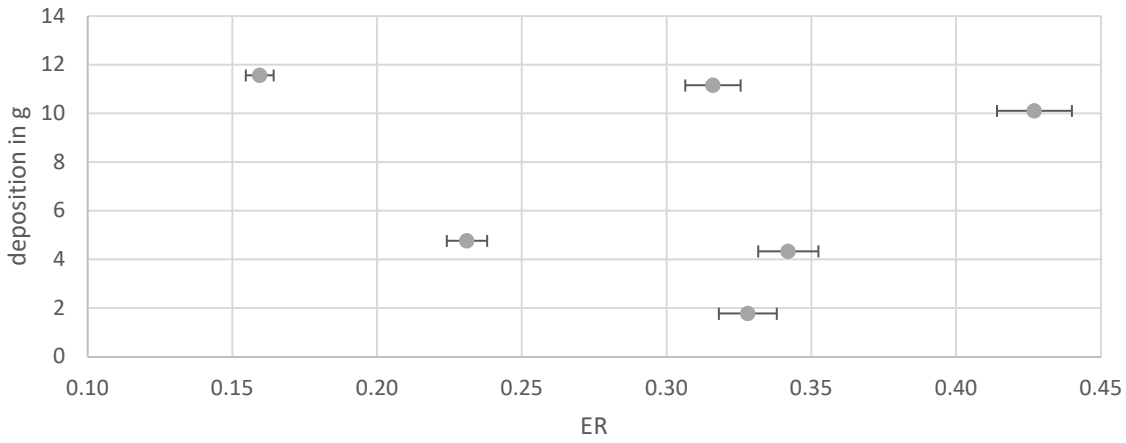

figure 47 Char and tar deposition on the steel wool in the condensate tube with an S/F ratio of 0.

Effect of the S/F ratio and ER on the LHV, CCE and CGE of the gasifier

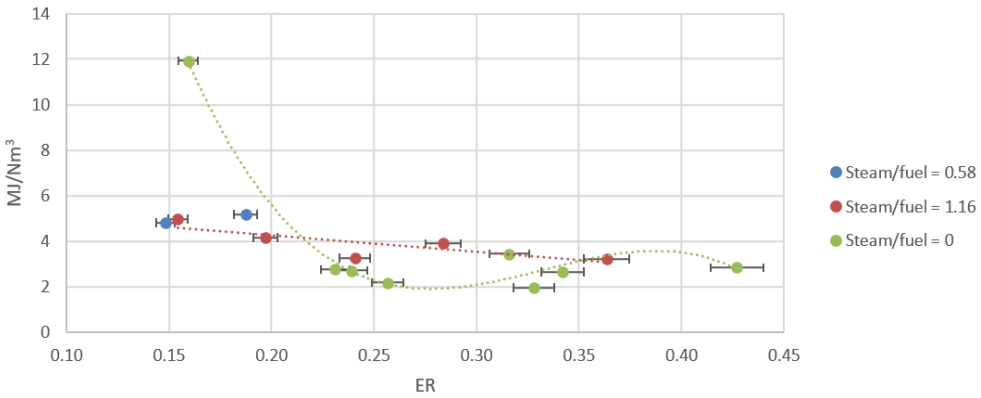

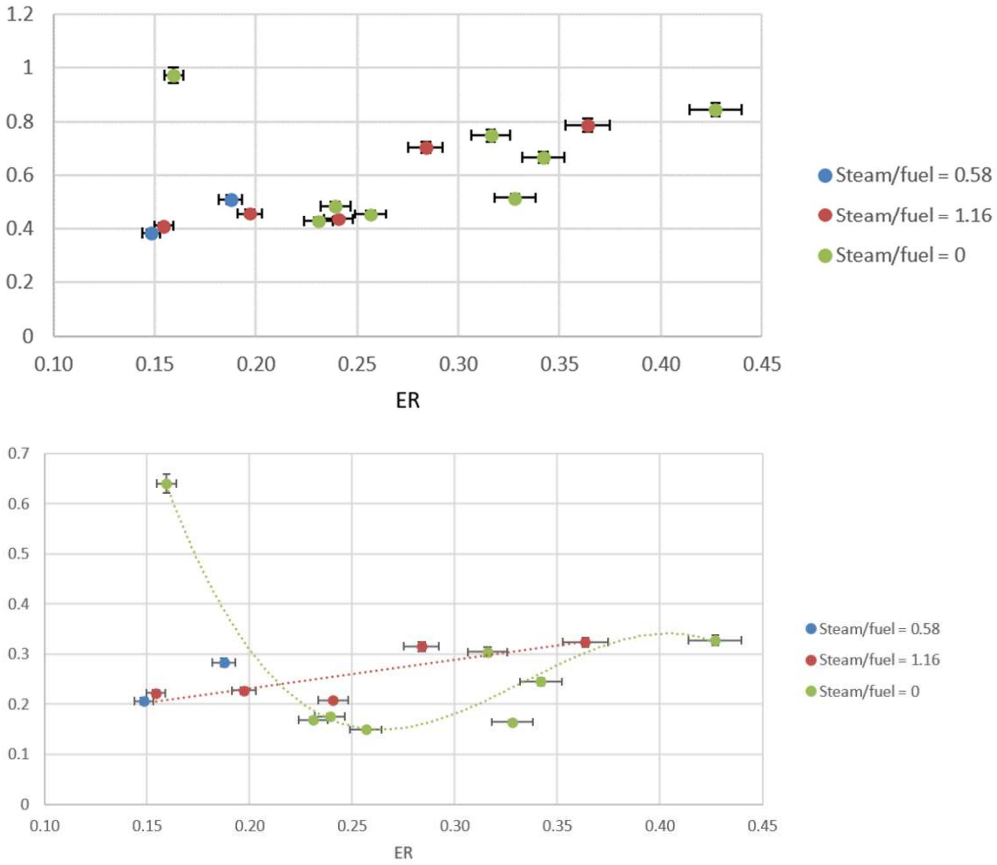

figure 48 (upper) Lower heating value of the dry product gas (middle) CCE for all different experiments (lower) CGE for all different experiments

In figure 48 the LHV, CCE and CGE of the dry product gas are shown for all the different experiments. The LHV, CCE and CGE are highest when S/F = 0 and ER ≈ 0.15 and were 11.9, 0.97 and 0.64 respectively. The composition of the gas was also very different for this gasifier configuration. However it should be noted that if a steam is added in this configuration the output of the reactor changes drastically, this is an indication that this is not a robust configuration of the gasifier as the output depends strongly on the composition of the input. An increased S/F ratio seems to have a slightly increasing effect on the LHV, CCE and CGE on the ER range of 0.25 to 0.3. At higher ER (ER>0.35) the LHV, CCE and CGE of the gasifier does not differ much due to a change in S/F ratio. Therefore it can be concluded that the output of the gasifier for energy purposes has a lower dependency on the input of the gasifier at these higher ER's. At the higher ER's the maximum CCE and CGE were found at ER = 0.427 and S/F = 0 and were 0.84 and 0.33 respectively.

The CGE found in this work differed much from the CGE's generally found in literature. The relation of the CGE and the ER found in literature in a study of Zhengh et al. (2016) for the gasification of bio-oil in an externally heated entrained flow gasifier at 1000 °C can be found in figure 49. The maximum CGE for gasification with air peaked at ER = 0.3 and was 74%. This is probably caused due to the higher reactor temperatures in the gasifier.

In the research of Tsekos et al. (2021) the gasification of woody biomass in a indirectly heated bubbling fluidized bed steam reformer was studied. The thermal power of 50 kW of the reactor was comparable to the thermal power in this work of 40 kW. The CGE and CCE that were found for the externally heated system were approximately up to 0.83 and 0.93 at an ER of 0.2 and a S/F ratio ranging from 0.8 to 1.2. However the overall efficiency of the system was at maximum approximately 0.43. Because the gasifier in tested in this thesis in an autothermal system the CGE of the system should be compared with the overall efficiency allothermal gasifiers. In this work an non-robust operation configuration was found with an CGE of 0.64 and a more stable configuration where the CGE was 0.33. These first CGE is much higher than the overall efficiency found in the

work of Tsekos et al.. However at the more robust point of operation the CGE is lower than in the work of Tsekos et al..

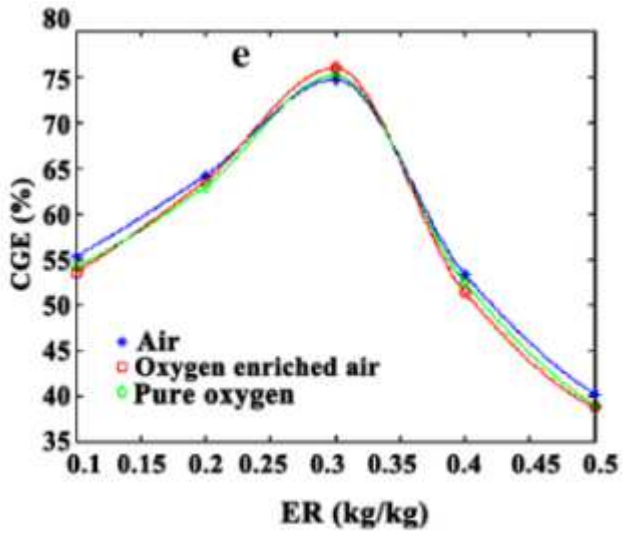

figure 49 The CGE found in an externally heated bio-oil air/oxygen entrained flow gasifier at 1000 °C (Zheng et al., 2016)

Effect of temperature on the CGE

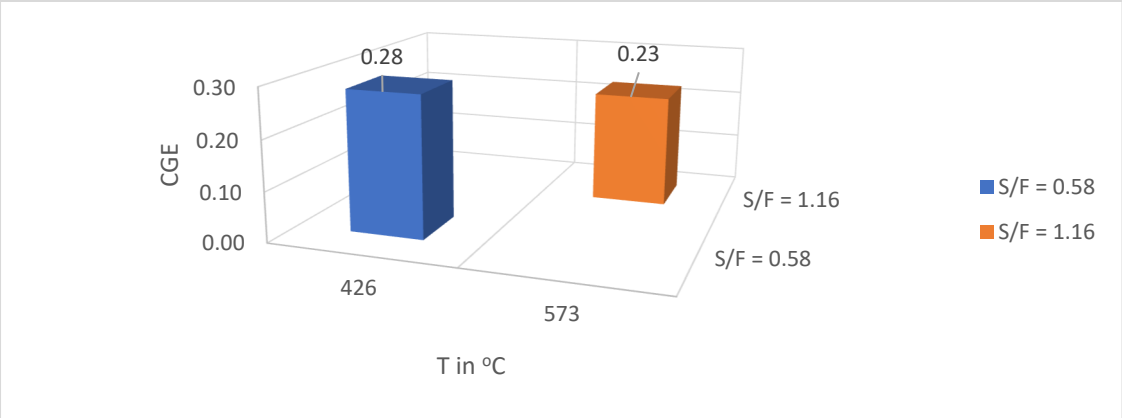

figure 50 The CGE at ER ≈ 0.2 at different temperatures and different S/F ratios. The 426 °C temperature was the steady state temperature for these conditions, the 573 °C experiment was in unsteady state with a preheated reactor

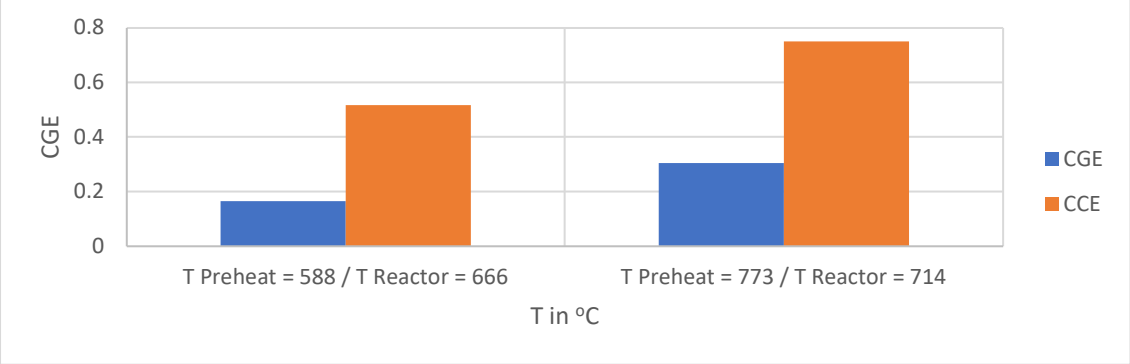

figure 51 The CCE and CGE at ER ≈ 0.32 and S/F = 0 at (left) low temperature in unsteady state and (right) at high temperature in steady state conditions

In figure 50 a comparison is made between two experiments where one experiment was done at low temperature, being the steady state temperature for this configuration. And one experiment at 147 °C higher, which was not in steady state for the corresponding configuration, with a preheated reactor. This ER of both experiments were both ER ≈ 0.2. The experiment was done to give an indication if a slight increase in temperature and S/F ratio could increase the CGE in this configuration. This could be expected because the temperature and the S/F ratio both stimulate the endothermic gasification reactions like the steam reforming reaction as discussed in Ch. 9.1. However instead of increasing the CGE, the CGE decreased from 0.28 to 0.23. This could be explained by stimulation of certain endothermic reaction by an increase in temperature which convert the oil into non-volatiles.

The effect of temperature change at a higher temperature can be derived from 2 experiments that have a comparable ER of 0.32 and a S/F ratio of 0. The resulting CGE and CCE of these experiments can be found in figure 51. The low temperature experiment was the experiment where the reactor was not yet in steady state, the high temperature experiment was the experiment where the reactor was already in steady state. The CGE and CCE increased from 0.16 and 0.53 to 0.30 and 0.75 respectively. Thus concluding that at this higher ER and higher temperature the change in temperature does have a increasing effect on the CGE. This could be caused by the stimulation of the endothermic reactions at the high temperatures.

Lessons learned from the operation of the experimental setup

Figure 46 Char deposit with an ash content of 11.0 m% in the reactor tube after operation at low temperature below the end of the boiling curve (566 °C)

In Figure 46 the deposited char is visible which was produced during operation at temperatures below the end of the boiling curve (566 °C) of the DKR350 pyrolysis oil. Char was deposited on the wall due to the evaporation of the volatiles. This learns that this method in not useful at these lower temperatures. What also can be seen in Figure 46 is that the structure of the gasifier is completely conserved. This means that despite the high preheating temperatures of up to 900 °C the temperatures never reached near the melting point of the stainless steel. This shows that no ceramics are required to ensure the structural integrity of such a gasifier at high temperatures. However a more corrosive resistant stainless steel alloy could be preferred above the AISI 304 that was used in this reactor.

figure 47 (left & right) Heavy soot deposition in the 60 mm recirculation tube with an ash content of 2.42 m%

In figure 47 the soot deposition in the recirculating tube can be seen. This soot deposition caused the clogging of the pitot tube and was part of the cause of the poor performance of the recirculation system as described in Ch. 8.5.

figure 52 (left) Look-through to the oil injection tube showing a clean tube after operation indicating no charring inside the oil injector lance. (right) Heavy charring on the outside of the water cooled oil injector lance, however the outlet of the oil injector is clean

The in and the outlet of the oil injection tube after operation can be seen in figure 52. Heavy char deposition on the outside of the injection lance can be noticed. However the inside of the oil injection lance is clean. This indicates adequate cooling of the injection nozzle and thus preventing charring and eventually clogging of the oil injector. The injector was cooled with water and therefore always <100 °C.

figure 53 (left) Tubing with tar deposition visible after operation with DKR350 pyrolysis oil and after flushing with diesel. (right) A broken oil pump used in the experiments which got clogged with the tars from the DKR350 pyrolysis oil

Tar deposition from the oil in the pumps and the tubes caused clogging of both the pumps and the oil lines as can be seen in figure 53. The tars did pass through a fuel filter for cars, therefore filtering is not the solution for this oil. A more robust pump should be used for handling the oil. The tars left in the oil feeding lines dried out after tests and became a solid material. This caused clogging in the oil lines during next operation of the system. The clogging can partially be prevented by flushing the feeding system after operation with a solvent for the tars. For this system diesel was used as a flushing fluid and water was used as a conservation fluid to prevent the tars from turning into a solid. However, the tars did not solve well in the diesel which can be seen in the left picture of figure 53 where the tubing is shown after operation and flushing with diesel.

Composition and autoignition characteristics of the char and soot deposit

The char and soot that is deposited on the reactor walls should be removed. This could be done by combustion. To test the combustibility of the char and soot deposit an autoignition and combustion test was performed on the char deposited on in the reactor tube as seen in Figure 46. In figure 54 the char sample that was tested can be seen before the combustion test and after the combustion test. The red color of the ash indicates a high concentration of iron which could come from the reactor wall or from the oil, as the oil contains 431 mg/kg of iron according to the lab report in appendix A. After heating the char up to 850 ^{o}C in a cup as in appendix B the weight of the residue reduced to 32% of its original weight. The char auto ignited at approximately 400 ^{o}C. The ash content of the char sample in figure 54 was determined in a commercial lab and was determined to be 11.0 m%.

figure 54 (left) The char with an ash content of 11.0 m% that was deposited in the reactor chamber at low temperature (<500 ^{o}C) operation with low equivalence ratio (<0.25) and high S/F ratio (≥0.58). (right) The leftovers of the char after heating the sample up to 850 ^{o}C with a fresh air supply. The red color could indicate a high concentration of iron in the char.

The soot that was deposited on the walls in the rest of the system was also collected and an autoignition/combustion test was performed on the sample. The tests performed can be found in appendix B. From these tests it was concluded that in an oxygen poor environment the soot ignited at 674 ^{o}C. The soot was completely combusted after heating it up to 790 ^{o}C with a negligible amount of ash left. Also, it was shown that in an environment with a higher oxygen supply the soot already fully combusted at a temperature of 660 ^{o}C. The ash content of the soot was determined in a commercial lab and was determined to be 2.43 m%.

10. Evaluation of the preliminary gasifier design and implementation

In this chapter the preliminary design and implementation will be evaluated with the results of the modelling and experiments.

The assumption in Ch. 5.3 that the product gas still contains a high amount of char, tar and other condensables is correct according to the low carbon conversion that was measured in the experiments and the char, tar and other condensates that were collected in the condenser. This means that the product gas should be cleaned in a gas treatment system as described in the implementation plan of Ch. 5.3. The product gas should therefore be combined with the pyrolysis gas and should therefore not exceed 600 ^{o}C. However the operation modes with ER > 0.3, which have a relatively high CCE and CGE, produce gasses with a higher temperature than 600 ^{o}C. Therefore there is need for gas cooling to prevent damaging the pyrolysis/gas treatment system.

The effects of recirculation could not be measured. Therefore no conclusions on the effect of recirculation on the stability or conversion can be derived. Also no conclusion can be made on the idea of evaporating the oils in the recirculating tube to increase the stability of the gasifier and to increase the conversion of the oil. However, the stability of the system does not seem to be an issue as tests were performed at reactor temperatures of <372 ^{o}C. Operation in steady state was possible at these temperatures indicating stable operation. Therefore the need for a stabilizing mechanism like the recirculation in the preliminary gasifier design is not required.

The in feeding into the reactor can be done with evaporation on the hot reactor wall instead of using an atomizer. With the right gasifier settings a carbon conversion of >0.8 can be achieved. A carbon conversion of almost 1 was also measured but this setting was less robust because the composition of the gas drastically changed after adding steam while keeping the rest of the settings constant. It could not be concluded if the unconverted carbon stayed in the reactor as solid carbon, or was entrained as solid carbon in the gas or was converted into volatile hydrocarbons. However, because the carbon conversion was reasonably high, it can be concluded that only a small amount of char formation on the reactor walls can occur. Therefore the evaporation on the reactor walls is a viable option for configurations with higher ER's. The CCE much lower than 1 does however indicate the need of gas cleaning as it indicates unconverted carbon in the product gas.

A cleaning program should be formulated where the reactor is heated to approximately 800 ^{o}C whereafter a sufficient supply of air is fed into the reactor which causes combustion of the char. The autoignition tests performed on the char deposition showed that in this manner all the char will be combusted whereafter only a small amount of ashes are left.

In figure 55 the final adjusted design for the gasifier is shown. No recirculation system is added this time because additional stabilization appeared to be unnecessary. An air preheating system is added as an increased temperature seems to have an increasing effect on the CCE and CGE. The gasifier chamber will be isolated to increase the residence time of the gas at high temperatures, after the isolated section the heat exchange with the air will be maximized to cool down the product gas and preheat the air. The oil is in injected with a water-cooled injection lance whereafter the oil flows and evaporates on a tilted reactor wall. The tilted position of the gasifier will ensure proper flow of the oil into the hot parts of the reactor, also of the heavier oil fractions.

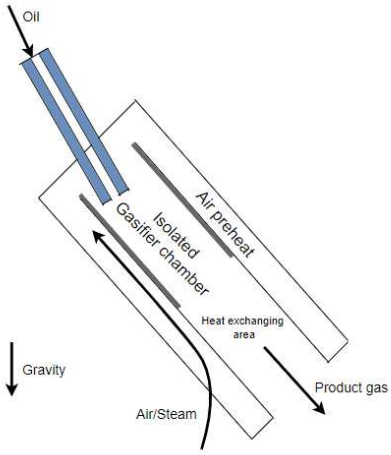

figure 55 The adjusted gasifier design. The gasifier is in tilted position to ensure proper distribution and flow of the oil over the gasifier chamber wall. The air is preheated with the product gas and the oil is injected with a water cooled injector.

From this study it cannot be concluded if the same gas treatment system can be used as for the pyrolysis gas. That is because the concentration of contaminants determining the need for gas treatment were not determined in this study because the gas sampling system did not perform as designed. It can however be concluded that the LHV of the product gas will be around 4 MJ/Nm^3 which is much lower than the 38 MJ/Nm^3 of the pyrolysis gas. To create a thermal output of the gasifier which is comparable to thermal power of the pyrolysis gas, the normalized volumetric flowrate of the product gas should be approximately 10 times the normalized flowrate of the pyrolysis gas. This large difference in flowrates could be a problem for the gas treatment system if the gasifier is implemented in such a way that it uses the same gas treatment system. In this study it is however assumed that the same gas treatment system should be used because the concentration of contaminants in the product gas is still unknown.

In figure 56 on the left the implementation of the gasifier without any heat integration can be seen. This will be called implementation option 1. The system uses the same gas treatment system as the pyrolysis reactor. In figure 56 on the right the resulting flowsheet can be seen with the components added marked in red. If the gasifier operates at an ER = 0.43 and a S/F = 0, the CGE = 0.33 according to the results of the experiments in this study. With this thermal power an additional 0.17 MW in thermal power of the product gas is created. To the total WER unit this delivers an increase of 0.17 MW / 2.5 MW = 6.8 percent point in thermal efficiency.

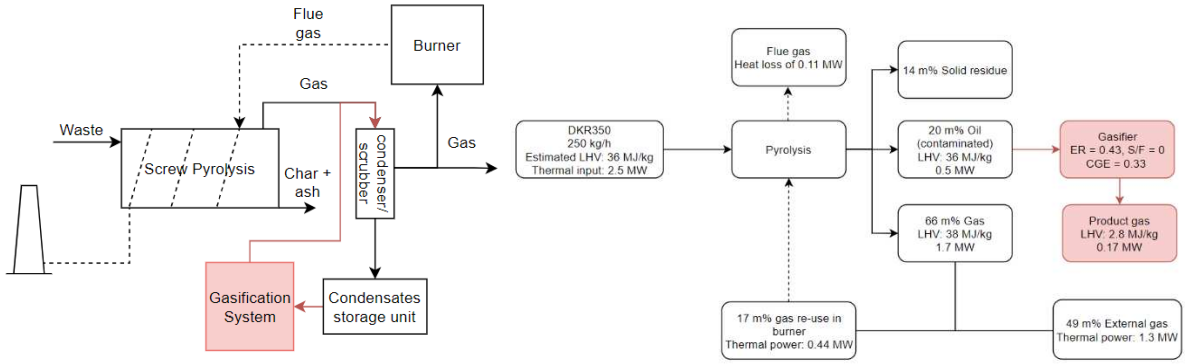

figure 56 Implementation option 1: (left) Example of implementation where the same condenser/scrubber system is used with the adjustments to the existing system in red. (right) The flowsheet with the adjustments on the left, with a gasifier operating on an ER = 0.43 and S/F = 0 with the CGE of 0.33 as determined in this study. The increase in thermal power of the product gas is 0.17 MW.

The gasifier could also replace the burner of the system which operates on the product gas. This gives the option of heating the system on the produced oils instead of heating it with the product gas. If a high supply of

oils is then produced the gasifier can be switched to gasification mode. Also, if it is switched back to burning mode is would burn the system clean of the deposited char and tars. Another advantage of this configuration would be that the gasifier is always on temperature and therefore there is no startup time delay when power is required. The startup burner of the gasifier can then also act as the backup burner for the pyrolysis system.

In figure 55 on the left side implementation option 2 is shown where the burner is replaced with the gasifier. The product gasses of the gasifier can either preheat the screw pyrolysis reactor whereafter they are joined with the pyrolysis gasses to go to the gas treatment system. Or if the gasifier is in combustion mode the flue gas can leave through the chimney after circulating the pyrolysis reactor while simultaneously cleaning the system of carbonaceous deposits. On the right of figure 55 the resulting flowsheet can be seen of implementation option 2. By replacing the burner, 0.44 MW of pyrolysis gas is saved. The remainder of the oil will be gasified in gasifier mode at ER =0.43 and S/F = 0, and thus according to the experiments with an CGE of 0.33. This will deliver an additional 0.02 MW. Thus the total increase of the thermal power of the WER unit will be 0.46 MW. This is an increase of 0.46 MW / 2.5 MW = 18 percent point in thermal efficiency. This is significantly more than the 6.8% gained with implementation option 1. However it should be noted that implementation option 2 could give problems due to deposition of tars and chars on the heating mantle of the pyrolysis reactor, which will reduce the heat transfer into the pyrolysis reactor.

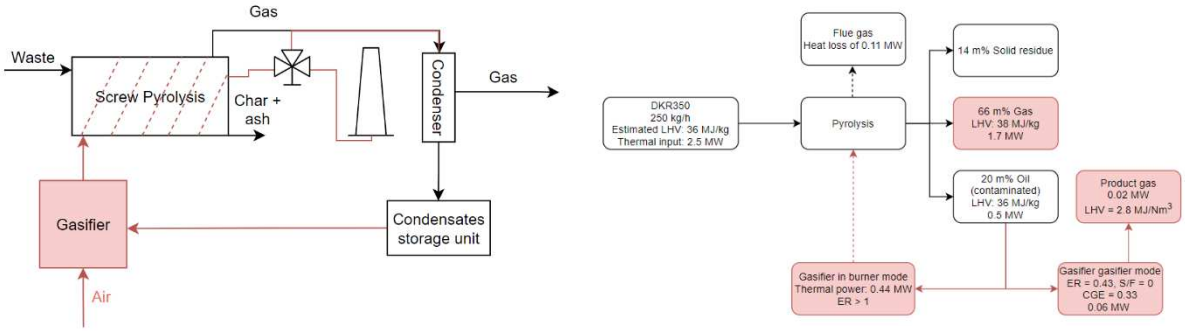

figure 57 Implementation option 2: (left) The design for the gasifier implementation where the same condenser/scrubber is used as for the pyrolysis gas and where the gas burner of the system is replaced by the gasifier. The added equipment is marked is red. (right) The resulting flowsheet with the adjustment of the system on the left. Because the gasifier replaces the gas burner the thermal output of the gas of the system increases with 0.44 MW. If the remainder of the oil is also gasifier the thermal power increases with 0.46 MW.

11. Conclusions

In this study a design was proposed and experimentally validated for the gasification of pyrolysis oil at small scale for energy applications. The gasifier was designed to be implemented at an existing waste energy recycling (WER) unit at Waste4me B.V. which processes waste streams in a pyrolysis reactor. The pyrolysis oil investigated in this study was produced from a DKR350 waste stream. To come up with a suitable design for the gasifier the current WER unit at the company was first reviewed to give a context to the design. From this context of design, the design constraints and criteria were formulated. Then a literature study was done into the different reaction occurring during gasification. Also the four different already commercially applied gasifier types, namely: Entrained flow, molten salt, fluidized bed and fixed bed were reviewed in literature and the relevant knowledge for the gasification of DKR350 pyrolysis oil was collected. With this knowledge the gasifier type 'non-slagging autothermal entrained flow low temperature gasifier' was selected as the best fit to the design constraints and criteria and shall therefore be implemented at the WER unit for the gasification of the DKR350 pyrolysis oil. Also a plan was proposed for the implementation of the gasifier, which was evaluated later on in the study. Next the selected gasifier type was further detailed into a conceptual preliminary gasifier design. The gasifier will operate at low temperatures to minimize the costs of construction of the gasifier, to maximize the efficiencies, to prevent slagging and to minimize startup time. However due to the lower rate of reactions at low temperatures, it can become harder to control the reactor, therefore it was tried to design a reactor which is robust in terms of properties of the feed oil. Also, the reactor should be controllable for different inputs and the caloric output of the gasifier should also be controllable to be able to meet a certain energy demand. Besides these properties the gasifier should still have a reasonable cold gas efficiency and carbon conversion. A design was proposed which aimed at meeting all these requirements. The design is a low temperature, air blown, non-slagging, autothermal entrained flow gasifier with a recirculation system which potentially enhances the robustness and the conversion of the gasifier. Then a simplified experimental setup is designed to validate the potential performance of the designed gasifier. The main aspects that were studied in these experiments were the lower limit of operation of the equivalence ratio (ER), the effects of recirculation, the composition of the product gas at different ER and steam/fuel (S/F) ratio's, the carbon conversion- and cold gas efficiency (CCE and CGE) and the performance of the oil injector and evaporator, which was an alternative system to the commonly used atomizers. The composition of the product gas was determined with a gas chromatograph for different ER and S/F ratios. After commissioning it became clear that the effects of recirculation could not be investigated as the performance of the recirculation system was not as designed. The conclusion derived from the results of the experiments were as following:

- The dry gas yield per unit oil increases approximately linear with the ER in the range of ER of 0.15 to 0.43 and is independent of the S/F ratio.
- The actual compositions deviated significantly from the compositions that would be expected from the gibbs equilibrium composition, therefore this is a poor predictor of the gasifier performance.
- The CO_2, H_2, C2-C5 concentrations decreased whereas the CO concentration increased with the addition of steam. The effects of steam on the CO_2, H_2 and CO concentrations contradict the effect of steam on the composition of the equilibrium composition.
- With a S/F of 1.16, an increase in the ER resulted in an increase of the CO_2 concentration, and a decrease of the CO concentration, which is expected from the effect of the ER on the equilibrium composition
- The highest CCE and CGE were found at an ER = 0.16 and S/F = 0 with values of 97% and 64% respectively, although to ensure a robust operation of the gasifier different settings are recommended as a high reduction in LHV, CCE and CGE was found when steam was added to the system.
- At ER > 0.35 the output of the system becomes less dependent on the input of the system, meaning that the composition, LHV, CCE and CGE became similar for different S/F ratios.
- CGE and the LHV of the dry gas increased slightly due to steam addition between ER 0.24 and 0.3.

- Carbon conversion is highest at ER=0.16 without steam. For the rest it increases with ER up to approx. 0.8 at higher ER's.
- At ER = 0.2, an increase in S/F ratio and temperature does not influence the dry gas composition
- At high temperatures (>580 °C) temperature seems to have an increasing effect on the CCE and CGE, while on low temperature (<580 °C) the opposite effect was found. However more data should be collected to draw a final conclusion on this topic.
- The oil injector showed no charring or clogging and while experiments showed reasonable CCE's and CGE's. Therefore it is concluded that the used oil injector is a suitable alternative for the commonly used atomizers.
- The water cooled injection lance prevented charring in the injector
- From the experiments it was concluded that the lower limit of operation of the (ER) is lower than 372 °C as the gasifier reached steady state at this temperature.

The gas sampling system did not perform as designed. The yield of condensable hydrocarbons, water and entrained char could therefore not be determined, and thus the CCE of the dry product gas is the only known value of the carbon mass balance.

With the knowledge gained from the experiments the preliminary gasifier design and the plan for implementation in the WER unit at Waste4me B.V. was then evaluated. For the implementation it was concluded that the product gas does need to be processed in a gas treatment system to clean it from the condensables and solid particles. Also, there is a need for cooling or heat exchange before the gasses can be combined with the pyrolysis gasses to prevent overheating and damaging the pyrolysis gas treatment system.

The effects of the recirculation on the stability as defined in paragraph 7.1 were not measured as the recirculation system did not meet the required performance due to heat losses. However, it was concluded that the lower limit of operation of the ER is below 372 °C and therefore there is no need anymore for a system which lowers the lower limit of operation even further as the reactor delivers a very poor performance at these temperatures in terms of LHV, CCE and CGE. Therefore, the operational temperature will be much higher and thus the lower operational limit will never be reached.

The CCE with the evaporation of the oil on the hot reactor wall was high (>0.8) for several configurations. It is therefore concluded that the evaporation system is a viable alternative for the atomizer, especially for the small scale installations as the channels of small scale atomizers clog easily.

The optimal configuration of the gasifier is at an ER > 0.35 because in this region the output of the gasifier becomes less dependent on the S/F ratio, indicating lower dependency of the output of the gasifier on the input of the gasifier. Also, at ER > 0.35 the CGE and CCE are larger except for the single configuration of ER = 0.16 and S/F = 0. Steam can be added to alter the composition of the product gas, but steam addition does not alter the CGE and CCE significantly at an ER > 0.35.

The char and tar collected from the reactor walls were combusted with ambient air and showed that only a negligible amount of ashes was left at 790 °C. Therefore, a combustion program is recommended for periodical cleaning of the gasifier.

For the implementation 2 options are proposed. In the first option all the pyrolysis oil is gasified with an CGE of 0.33, increasing the thermal efficiency of the WER unit with 6.8 percent point from 52% to 58%. In implementation option 2 the gasifier replaced the burner, which will result in an increase of thermal efficiency of 18 percent point of the WER unit to 70%.

12. Recommendations

For the implementation of gasifier as the heating system of the WER unit the parameters that can influence the product temperature of the gasifier should be investigated further with an experimental study. To fully replace the burner of the WER unit it should also be studied if for all the waste compositions that are processed with the WER unit there is enough oil production to heat the system.

Further heat integration could also be studied, where the air is preheated with the heat of the pyrolysis reactor for example. However, this would make the two reactors dependent on each other and therefore it is important that also the effects of preheating the air are researched to determine the effects on system output and process conditions. Also, the preheating of the air could be interesting to study as this could potentially improve the CCE and CGE. According to Le Chatelier's principle the endothermal gasification reactions are stimulated at higher temperatures which would improve the CCE and CGE. An indication for this effect was also found in this study of this effect between two different experiments at temperatures above 580 ^{o}C where the CCE and CGE improved with temperature. However, at low temperatures the opposite was true, therefore it is important to first further study this effect before it can be employed.

In the experimental part of this study the oil was evaporated by dripping it on the hot reactor wall. However, the heating rates are much lower in this manner than one would have with an atomizer. Therefore, probably the char formation is much higher than one would have with an atomizer. Employing an atomizer in the system could therefore further improve the CCE and CGE of the gasifier.

In this study the effects of the oil feed flow into the reactor and the residence time were not studied. Therefore, it would be interesting to study effect of the residence time on the gasifier output and process conditions by increasing the oil flow feed while keeping the ER and the S/F ratio constant.

Besides the previously mentioned research recommendations, also some recommendations are made for upgrading the current experimental setup:

- The gas sampling system should be upgraded in such a way that the production of non-volatile hydrocarbons, water and char can be measured so that the cause of the reduction in carbon conversion can be further investigated
- The tests should be performed with an online GC. Then the product gas can be monitored over a longer period of time and the change of dilution of the gas samples with air is reduced.
- The oil feed system requires more robust pumps to ensure a more constant oil flow and thus better reactor control
- The air feed system requires an upgrade for more accurate flow measurements and the compressed air feed system should need an upgrade to ensure a more constant air flow into the reactor.

References

Brahim, A., Prévost, M., & Bugarel, R. (1983). Momentum transfer in a vertical down flow liquid jet ejector: case of self gas aspiration and emulsion flow. International Journal of Multiphase Flow, 10(1), 79–94. https://doi.org/10.1016/0301-9322(83)90061-7

Ashraf, C., Jain, A., Xuan, Y., & van Duin, A. C. T. (2017). ReaxFF based molecular dynamics simulations of ignition front propagation in hydrocarbon/oxygen mixtures under high temperature and pressure conditions. *Physical Chemistry Chemical Physics*, *19*(7), 5004–5017. https://doi.org/10.1039/c6cp08164a

Barclay, K., Birk, J., & Parkins, W. (1977). *Process for production of synthesis gas.* https://www.osti.gov/biblio/7106062

Basu, P. (2018). Tar production and destruction. In *Biomass Gasification, Pyrolysis and Torrefaction: Practical Design and Theory* (pp. 189–210). Elsevier. https://doi.org/10.1016/B978-0-12-812992-0.00006-6

Chang, Y., & Chen, Y. (2000). Enhancement of a steam-driven ejector using a novel application of the petal nozzle. Journal of the Chinese Institute of Engineers, 23(6), 677–686. https://doi.org/10.1080/02533839.2000.9670589

Contin, V., Beart, T., & Toepoel, V. R. (2020, oktober). Business Case Report DKR350. Waste4Me B.V.

Cover, A. E., & Schreiner, W. C. (1974, October 6). Molten salt processing of fuels. *Society of Petroleum Engineers - Fall Meeting of the Society of Petroleum Engineers of AIME, FM 1974*. https://doi.org/10.2118/4995-ms

Creager, N. R., Creager, N., Brown, R. C., Kong, S.-C., & Hoff, S. J. (2016). *Gasification of liquid sprays in an entrained flow gasifier*. https://lib.dr.iastate.edu/etd/15140

Dahmen, N., Henrich, E., Dinjus, E., & Weirich, F. (2012). The bioliq® bioslurry gasification process for the production of biosynfuels, organic chemicals, and energy. *Energy, Sustainability and Society*, *2*(1), 1. https://doi.org/10.1186/2192-0567-2-3

Datta, R., & James, P. (2016). Molten salt pyrolysis for bio-oil and chemicals (WO2017007798A1). USA patent office.

de Beld, B. van, & Prins, W. (2002). *Entrained flow gasification of bio-oil for synthesis gas*. https://www.researchgate.net/publication/303189518_Entrained_flow_gasification_of_bio-oil_for_synthesis_gas

Dou, B., Gao, J., Sha, X., & Baek, S. W. (2003). Catalytic cracking of tar component from high-temperature fuel gas. *Applied Thermal Engineering*, *23*(17), 2229–2239. https://doi.org/10.1016/S1359-4311(03)00185-6

Duchesne, M. A. (2012). *SLAGGING IN ENTRAINED-FLOW GASIFIERS*. https://ruor.uottawa.ca/handle/10393/23353

Eikeland, M. S., Thapa, R. K., & Halvorsen, B. M. (2015). Aspen Plus Simulation of Biomass Gasification with Known Reaction Kinetic. *Proceedings of the 56th Conference on Simulation and Modelling (SIMS 56), October, 7–9, 2015, Linköping University, Sweden*, 153. https://doi.org/10.3384/ecp15119149

Elies, D. J. (2012). *Autoignition of Hydrogen and Syngas with Air in a Turbulent Flow Reactor*. https://etda.libraries.psu.edu/catalog/16294

Ewing, C. T., & Stern, K. H. (1974). Equilibrium vaporization rates and vapor pressures of solid and liquid sodium chloride, potassium chloride, potassium bromide, cesium iodide, and lithium fluoride. *Journal of Physical Chemistry*, *78*(20), 1998–2005. https://doi.org/10.1021/j100613a005

Fazly, M. (2016). Non-slagging entrained flow gasification of pyrolysis oil from radiata pine woody biomass. *Engineering: Theses and Dissertations*, 188. https://doi.org/10.26021/1193

Fleck, S., Santo, U., Hotz, C., Jakobs, T., Eckel, G., Mancini, M., Weber, R., & Kolb, T. (2018). Entrained flow gasification Part 1: Gasification of glycol in an atmospheric-pressure experimental rig. *Fuel*, *217*, 306–319. https://doi.org/10.1016/j.fuel.2017.12.077

Francisco, S., Maruyama, H., Takahashi, S., Iritani, J., & Miki, H. (2000). *Status of the EAGLE Project: Coal Gas Production Technology Acceptable for Fuel Cells*.

Fuels and Chemicals - Autoignition Temperatures. (2003). Engineering Toolbox. Retrieved October 21, 2021, from https://www.engineeringtoolbox.com/fuels-ignition-temperatures-d_171.html

Furusjö, E., Ma, C., Ji, X., Carvalho, L., Lundgren, J., & Wetterlund, E. (2018). Alkali enhanced biomass gasification with in situ S capture and novel syngas cleaning. Part 1: Gasifier performance. *Energy*, *157*, 96–105. https://doi.org/10.1016/j.energy.2018.05.097

Girods, P., Gastagno, F., Lelait, L., & Rogaume, Y. (2009). *Gasification tar reduction by sparging in a molten salt reactor*.

Holthoon, E. van. (2010). *Shell Gasification - Leading Technology Across Multiple Applications*. https://www.kivi.nl/uploads/media/565f102528109/Kivi_Gasification_Shell_Mar_2010.pdf

Huang, B.J. (1998) A 1-D analysis of ejector performance

Kawase, M., & Otaka, M. (2013). Removal of H2S using molten carbonate at high temperature. *Waste Management*, *33*(12), 2706–2712. https://doi.org/10.1016/j.wasman.2013.08.002

Kohl, A. L. (1986). Black liquor gasification. The Canadian Journal of Chemical Engineering, 64(2), 299–304. https://doi.org/10.1002/cjce.5450640221

Kohl, A. (2008). Gasification of sulfur-containing carbonaceous fuels (US20080141591A1). US patent office.

Law, C. K. (2010). *Combustion Physics* (1st ed.). Cambridge University Press.

Leijenhorst, E. J., Wolters, W., van de Beld, B., & Prins, W. (2014). Autothermal Catalytic Reforming of Pine-Wood-Derived Fast Pyrolysis Oil in a 1.5 kg/h Pilot Installation: Performance of Monolithic Catalysts. *Energy & Fuels*, *28*(8), 5212–5221. https://doi.org/10.1021/ef501261y

Lewis, Aaron D., "Gasification of Biomass, Coal, and Petroleum Coke at High Heating Rates and Elevated Pressure" (2014)

Li, J., Xie, Y., Zeng, K., Flamant, G., Yang, H., Yang, X., Zhong, D., Du, Z., & Chen, H. (2020). Biomass gasification in molten salt for syngas production. *Energy*, *210*, 118563. https://doi.org/10.1016/j.energy.2020.118563

Li, L. K. B., Dressler, D. M., Green, S. I., Davy, M. H., & Eadie, D. T. (2009). EXPERIMENTS ON AIR-BLAST ATOMIZATION OF VISCOELASTIC LIQUIDS, PART 1: QUIESCENT CONDITIONS. Atomization and Sprays, 19(2), 157–190. https://doi.org/10.1615/atomizspr.v19.i2.30

Lyke, S. E., Sealock, L. J. Jr., & Roberts, G. L. (1983). *Hot gas cleanup using solid supported molten salt for integrated coal gasification/molten carbonate fuel cell power plants. Topical report, October 1982-December 1983*. https://doi.org/10.2172/5134109

Magalhaes, E. M. (2011). COMBUSTION STUDY OF MIXTURES RESULTING FROM A GASIFICATION PROCESS OF FOREST BIOMASS. *Engineering Sciences*, 1. https://tel.archives-ouvertes.fr/tel-00623073/document

Magrini-Bair, K.; Czernik, S.; French, R.; Parent, Y.; Ritland, M.; Chornet, E. U.S. DOE Hydrogen Program Review; National Renewable Energy Laboratory: Golden, CO, (2002)

Marda, J. R., DiBenedetto, J., McKibben, S., Evans, R. J., Czernik, S., French, R. J., & Dean, A. M. (2009). Non-catalytic partial oxidation of bio-oil to synthesis gas for distributed hydrogen production. *International Journal of Hydrogen Energy*, *34*(20), 8519–8534. https://doi.org/10.1016/j.ijhydene.2009.07.099

Maund, J. K., & Earp, D. M. (1988). Fuels from Biomass by Conversion in Molten Salts. In *Research in Thermochemical Biomass Conversion* (pp. 542–556). Springer Netherlands. https://doi.org/10.1007/978-94-009-2737-7_42

Mcmahon, J. F., & Ernest, S. (1962). Production of hydrogen-containing gases (US3252774A). United States Patent Office.

Mevissen, N., Schulzke, T., Unger, C. A., & an Bhaird, S. M. (2009). Thermodynamics of autothermal wood gasification. *Environmental Progress & Sustainable Energy*, *28*(3), 347–354. https://doi.org/10.1002/ep.10393

Namkhat, A., & Jugjai, S. (2010). Primary air entrainment characteristics for a self-aspirating burner: Model and experiments. *Energy*, *35*(4), 1701–1708. https://doi.org/10.1016/j.energy.2009.12.020

NIST WebBook. (2021). NIST Chemistry WebBook. Retrieved September 29, 2021, from https://webbook.nist.gov/

Moersch, O., Spliethoff, H., & Hein, K. (2000). Tar quantification with a new online analyzing method. Biomass and Bioenergy, 18(1), 79–86. https://doi.org/10.1016/s0961-9534(99)00068-9

Pang, S. (2016). Fuel flexible gas production: Biomass, coal and bio-solid wastes. In *Fuel Flexible Energy Generation: Solid, Liquid and Gaseous Fuels* (pp. 241–269). Elsevier Inc. https://doi.org/10.1016/B978-1-78242-378-2.00009-2

Patah, F. A. P. (2016). *Non-slagging entrained flow gasification of pyrolysis oil from radiata pine woody biomass.* https://ir.canterbury.ac.nz/handle/10092/13284

Perondi, D., Restelatto, D., Manera, C., Godinho, M., Zattera, A. J., & Faria Vilela, A. C. (2019). The role of CaO and its influence on chlorine during the thermochemical conversion of shredder residue. *Process Safety and Environmental Protection*, *122*, 58–67. https://doi.org/10.1016/j.psep.2018.11.022

Postma, R. S., Kersten, S. R. A., & van Rossum, G. (2016). Potassium-Salt-Catalyzed Tar Reduction during Pyrolysis Oil Gasification. *Industrial & Engineering Chemistry Research*, *55*(26), 7226–7230. https://doi.org/10.1021/acs.iecr.6b01095

Prins, M. J. (2005). Thermodynamic analysis of biomass gasification and torrefaction. *Technische Universiteit Eindhoven*, 15. https://doi.org/10.6100/IR583729

Pritchard, R. (1977). *Handbook of industrial gas utilization: Engineering principles and practice* (1st Edition). Van Nostrand Reinhold Co.

Sakaguchi, M., Watkinson, A. P., & Ellis, N. (2010). *Steam Gasification of Bio-Oil and Bio-Oil/Char Slurry in a Fluidized Bed Reactor*. https://doi.org/10.1021/ef100604z

Saleh, A. R., Sudarmanta, B., Mujiarto, S., Suharno, K., & Widodo, S. (2020). Modeling of oil palm frond gasification process in a multistage downdraft gasifier using aspen plus. *Journal of Physics: Conference Series*, *1517*, 012036. https://doi.org/10.1088/1742-6596/1517/1/012036

Scheirs, J., & Kaminsky, W. (2006). Feedstock Recycling and Pyrolysis of Waste Plastics. Journal of Hazardous Materials, 147(1–2), 682–683. https://doi.org/10.1016/j.jhazmat.2007.04.035

Setten, van, B. A. A. L., Bremmer, J., Jelles, S. J., Makkee, M., & Moulijn, J. A. (1999). Ceramic foam as a potential molten salt oxidation catalyst support in the removal of soot from diesel exhaust gas. *Catalysis Today*, *53*(4), 613–621. https://doi.org/10.1016/S0920-5861(99)00149-2

Shen, H. P. S., & Oehlschlaeger, M. A. (2009). The autoignition of C8H10 aromatics at moderate temperatures and elevated pressures. *Combustion and Flame*, *156*(5), 1053–1062. https://doi.org/10.1016/j.combustflame.2008.11.015

Shin, E.-J., Nimlos, M. R., & Evans, R. J. (2001). The formation of aromatics from the gas-phase pyrolysis of stigmasterol: kinetics. *Fuel*, *80*(12), 1681–1687. https://doi.org/10.1016/s0016-2361(01)00054-0

Singh, G. (1999). ENTRAINMENT AND MIXING STUDIES FOR A VARIABLE DENSITY CONFINED JET. *Numerical Heat Transfer, Part A: Applications*, *35*(2), 205–224. https://doi.org/10.1080/104077899275335

Singh, G., Sundararajan, T., & Bhaskaran, K. A. (2003). Mixing and Entrainment Characteristics of Circular and Noncircular Confined Jets. *Journal of Fluids Engineering, Transactions of the ASME*, *125*(5), 835–842. https://doi.org/10.1115/1.1595676

Sovani, S. D., Sojka, P. E., & Lefebvre, A. H. (2001). Effervescent atomization. *Progress in Energy and Combustion Science*, *27*(4), 483–521. https://doi.org/10.1016/s0360-1285(00)00029-0

Sugiura, K., Minami, K., Yamauchi, M., Morimitsu, S., & Tanimoto, K. (2007). Gasification characteristics of organic waste by molten salt. *Journal of Power Sources*, *171*(1), 228–236. https://doi.org/10.1016/j.jpowsour.2006.11.007

Tian, H., Wang, W., Ding, J., Wei, X., & Huang, C. (2016). Preparation of binary eutectic chloride/expanded graphite as high-temperature thermal energy storage materials. *Solar Energy Materials and Solar Cells*, *149*, 187–194. https://doi.org/10.1016/j.solmat.2015.12.038

Tremel, A., & Spliethoff, H. (2013). Gasification kinetics during entrained flow gasification - Part III: Modelling and optimisation of entrained flow gasifiers. *Fuel*, *107*, 170–182. https://doi.org/10.1016/j.fuel.2013.01.062

Tsekos, C., Del Grosso, M., & De Jong, W. (2021). Gasification of woody biomass in a novel indirectly heated bubbling fluidized bed steam reformer. Fuel Processing Technology, 224, 107003. https://doi.org/10.1016/j.fuproc.2021.107003

Vargas, A. C., García, A. M., Arrieta, C. E., Sierra del Rio, J., & Amell, A. (2020). Burning Velocity of Turbulent Methane/Air Premixed Flames in Subatmospheric Environments. *ACS Omega*, *5*(39), 25095–25103. https://doi.org/10.1021/acsomega.0c02670

Veksha, A., Giannis, A., Oh, W. da, Chang, V. W. C., Lisak, G., & Lim, T. T. (2018). Catalytic activities and resistance to HCl poisoning of Ni-based catalysts during steam reforming of naphthalene. *Applied Catalysis A: General*, *557*, 25–38. https://doi.org/10.1016/j.apcata.2018.03.005

Nikkanen, V. (2014). Molten Salt Reactors in Gasification and Gas Purification. 6th International Freiberg Conference on IGCC & XtL Technologies Dresden. https://tu-freiberg.de/sites/default/files/media/professur-fuer-energieverfahrenstechnik-und-thermische-rueckstandsbehandlung-16460/publikationen/2014-08-3.pdf

Vogels, J. (2010). Industrial Scale Hydrogen Production from Biomass via CHOREN's Unique Carbo-V-process. In *Essen Schriften des Forschungszentrums Jülich / Energy & Environment* (Vol. 78). Zentralbibliothek, Verlag.

Walker, P., Rusinko, F., & Austin, L. (1959). Gas Reactions of Carbon. Advances in Catalysis, 133–221. https://doi.org/10.1016/s0360-0564(08)60418-6

Wang, D.; Fan, L.-S. (2013). "Particle characterization and behavior relevant to fluidized bed combustion and gasification systems". In Scala, Fabrizio (ed.). Fluidized Bed Technologies for Near-Zero Emission Combustion and Gasification. Elsevier. pp. 42–76 [p. 45]. doi:10.1533/9780857098801.1.42.

Wang, X. F., Chin, J. S., & Lefebvre, A. H. (1989). Influence of Gas-Injector Geometry on Atomization Performance of Aerated-Liquid Nozzles. *International Journal of Turbo and Jet Engines*, *6*(3–4), 1. https://doi.org/10.1515/tjj.1989.6.3-4.271

Waste4me. (2021). Waste4ME B.V. Retrieved October 18, 2021, from https://www.waste4me.com

White, F. (2011). Fluid Mechanics (7th edition). McGraw-Hill Education.

Williams, A. (1990). Combustion of Liquid Fuel Sprays. In *Combustion of Liquid Fuel Sprays*. Elsevier. https://doi.org/10.1016/c2013-0-00958-9

Xu, M., Hu, H., Yang, Y., Huang, Y., Xie, K., Liu, H., Li, X., Yao, H., & Naruse, I. (2018). A deep insight into carbon conversion during Zhundong coal molten salt gasification. *Fuel*, *220*, 890–897. https://doi.org/10.1016/j.fuel.2017.12.051

Yosim, S. J. (1981). The Molten Salt Coal Gasification Process. *Proceedings of The Electrochemical Society*, *9*, 439–451. https://doi.org/10.1149/198109.0439PV

Zheng, J.-L., Zhu, M.-Q., Wen, J.-L., & Sun, R.-. (2016). Gasification of bio-oil: Effects of equivalence ratio and gasifying agents on product distribution and gasification efficiency. *Bioresource Technology*, *211*, 164–172. https://doi.org/10.1016/j.biortech.2016.03.088

Appendix A: DKR350 GC screening oil lab report and boiling curve

ASG Analytik-Service

ASG Analytik-Service AG
Trentiner Ring 30 • 86356 Neusäss • Germany

Ingenia Consultants and Engineers
Esp 118
5633 AA Eindhoven
NETHERLANDS

Your reference	: Dik
Your order no.	: B001-2180268
Date of order	: 07.01.2021
Sample Receipt	: 08.01.2021
Sampling	: Customer
Start of test period	: 08.01.2021
End of test period	: 09.02.2021
Report date	: 09.02.2021
Page	: 1 of 2

Report No. : 2900104-2

Sample	ASG-ID	Parameter	Method	Result
Pyro-oil #0034	2900104_001	GCxGC MS Screening	ASG 2221 HT-GCxGC-MS	**siehe Anhang**

A volume of 500mg was diluted with dichloromethane and 1,0 µl was injected on-column for the analysis. The file named „ASG 2221_2900104_Chromatogramm.png" displays the 2D-Chromatogram. Different regions, comprising the main substance classes, are displayed in the chromatogram. The file „ASG 2221_2900104_Auswertung.xlsx" contains detailed spreadsheets of the identified substance classes. Based on the result of the simulated distillation (SimDist HT), it could be assumed that the sample is fully eluting by HT-GCxGC-TOFMS. However, compounds with boiling points below 100°C are discriminated by this method. A percentage of approximately 6% (area percentage) could not be assigned to certain classes. With a high probability these components consist of various aromatic compounds with unsaturated side chains as well as poly- and heteroaromatic compounds. Data evaluation was achieved by automated tools and can contain false positive/negative results. Several single compounds were identified manually due to their exposed location and high similarity to the mass spectra library.

Several different classes of Oxygenates could be identified. Phenols were identified as most prominent oxygen-contained compound class with more than 16% (area percentage).

DKR350 pyrolysis oil composition tables determined by high temperature gas chromatography:

	n-Alkanes	iso-Alkanes	Naphthenes/D	Dinaphthenes	Polynaphthen	Alkylbenzenes	Naphtheneob	Indenes/Alker	Naphthalenes	Biphenyls/Dip	Fluorenes	Anthracenes/	Pyrenes/Fluor	Total
C6						1.44%								1.44%
C7	<0.01%	<0.01%	0.11%	0.53%		6.45%								7.09%
C8	0.03%	0.23%	0.84%	0.41%		12.94%								14.45%
C9	0.06%	0.32%	1.20%	0.39%		4.93%	5.84%	0.76%						13.48%
C10	0.05%	0.03%	0.58%	0.21%		0.78%	0.77%	0.92%	1.74%					5.09%
C11	0.05%	0.67%	0.59%	0.04%		0.20%	0.47%	0.63%	1.30%					3.95%
C12	0.03%	0.08%	0.75%	0.08%		0.04%	0.14%	0.23%	0.57%	0.60%				2.51%
C13	0.03%	0.00%	0.18%	0.02%		0.05%	<0.01%	0.02%	0.21%	0.37%	0.21%			1.09%
C14	0.02%	0.72%	0.20%			0.01%	<0.01%		0.06%	0.27%	0.28%	0.25%		1.81%
C15	0.03%	0.09%	0.26%						<0.01%	0.04%	0.11%	0.21%		0.74%
C16	0.02%	0.02%	0.07%								0.02%	0.07%	0.10%	0.30%
C17	0.02%	0.29%	0.08%									<0.01%	0.02%	0.41%
C18	0.01%	0.03%	0.11%									0.01%	<0.01%	0.16%
C19	0.01%	0.02%	0.02%											0.05%
C20	0.01%	0.19%	0.07%											0.27%
C21	0.01%	0.02%	0.01%											0.04%
C22	0.01%	0.06%	0.05%											0.11%
C23	0.01%	<0.01%												0.01%
C24	0.01%	<0.01%												0.01%
Various		0.10%			0.29%									0.45%
Total	0.39%	2.86%	5.19%	1.68%	0.29%	26.84%	7.22%	2.56%	3.87%	1.28%	0.62%	0.54%	0.12%	53.45%
												Total		92.81%

S-Compound Groups	
Thiophenes	0.03%
Benzothiophe	0.03%
N-Compound Groups	
Nitrils	1.66%
Dinitrils	0.28%
Pyridins	0.09%
Benzonitrils	0.08%
Indoles	0.02%
Carbazoles	0.01%
Quinolines	0.16%
O-Compound Groups	
Alcoholes	0.13%
Aldehydes/Ke	0.53%
Various Oxyge	0.92%
Phenoles	16.62%
Benzofuranes	0.84%
PAK-Groups	
Phenyl-Napht	0.27%
Benzoanthrac	0.03%
Benzopyrenes	0.01%
Benzofluoren	0.07%
Cl-Compound Groups	
Chloralkanes	0.46%
Total	22.26%

Single Compounds	
Styrene	10.99%
Caprolactam	1.13%
Benzenebutar	2.16%
1,3-Dicyanobe	0.22%
Phenol, 2-chlo	0.06%
Benzeneaceto	0.12%
N-n-Propylpht	0.10%
1H-Isoindole-	0.55%
Biphenylene	0.07%
Benzene, 1,1'-	1.69%
Total	17.10%

DKR350 pyrolysis oil boiling point curve:

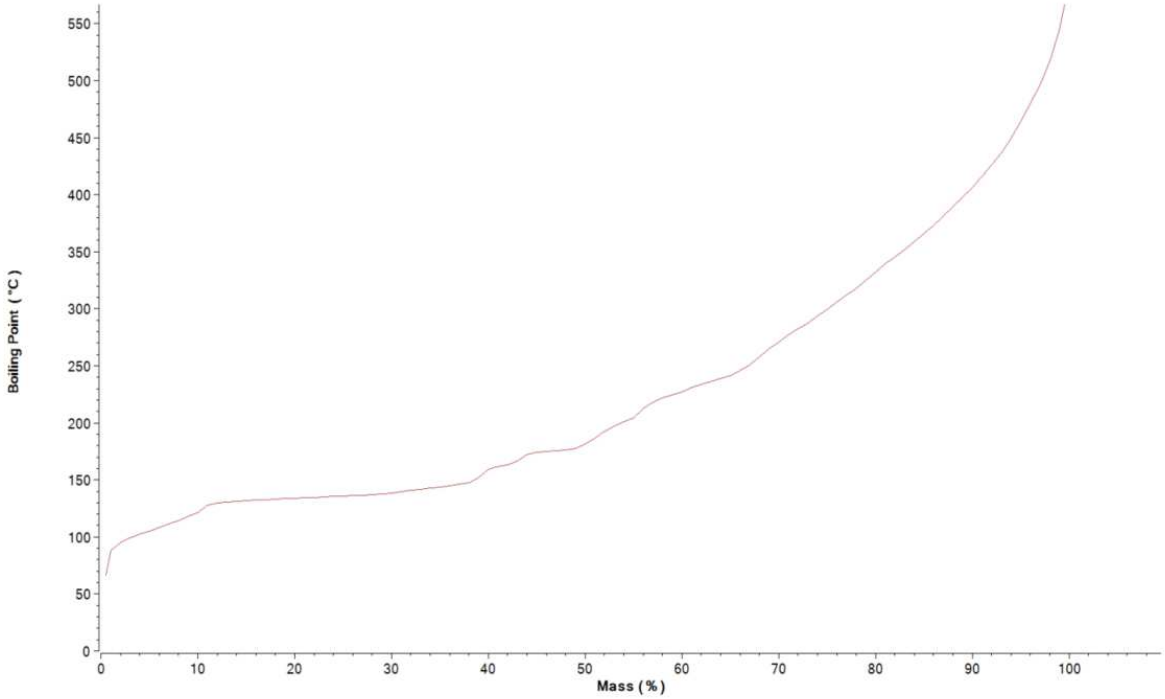

DKR350 pyrolysis oil properties and contaminant concentrations

Sample	ASG-ID	Parameter	Method	Result	Unit
Pyro-oil #0034	2900104_001	Kin. viscosity (25 °C)	ASTM D 7042 :2020	-*	mm^2/s
		Flash point	DIN EN ISO 3679 :2015	+11,0	°C
		Simulated Distillation	ASTM D 7169 :2020	see attachment	
		Chlorine content	DIN EN 15408 :2011	0,356	% (m/m)
		Fluorine content		0,015	% (m/m)
		Bromine (Br) content		0,023	% (m/m)
		Iodine content		<0,001	% (m/m)
		Silver (Ag)	ASG 1704-ICP-OES	<1	mg/kg
		Aluminium (Al)		<5	mg/kg
		Barium (Ba)		<1	mg/kg
		Beryllium (Be)		<5	mg/kg
		Bismuth (Bi)		<5	mg/kg
		Calcium (Ca)		<5	mg/kg
		Cadmium (Cd)		<0,5	mg/kg
		Cobalt (Co)		<1	mg/kg
		Chromium (Cr)		<1	mg/kg
		Copper (Cu)		<1	mg/kg
		Iron (Fe)		431	mg/kg
		Potassium (K)		<10	mg/kg
		Lithium (Li)		<1	mg/kg
		Magnesium (Mg)		<5	mg/kg
		Manganese (Mn)		1	mg/kg
		Sodium (Na)		<10	mg/kg
		Nickel (Ni)		<1	mg/kg
		Lead (Pb)		<10	mg/kg
		Strontium (Sr)		<1	mg/kg
		Thallium (Tl)		<0,5	mg/kg
		Vanadium (V)		<1	mg/kg
		Zinc (Zn)		7	mg/kg

*not possible (sample contains too many particles)

Appendix B: Reactor char deposit autoignition test

In this appendix the autoignition test on the char which was deposited on the reactor chamber will be discussed.

Setup

The char was collected from the walls of the chimney. The autoignition test was performed in an oven with a glass window wherethrough the ignition could be seen visually. The lid was opened a bit which made ventilation the ambient air possible. The oven that was used can be seen in figure B2. The temperature was measured by thermocouples and the moment of ignition was determined visually. The test was performed in two different configurations which can be seen in figure B1. The first test that was performed was done by placing a 10 ml cup with char deposit in it inside the oven with a thermocouple inside the char and a thermocouple right above the cup. The first test was performed 2 times. The second test was performed by placing a 25 ml cup upside down with the char deposit on top of it. One thermocouple was placed right above the char pile.

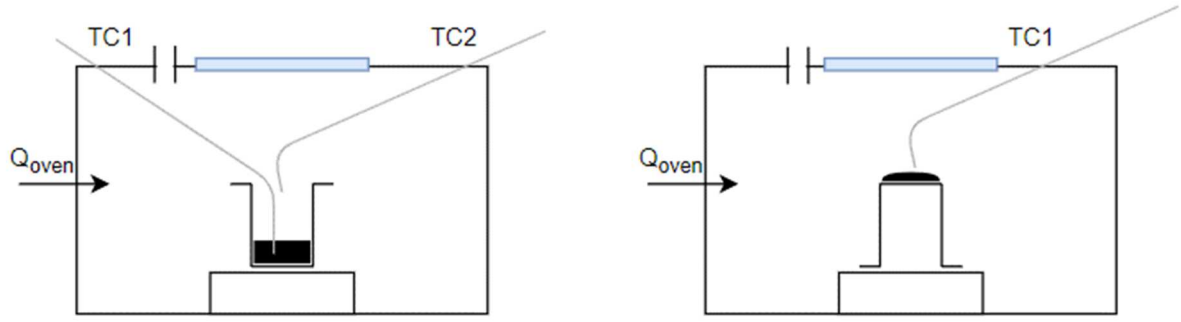

figure B.1 The setup of the autoignition test in a ceramic oven with a glass window and ventilation with ambient air in two different configurations: 1. 10 mm cup with a thermocouple inside and a thermocouple above the cup (left). 2. A 25 ml cup upside down with the char on top and a thermocouple above it (right).

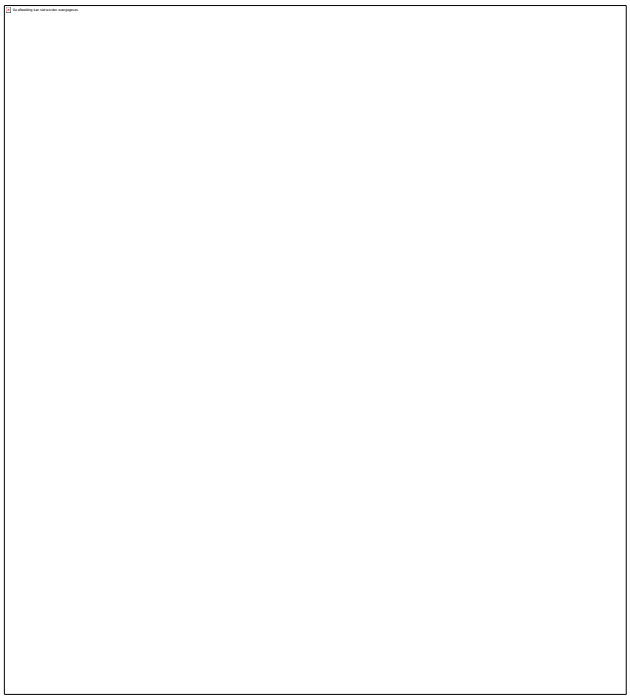

figure B.2 The oven with a glass window and 2 thermocouples which was used in the autoignition test of the char deposit

Results & discussion

Test 1: Configuration 1

The first test failed because the moment of autoignition could not be seen. However after the test the cup was empty so the char deposit did evaporate or combust. The test also failed because thermocouple 1 began interfering with some other electrical components as can be seen in figure B3 The temperature above the cup was always 0 – 80 °C higher than in the cup.

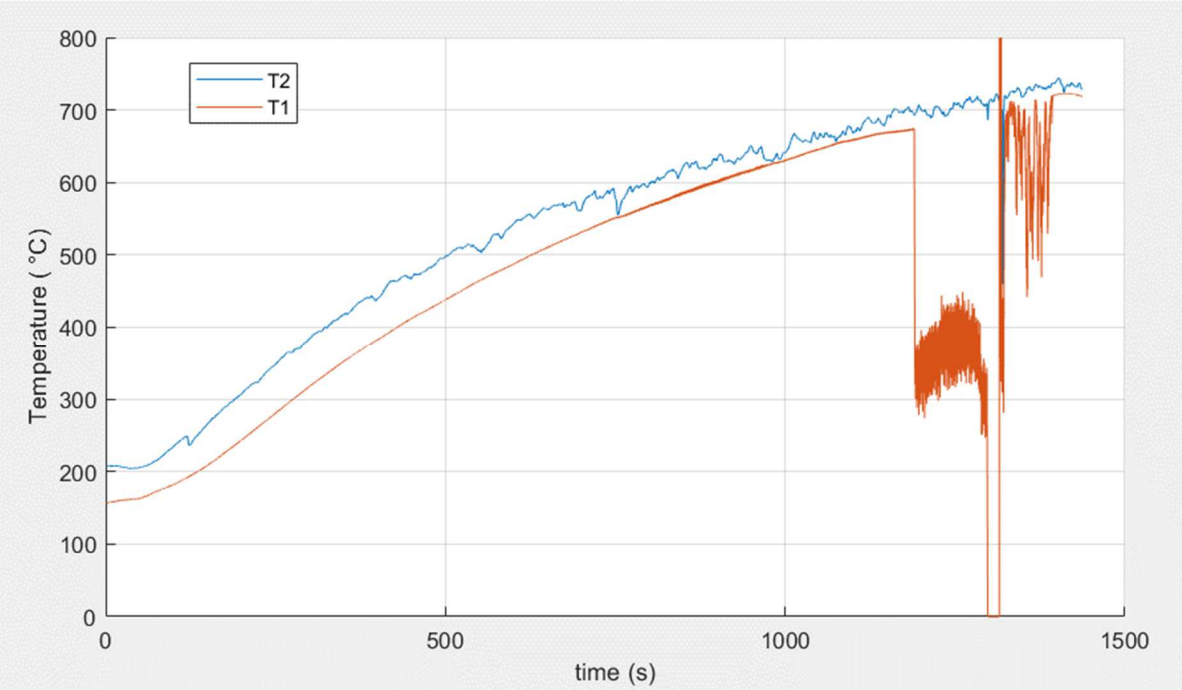

figure B3 The temperature in the oven plotted against time during autoignition test 1 with configuration 1

Test 2: Configuration 1

In this test the cup was filled with more char residue so that the visual observation of the moment of autoignition became easier. Also the lid was opened more than in test 1 so that there was more ventilation with the ambient air. The temperature measured with the thermocouples can be seen in figure B4. The temperature above the cup was almost always lower than inside the cup. This difference in results with test 1 was likely caused because of the increased amount of ventilation. The visual observations during the tests are as following:

Until 670 °C measured on with T1 in the cup there was only a decrease in char volume but no ignition. At 674 °C at T1 the gas above the cup ignited. At this point T2 was 650 °C. At 700 °C at T1 the combustion stopped but there was still some black residue at the bottom of the cup. At 790 °C at T1 the black residue was completely gone and only a small amount of white/grey ash was left.

Due to the small cup that was used in this test there was probably gas accumulation above the char. Therefore the autoignition was probably the autoignition temperature of the evaporated gasses instead of the autoignition temperature of the char. Before autoignition is was also observed that the char volume had already decreased, indicating an evaporation of the char.

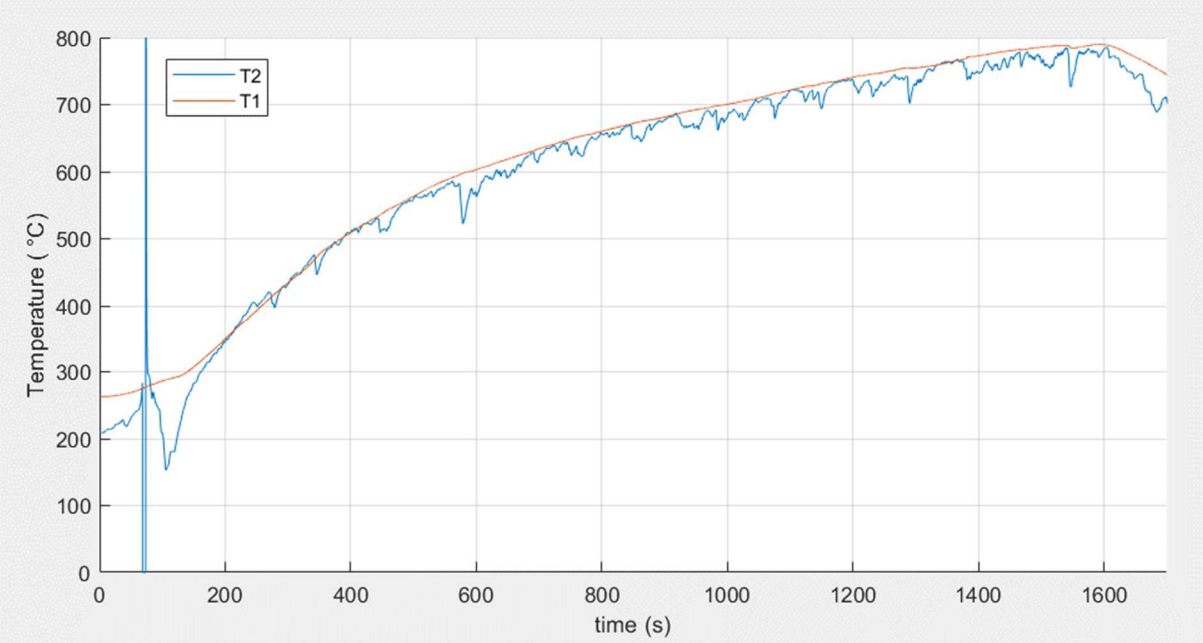

Figure B4 The temperature in the oven plotted against time during autoignition test 2 with configuration 1. The first ignition was observed at 674 °C.

Test 3: Configuration 2

The third test was done with configuration 2. The measured temperature plotted against time can be seen in figure B5. The visual observations are as following:

At 600 °C the char had decreased in volume. At 630 °C most of the char was gone. At 650 °C only some small black grains were left. At 660 °C al of the char was gone.

In this test no autoignition temperature could be determined. However it can be concluded that with enough supply of heated ambient air the char will disappear when heated to 660 °C. When compared to test 2 this test shows that with enough unreacted but heated ambient air supply the temperature at which the char will disappear is lower than with a lower supply of unreacted heated ambient air. The fact that no ignition was observed confirms the conclusion from test 2 that there is also evaporation instead of combustion. However is could also be that the combustion was not observable with the naked eye.

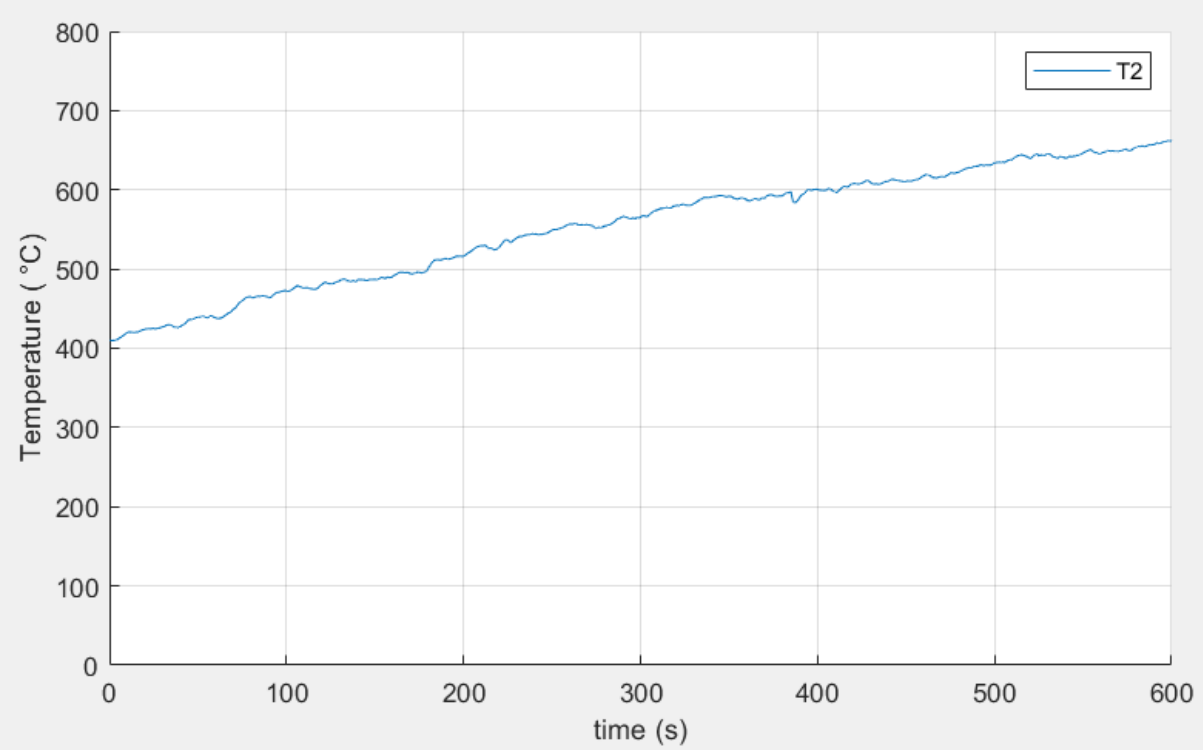

figure B5 The temperature in the oven plotted against time during autoignition test 3 with configuration 2. No ignition was observed, however at 660 °C all of the char was gone.

Conclusion

It was not possible to determine a definitive autoignition temperature of the char as the ignition was not always observed and the autoignition temperature also seems to depend on the configuration of the test. However it could be concluded that the char most probably contains a high amount of condensables which condensate on the relatively cold reactor wall as a large amount of the char evaporated instead of combusted. Test 2 showed that vapor coming from the char will autoignite at 674 °C. Test 2 also showed that the residue that is left after evaporation and combustion of the gasses will be fully disappeared at a temperature of 790 °C leaving only ashes. Test 3 showed that with a sufficiently high amount of heated ambient air it is possible to get rid of the char deposit at a temperature of 660 °C.

Appendix C: Short HAZOP Study of the setup

This hazard an operability study was performed to identify and prevent problems and risks of the experimental setup. The HAZOP study is based on the HAZOP study of Patah (2016) who designed an experimental setup for the gasification of bio-oil in an externally heated oxygen blown gasifier.

In table 5 the results of the HAZOP study are shown. The only case where extra control measures are required is when there is a flameout of the flare. Because this can cause a risk of explosion and fire the ATEX zones will be identified and the corresponding safety measures will be followed. Besides for the protection of the personnel 2 operators will operate the installation and suitable personnel protective equipment will be worn.

Score	Order of magnitude Frequency or Likelihood	Qualitative
+1	About once per month (10^{1})	Expected to occur frequently or regularly
0	Once per year (10^{0})	Likely to occur occasionally/several times during plant lifetime
-1	10% chance per year (10^{-1}) (once every 10 years)	Probably will happen more than once during plant lifetime
-2	1% chance per year (10^{-2}) (once every 100 years) (100 plant, once/year)	Not expected to occur but could occur during plant lifetime
-3	1 in 1,000 chance per year (10^{-3})	Would be very surprising if happened during plant lifetime
-4	1 in 10,000 chance per year (10^{-4})	Extremely remote, or not expected to be possible

Table 1 HAZOP score (O) for the change of occurrence (Patah, 2016)

Score	Effects expected to occur exclusively On-Site	Effects expected to occur Off-site
6		• Catastrophic release to environment • Long term effects • Substantial fines/penalties expected
5	• Catastrophic release to facility • Long term effects • Substantial fines/penalties expected	• Major release to environment • Long term impact likely • Fines/penalties likely
4	• Major release to facility • Long term impact likely • Fines/penalties likely	• Minor release to facility/outside help needed • Short term impact likely • Legal/public relation consequences
3	• Minor release to facility/outside help needed • Short term impact likely • Legal/public relation consequences	• Major release handled with internal resources • No legal/public relation consequences
2	• Major release handled with internal resources • No legal/public relation consequences	• Minor release handled with internal resources • No legal/public relation consequences
1	• Minor release handled with internal resources • No legal/public relation consequences	• Environmental impact unlikely
0	• Environmental impact unlikely	none

Table 2 HAZOP score (E) for the environmental impact (Patah, 2016)

Score	Unlikely but might affect one person On-site (10% of time)	Likely to affect 1-2 people On-site	Likely to affect 5-20 people On-site or Off-site
6			Fatality
5		Fatality	Immediate impairment, Permanent health effects
4	Fatality	Immediate impairment, Permanent health effects	Severe injury, Lost time
3	Immediate impairment, Permanent health effects	Severe injury, Lost time	Injury requiring medical treatment
2	Severe injury, Lost time	Injury requiring medical treatment	Minor injury
1	Injury requiring medical treatment	Minor injury	Probably none
0	Minor injury	Probably none	None

Table 3 HAZOP score (P) for impact on the health of people (Patah, 2016)

Score	Probability of safeguard failure	Example
0	100%	• No safeguards • Operator in difficult position
1	10%	• Single operator with adequate time (> 5 min) fails to do correct thing 1 out of 10 times
2	1%	• Single set of hardware, functionally tested • Automatic shutdown procedure
3	0.1%	• Passive protection (explosion disk) • Combination of Score 1 & 2
4	0.01%	• Two independent sets of hardware

Table 4 HAZOP score (SG) to rate the safeguard measures (Patah, 2016)

Risk level	Risk rating score	Descriptions
1	-4 to -1	Low risk, existing safeguards are adequate
2	0 to 3	Low risk, but risk control measures are required
3	4 to 8	High risk, risk control measures and additional protective measures are needed
4	9 to 13	Very high risk, this part or process cannot be operated unless risk control measures and additional protective measures have been conducted to reduce the risk and hazard

Table 5 Identified risks levels of the HAZOP study (Patah, 2016)

#	Deviation	Cause	Score O from table 1	Consequence	Score E from table 2	Score P from table 3	Safeguards	Score SG from table 4	Risk rating = O+E+P-SG	Risk Level from table 5	Required control actions
1	Reduction or stop of the compressed air inflow	Defect of compressor	-2	Reactions stops due to low ER due to a reduction in air inflow. If the reactions stop there will be unreacted oxygen inside the reactor giving an explosive mixture.	1	4	Construction of reactor vessel in such way that pressure can escape Build the reactor strong enough to withstand an explosion (will be explained in the text) Temperature drop alarm on control panel at a decrease of 5 K/s Operating panel at distance, reducing the risk at the event of an internal explosion Use no valve between gasifier and secondary burner. If an oxygen/fuel mixture exists this will cause combustion propagation from the secondary burner instead of explosion from inside the reactor	4	-1	1	Only test lower operation limit when reactor vessel is <600 C°. Check wall temperature and gas temperature before testing. Remove measuring devices that can be damaged by high pressures. Stop oxygen and fuel inlet when alarm sounds, and let reactor cool down before venting with air. Verify the reactor wall temperature.
		Blockage of compressed air hoses	-2		1	4		4	-1	1	
2	Reduction or stop of the compressed air inflow	Failure of the oil pump	-2	This will first cause the temperature to rise due to a high ER whereafter all the reactions stop due to shortage of fuel.	0	0	Thermocouple in reactor to detect the temperature	1	-3	1	Reduce the air flow into the reactor if the temperature rises above a 1000 °C. This is below the rating of the thermocouples of 1100 °C and below the maximum temperature of the rest of the reactor components.
		Blockage of the feeding system	-2		0	0		1	-3	1	
3	Explosive/combustible gas outside reactor	Leaking reactor	-2	Explosive/combustible gas accumulation outside reactor (if the secondary burner stops, the combustible gasses will blow unburned into the	1	3	Pressure/leak testing of the reactor Operation outside	3	-1	1	Wear gas mask if near the reactor Wear LEL gas detector if near reactor
4		Secondary burner flameout	0		1	3		2	2	2	

				atmosphere, causing risk of explosion/fire) The gas can be poisonous for the personnel around the reactor			Use a high temperature stabilization burner in the secondary burner to prevent secondary burner flameout				Check flame of secondary burner Control with 2 operators Control panel on the upwind side **Identify Atex zone and follow the Atex recommendations**
5	Reduction in cooling water	Blockage in cooling water system	-2	Steam formation in cooling cylinder which causing pressure build up in cooling water.	0	2	Temperature sensor in cooling water outlet	1	-1	1	Check cooling water outlet temperature Check cooling water flow
		Failure of the cooling water pump	-2	Charring of the oil in the oil inlet, oil flow will reduce or stop. See issue #2.	See issue #2.	See issue #2.		See issue #2.	See issue #2.	See issue #2.	

Table 6: The results of the short Hazop study performed on the test setup

Appendix D: Oil elemental analysis, heating value and water content lab report

GBA GROUP ENVIRONMENT

GBA Gesellschaft für Bioanalytik mbH · Bruchstr. 5c · 45883 Gelsenkirchen

Ingenia Consultants & Engineers BV

Esp 118

5633 AA Eindhoven

Test Report No.: 2021P225405 / 1

Order/Sample-No.	21209365 / 001
Date of Arrival	23.07.2021
Taking of samples	durch den Auftraggeber
Date of sample	19.07.2021
Material	Öl
Sample Name	DKR 350 : Pyrolytic Oil
Start / End of analyses	23.07.2021 - 28.07.2021
Amount of sample	ca. 400 ml

Parameter	Result	Unit	Methods
water content (Karl Fischer)	10000	ppm	DIN EN 60814: 1999-03*; VDE 0370-20: 1999-03 22
Higher heating value (as received)	38900	kJ/kg	DIN EN 15170: 2009-05* 22
Lower heating value (as received)	36100	kJ/kg	berechnet mit Faktor 22

With * marked methods are accredited methods. Detection limits (DL) may vary depending on the matrix of the sample.
Testing laboratory: 22GBA Herten

Gelsenkirchen, 28.07.2021

i. A. Jan-Niklas Franzen
Projektbearbeitung

GBA Gesellschaft für Bioanalytik mbH
Bruchstr. 5c, 45883 Gelsenkirchen
Telefon +49 (0)209 / 97 619 - 0
Fax +49 (0)209 / 97 619-785
E-Mail gelsenkirchen@gba-group.de
www.gba-group.com

HypoVereinsbank
IBAN DE45 2003 0000 0050 4043 92
SWIFT BIC HYVEDEMM300
Commerzbank Hamburg
IBAN DE87 2004 0000 0449 6444 00
SWIFT-BIC COBADEHHXXX

Sitz der Gesellschaft:
Hamburg
Handelsregister:
Hamburg HRB 42774
USt-Id.Nr. DE 118 554 138
St.-Nr. 47/721/00196

Geschäftsführer:
Ralf Murzen,
Dr. Roland Bernerth,
Kai Pinke,
Dr. Dominik Obelser

30 Jahre 1989-2019

ASG
Analytik-Service
Gesellschaft

ASG Analytik-Service Gesellschaft mbH
Trenkner Ring 30 • 86356 Neusäss • Germany

Ingenia Consultants and Engineers
Esp 118
5633 AA Eindhoven
NETHERLANDS

Your reference	:	Dik
Your order id.	:	B006-2180268
Date of order	:	22.07.2021
Sample receipt	:	29.07.2021
Sender	:	Customer
Start of test period	:	30.07.2021
End of test period	:	06.08.2021
Report date	:	06.08.2021
Page	:	1 of 1

Report No.: 2905357-1

Sample	ASG-ID	Parameter	Method	Result	Unit
DKR 350, Pyrolytic Oil	2905357_001	Carbon content	DIN 51732 :2014	82,0	% (m/m)
		Hydrogen content		8,65	% (m/m)
		Oxygen content	DIN 51732 :2014 mod.	6,7	% (m/m)

Jürgen Stocker (Manager of Elemental Analysis Group)

Appendix E: Calculation of the equilibrium constants with MATLAB

In this appendix the methodology of determining the equilibrium constants at temperatures above the standard temperatures are

The equilibrium constants of reactions can will be determined in a matlab script using the correlations of the NIST Webbook for the heat capacity, standard enthalpy and the standard entropy.

The equilibrium equation is as following:

$$\mathrm{K} = \frac{[C]^c[D]^d}{[A]^a[B]^b}$$

$$\mathrm{aA} + \mathrm{bB} \rightleftharpoons \mathrm{cC} + \mathrm{dD}$$

The correlations for the heat capacity, standard enthalpy and standard entropy from the NIST Webbook are:

$$Cp^\circ = \mathrm{A} + \mathrm{B} * t + \mathrm{C} * t^2 + \mathrm{D} * t^3 + \mathrm{E}/t^2$$

$$H^\circ - H^\circ_{298.15} = \mathrm{A} * t + \mathrm{B} * t^2/2 + \mathrm{C} * t^3/3 + \mathrm{D} * t^4/4 - \mathrm{E/t} + \mathrm{F} - \mathrm{H}$$

$$S^\circ = A * \ln(t) + B * t + C * t^2/2 + D * t^3/3 - E/(2 * t^2) + G$$

Where t = T/1000 and T is in the temperature in Kelvin.

Calculate heat of reaction with:

$$\Delta H_{rxn}(Tref) =$$

Correct heat of reaction for temperature change from reference temperature.

$$\Delta H_{rxn}(\mathrm{T}) = \Delta H_{rxn}(T_{ref}) + \sum_i \nu_i \left(H_i(T) - H_i(T_{ref})\right)$$

Where v represents the stoichiometric ratio's of the reactions. Calculate gibbs free energy of reaction from:

$$\mathrm{dG} = \mathrm{dH} - \mathrm{d}(\mathrm{T} \cdot S)$$

Then calculate equilibrium constant from:

$$\Delta G^\circ = -\mathrm{RT}\ \ln K$$

The equilibrium constants were calculated with Matlab and the results can be seen in paragraph 9.1 of the report. The matlab script used is as following:

```
clear all
close all

% reactor temperatuur
T = 400:20:1000; %in celsius
T = T + 273.15; % to kelvin

% Reaction 1: CH4 + 2 H2O -> CO2 + 4 H2
% Reaction 2: CO + H2O -> CO2 + H2

t = T/1000;

% H2
```

```
% T = 298-1000K valid temperature range
A =  33.066178;
B = -11.363417;
C =  11.432816;
D = -2.772874;
E = -0.158558;
F = -9.980797;
G =  172.707974;
H =  0.0;

Hf_29815_H2 = 0.0; % kJ/mol
S_29815_H2 = 130.68; % J/mol/K

dH_H2 = A*t + B*t.^2/2 + C*t.^3/3 + D*t.^4/4 - E./t + F - H;
S_H2 = (A*log(t) + B*t + C*t.^2/2 + D*t.^3/3 - E./(2*t.^2) + G);

%H2O
% 500-1700 K valid temperature range
A =   30.09200;
B =   6.832514;
C =   6.793435;
D =  -2.534480;
E =   0.082139;
F =  -250.8810;
G =   223.3967;
H =  -241.8264;

Hf_29815_H2O = -241.83; %this is Hf.
S_29815_H2O = 188.84;

dH_H2O = A*t + B*t.^2/2 + C*t.^3/3 + D*t.^4/4 - E./t + F - H;
S_H2O = (A*log(t) + B*t + C*t.^2/2 + D*t.^3/3 - E./(2*t.^2) + G);

%CO
% 298. - 1300K valid temperature range
A =   25.56759;
B =   6.096130;
C =   4.054656;
D =  -2.671301;
E =   0.131021;
F =  -118.0089;
G =   227.3665;
H = -110.5271;

Hf_29815_CO = -110.53; %this is Hf kJ/mol.
S_29815_CO = 197.66;

dH_CO = A*t + B*t.^2/2 + C*t.^3/3 + D*t.^4/4 - E./t + F - H;
S_CO = (A*log(t) + B*t + C*t.^2/2 + D*t.^3/3 - E./(2*t.^2) + G);

%CO2
% 298. - 1200.K valid temperature range
A =   24.99735;
B =   55.18696;
C =  -33.69137;
D =   7.948387;
E =  -0.136638;
F =  -403.6075;
G =   228.2431;
H =  -393.5224;

Hf_29815_CO2 = -393.51; %this is Hf.
S_29815_CO2 = 213.79;
```

```
dH_CO2 = A*t + B*t.^2/2 + C*t.^3/3 + D*t.^4/4 - E./t + F - H;
S_CO2 = (A*log(t) + B*t + C*t.^2/2 + D*t.^3/3 - E./(2*t.^2) + G);

%CH4
%Temperature (K)    298. - 1300
A=  -0.703029;
B=  108.4773;
C=  -42.52157;
D=  5.862788;
E=  0.678565;
F=  -76.84376;
G=  158.7163;
H=  -74.87310;

Hf_29815_CH4 = -74.6; %this is Hf.
S_29815_CH4 = 188.66;

dH_CH4 = A*t + B*t.^2/2 + C*t.^3/3 + D*t.^4/4 - E./t + F - H;
S_CH4 = (A*log(t) + B*t + C*t.^2/2 + D*t.^3/3 - E./(2*t.^2) + G);

%standard heat of reaction K1 & K2

Hrxn1_29815 = Hf_29815_CO2 + 4*Hf_29815_H2 - Hf_29815_CH4 - 2*Hf_29815_H2O;
Srxn1_29815 = S_29815_CO2 + 4*S_29815_H2 - S_29815_CH4 - 2*S_29815_H2O;
Grxn1_29815 = Hrxn1_29815 - 298.15*(Srxn1_29815)/1000;

Hrxn2_29815 = Hf_29815_CO2 + Hf_29815_H2 - Hf_29815_CO - Hf_29815_H2O;
Srxn2_29815 = S_29815_CO2 + S_29815_H2 - S_29815_CO - S_29815_H2O;
Grxn2_29815 = Hrxn2_29815 - 298.15*(Srxn2_29815)/1000;

%corrected for temperature
Hrxn1 = Hrxn1_29815 + dH_CO2 + 4*dH_H2 - dH_CH4 - 2*dH_H2O;
Grxn1 = Hrxn1 - T.*(S_CO2 + 4*S_H2 - S_CH4 - 2*S_H2O)/1000;

Hrxn2 = Hrxn2_29815 + dH_CO2 + dH_H2 - dH_CO - dH_H2O;
Grxn2 = Hrxn2 - T.*(S_CO2 + S_H2 - S_CO - S_H2O)/1000;

%equilibrium constant calculation
R = 8.314e-3; %kJ/mol/K
K1 = exp(-Grxn1/R./T);
K2 = exp(-Grxn2/R./T);
```

Appendix F: Product specification of DKR 350 Waste

Der Grüne Punkt –
Duales System Deutschland GmbH

Product Specification 04/2009
Fraction-No. 350

Sorting fraction:	**MIXED PLASTICS**

A Specification/Description

Used, completely emptied, system-compatible articles made of plastics that are typical for packaging (PE, PP, PS, PET) incl. packaging parts such as caps, lids, labels etc.

The supplementary sheet is part of this specification!

B Purity

At least 90 mass % in accordance with the Specification/Description.

C Impurities

Max. total amount of impurities	10 mass %
Metallic and mineral impurities with an item weight of > 100 g are not permitted!	
Paper, cardboard	< 5 mass %
Other metal articles	< 2 mass %
PET bottles, transparent	< 4 mass %
PVC articles other than packaging	< 0.5 mass %
Other residual materials	< 3 mass %

Examples of impurities:
- Glass
- Composite paper/cardboard materials (e.g. beverage cartons)
- Other materials (e.g. rubber, stones, wood, textiles, nappies)
- Compostable waste (e.g. food, garden waste)

D Delivery form

- Transportable bales
- Dimension and density of the bales must be chosen so as to ensure that a tarpaulin truck (loading area 12.60 m x 2.40 m; lateral loading height min. 2.60 m) can be loaded with a minimum loading of 21 t
- Dry-stored
- Produced with conventional bale presses
- Identified with DSD bale label stating the sorting plant No., fraction No. and production date